University of Arkansas, Fayetteville

ScholarWorks@UARK

5-2021

Peptoid-Based Microsphere Coatings for Biomaterial Applications

Jesse Leland Roberts
University of Arkansas, Fayetteville

Follow this and additional works at: https://scholarworks.uark.edu/etd

Part of the Biomaterials Commons, Molecular, Cellular, and Tissue Engineering Commons, Polymer and Organic Materials Commons, and the Polymer Science Commons

Peptoid-Based Microsphere Coatings for Biomaterial Applications

A dissertation submitted in partial fulfillment
of the requirements for the degree of
Doctor of Philosophy in Engineering

by

Jesse Leland Roberts
University of Arkansas
Bachelor of Science in Chemistry, 2015
University of Arkansas
Master of Science in Chemical Engineering, 2017

May 2021
University of Arkansas

This dissertation is approved for recommendation to the Graduate Council.

_____
Shannon Servoss, Ph.D.
Thesis Director

_____
Jorge Almodovar, Ph.D.
Committee Member

_____
Chris Griggs, Ph.D.
Ex-Officio Committee Member

_____
Christa Hestekin, Ph.D.
Committee Member

_____
Audie Thompson, Ph.D.
Committee Member

Abstract

Peptoids are peptidomimetic oligomers that predominantly harness similarities to peptides for biomimetic functionality. The incorporation of chiral, aromatic side chains in the peptoid sequence allows for the formation of distinct secondary structures and self-assembly into supramolecular assemblies, including microspheres. Peptoid microspheres can be coated onto substrates for potential use in biosensor technologies, tissue engineering platforms, and drug-delivery systems. They have potential for use in biomedical applications due to their resistance to proteolytic degradation and low immunogenicity. This dissertation focuses on the physical characteristics and robustness of the peptoid microsphere coatings in various physiological conditions, along with their ability to serve as ELISA microarray and tissue engineering substrates. We have shown that the peptoid microspheres are suitable substrates for layer-by-layer technologies to create biomimetic artificial extracellular matrices for tissue engineering. Overall, this study demonstrates that peptoid microsphere coatings are suitable materials for many biological applications.

Acknowledgements

I would first like to thank my advisor, Dr. Shannon Servoss, whose expertise was invaluable in developing and pushing me to be a better scientist and person in her lab. Her patient and motivating leadership empowered me to thrive throughout my graduate studies. She accepted me in her lab as an undergraduate chemistry student and allowed for me to pursue my goal of obtaining my doctorate degree. I would like to thank my committee members Dr. Jorge Almodovar, Dr. Chris Griggs, Dr. Christa Hestekin, and Dr. Audie Thompson for their valuable input and guidance throughout my project. I would also like to thank Dr. Tammy Lutz-Rechtin for her mentorship and support through my research work and life. She was always there to chat with when I needed it most. Dr. Rohana Liyanage deserves many thanks for consultation and help with challenging research complications and the characterization of samples.

To my fellow lab members, Joshua Corbitt, Aubrey Schultz, Meagan Olsen, Kaitlyn Brinza, and Harris Blankenship, thank you all for the assistance and encouragement that you gave me throughout my studies. It was a fulfilling experience working alongside all of you. To all my friends that I have made while in graduate school, thank you for the many memories that we made together. Whether it was trips to conferences or trips to Dickson St for lunch, I truly enjoyed your company. You all made graduate school worth it.

I would like to thank my parents, Alesia and Darrell Roberts, for their constant love and support during my entire life. You were both a pillar and foundation to my success, where I knew I could always come back to you for help. Thank you to my sister, Darla Roberts, for her morale support and love throughout my studies. As a competitive big brother, I have always viewed myself as your role-model, which has kept me going straight my entire life. In fact, you

are my role-model as well. I would also like to thank the rest of my family, including all my aunts, uncles, heavenly grandparents, cousins, and in-laws for their investment in my success.

Finally, I would like to thank the girl that has been my biggest supporter, my wife, Madelyn. I believe she deserves a doctorate by association, as she has been the rock to my graduate studies. Thank you for taking extra duties while I was in lab or up late writing. There was never a moment that your belief in me faded, nor did your encouragement dwindle when my own morale did. You were a constant reminder to stay positive through the tough times, and with that I will forever love and support you. My two dogs, Jax and Tilly Mae, also deserve credit for being emotional support vessels that allowed me to decompress and take my mind off school.

Table of Contents

1. Introduction

Biomaterial research is an exciting field that has grown steadily over the last several decades. Biomaterials are made of either synthetic or natural components that are with biological systems [1]. They are typically designed to produce a precise reaction with the biological system for a specific application [2]. In 1987, the term, biocompatibility, was explained as the ability of a material to perform with an appropriate host response in a specific application [3, 4]. More specifically, the material does not induce undesirable responses and is not toxic, while also promoting the functionality of the device for its application [4].

Progress in biomaterial design and engineering has enabled novel biomaterials to be prime candidates for applications in biosensing [5], tissue regeneration [6], and drug delivery systems [7]. Each specific application has guidelines for the biomaterial designation. For instance, drug delivery materials must allow for the controlled and targeted delivery of drugs without causing an unwanted immune response [8]. Therefore, it is important to create biomaterials with ideal properties and biocompatibility for the desired application.

1.1 Types of Biomaterials

Biomaterials can be divided into different material classes, including metals, ceramics, polymers, and composites [9]. Each type of material has unique surface chemistries and compositions that dictate their biological functionality. These properties can be tuned to have a desired effect on the biological response and outcome [10]. Metals are often used as medical implants in various parts of the body due to their inertness and excellent mechanical properties that prevent wear and fatigue of the material. Generally, the metal materials must be coated with a biopolymer to promote bio-functionality, such as blood compatibility and bioactivity necessary for successful implantation [11]. Ceramics, like metals, are commonly used as implants and for

1

the repair of damaged body parts. Alumina and zirconia are bio-inert ceramics, while calcium phosphates and glass-ceramics are considered bio-active ceramics. Both classes are used for the repair of diseased parts of the body by mimicking the natural calcified tissue [12]. Although useful as implants, metal and ceramic biomaterials are limited in other applications due to their difficult and expensive manufacturing process, and their lack of bio-functionality [11, 12].

1.2   Biopolymers

Biopolymers are chained molecules that are produced from living matter. The monomer units of biopolymers typically consist of amino acids for proteins/peptides, saccharides for sugars, or nucleotides for nucleic acids [13]. Peptides, specifically, are used in a variety of biomedical applications such as treatment for type 2 diabetes, prostate cancer, anemia, and many other diseases [14]. Peptides make excellent biotherapeutic and biomaterial candidates due to their good safety, efficacy, and high selectivity [15]. However, they are relatively chemically unstable due to the ease of proteolytic degradation *in vivo* causing their half-lives to be drastically reduced [16]. Proteins and peptides are also prone to aggregation, which can directly reduce their function and activity [17]. Synthetic peptides are of great interested because of their ease of synthesis and ability to mimic peptide sequences utilized in nature. They possess many of the advantages as natural peptides (e.g. biocompatibility, bioavailability, low toxicity), but are also prone to degradation when exposed to proteolytic enzymes [18, 19].

The disadvantages of peptides have led researchers to pivot to new classes of non-natural polymers, called peptidomimetics, that are designed to mimic the function of natural peptides [16, 20]. These polymers often mimic the secondary and tertiary structure of peptides, but small structural differences result in more protease resistant molecules [21]. Examples of these molecules includes β-peptides and poly-N-substituted glycines (peptoids) [21, 22, 23]. These

compounds have shown excellent bioavailability and the ease of synthesis makes them ideal candidates for many biomedical applications.

1.3 Applications for Biopolymers

1.3.1 Drug Delivery Systems

Although many biotherapeutic drugs have proven successful as treatment options for various diseases, there are still complications with delivery. Traditional routes, including oral, sub mucosal (nasal), parenteral (injection), and transdermal (through the skin) [24], are not feasible due to enzymatic degradation and low absorption efficiency [25]. The oral delivery of biotherapeutic proteins faces issues with poor absorbance within the gastrointestinal system and chemical degradation due to harsh enzymes within the digestive system, resulting in the loss of activity and function [26]. These pH-sensitive drugs are prone to degradation within the colon's harsh environment [27]. Subcutaneous injections and transdermal administration routes are challenging due to immunogenic potential and unwanted immune responses [28]. It has been reported that subcutaneous degradation occurs with protein-based drugs due to the lymphatic transfer of these proteins when delivered parenterally [29]. Nasal drug delivery is of interest due to the high vascularity and permeability within the nasal mucosa [30, 31]. As seen with other delivery methods, the body's immune defense mechanism bodes an even bigger issue. If the biotherapeutic causes any irritation in the nasal mucosa, then the mucocillary clearance mechanism will cause the drug to be rapidly diluted, increasing the clearance by forming nasal mucus that will be eliminated from the nose [32]. For this reason, drug delivery systems are growing in interest to combat the immunogenicity issues of protein therapeutics.

Drug delivery systems help facilitate the successful delivery of a drug candidate to specific body sites. Currently, most drug delivery systems are within the colloidal size range (1-

1000nm), and act to release the drug at a controlled rate for a prolonged period of time [33]. The drug is typically kept within a solid inner matrix that is layered by a permeable outer polymeric membrane through which the drug diffuses [34].

Focus has been on biopolymer drug delivery systems created from both synthetic and natural polymers, such as polylactic-co-glycolic acid (PLGA) nanoparticles and lipid-based carriers, respectively. PLGA nanoparticles are attractive for drug delivery due to their biodegradability and biocompatibility, FDA approval in parenteral administration systems, well-described production and characterization methods, protections from drug degradation, sustained release capabilities, possibility to modify surface properties, and target specificity for desired organs or cells [35]. Despite these desirable properties, PLGA-nanoparticles have their limitations when dealing with certain biotherapeutics such as peptides and proteins. The synthesis process of these nanoparticles involves factors and processes that may cause the protein to become aggregated and denatured [36]. Another issue associated with the use of nanoparticles is the complexity of cellular uptake and the unknown stability and cytotoxicity of the nanoparticles following metabolism [37, 38]. Liposomes and lipid-based carriers have already had a major impact on targeted therapeutic protein delivery. Liposomes are defined as phospholipid vesicles consisting of multiple lipid bilayers enclosing discrete aqueous spaces [39]. Liposomes and lipid-based carriers are advantageous as drug delivery systems due to their biocompatibility, ability to self-assemble, extended drug circulation time, and their ability to carry multiple drugs at once [40]. However, as with other drug delivery systems, lipid-carriers are still susceptible to enzyme degradation, primarily in the spleen and liver [41].

Therefore, it is necessary to create a robust drug delivery system that better protects the therapeutic drug from enzymatic degradation, while also promoting the selective release at the target location.

1.3.2 Disease Detection

The overall knowledge and treatment options for various types of cancers has drastically increased over the past several decades. Although there is much optimism within the cancer biology field, as seen by increased cancer survival rates, there is still plenty of work to be done towards diagnostic tools. Diagnosis of a disease typically follows the first sign of symptoms, which in many cancers, is considerably too late. There is a direct correlation between mortality rates and disease progression [42]. If caught early, many forms of cancer and other diseases can be treated effectively. However, early stages of cancer are often asymptomatic, and diagnosis relies on the observation of tumor growth. The National Cancer Institute's SEER Program studied this correlation and showed that the 5 year survival rate in skin cancer (92%) and breast cancer (89%) were must higher than those for internal organs, such as lung cancer (21%) and pancreatic cancer (10%) [43]. The most common diagnostic techniques include taking a biopsy of the tumor site or performing imaging techniques (e.g. CT scan, MRI, ultrasound, nuclear scan, or PET scan) [44]. Unfortunately, these techniques do not provide a platform for early detection due to the tumor already being present.

The early detection of disease reduces the economic burden by decreasing the amount and extensiveness of treatments, while also decreasing the mortality associated with the disease [45]. Ideal diagnostic technologies would be able to detect molecular changes present in asymptomatic populations during the onset of disease with high specificity. Researchers have focused their efforts on developing biomarker-based technologies due to their sensitivity and

ability to provide information on the state of a biological process [46]. Cancer biomarkers can display the genotoxicity, hyperproliferation, hyperplasia, inflammation, mutations, altered patterns of gene and protein expression, promoter methylation, and enzymatic changes that occur in response to disease [46, 47]. Protein-based biomarkers provide a natural platform that relies on the identification of altered protein expression levels in disease states [48, 49]. To detect and quantify the protein levels, researchers have looked at antibody-based arrays because of their high target specificity [50]. Unfortunately, the approval rate for these biomarkers is hampered by the molecular heterogeneity for various populations of tumor tissues.

Enzyme-linked immunosorbent assay (ELISA) microarray technology was developed in the early 2000's [51, 52] for the purpose of analyzing numerous biomarkers in parallel with higher sensitivity than traditional immunoassays [53, 54]. It is considered a low-cost and efficient screening technology that uses small volumes of clinical samples and expensive antibodies to test multiple proteins at the same time, also known as multiplex [55]. The design of ELISA microarray involves the immobilization of small amounts of antibodies onto a solid support in an ordered pattern, a microarray [52]. The antibodies bind protein analytes onto the surface, in which the microarrays are then incubated with the clinical sample and tagged for fluorescent detection.

The challenge to ELISA microarray and other protein/antibody microarrays is producing a slide surface that promotes strong antibody attachment, without disrupting the high binding capacities, signal-to-noise ratios, and reproducibility. These surface structures also have to be robust enough to retain high specificity and sensitivity levels through rigorous processing conditions and prolonged storage periods [56, 57]. These microarray surfaces are typically defined as either two-dimensional or three-dimensional surfaces. Glass slides are frequently used

for two-dimensional solid support platforms, where they must be functionalized with various chemicals (e.g. aldehyde, aminosilane, epoxysilane, mercaptosilane, polystyrene, and poly-L-lysine) to promote antibody attachment [58]. The covalent attachment of antibodies to two-dimensional surfaces results in strong attachment, but the close contact with the surface can affect the protein structure and function [59].

Three-dimensional surfaces immobilize proteins through physical adsorption from the hydrophobic interactions within their structures. This results in the proteins maintaining their native structure forming a more optimal surface with increased binding capacities and signal intensities [60]. In theory, increasing the surface area by using three-dimensional substrates for antibody attachment should enhance the microarray results by providing more sites of attachment to increase signal intensity and the dynamic range. Polymer-based surfaces that increase surface area such as polyacrylamide [47, 61], agarose [62], and nitrocellulose [63] suffer from low signal-to-noise ratios due to absorption of protein in the porous coating [64].

1.3.3 Tissue Engineering

According to an American Heart Association study in 2015, there are nearly 800,000 persons in the United States that suffer from stroke and over 140,000 die each year. Strokes are the fifth leading cause of death and considered the leading cause for serious long-term disability [65]. A stroke occurs when blood is restricted from the brain by either a blood clot (ischemic) or ruptured blood vessel (hemorrhagic) causing irreversible damage through the formation of cavities, or areas of dead brain tissue [66]. Current treatment options are limited to surgically repairing the ruptured blood vessel or using tissue plasminogen activator (tPA) to break up the clot. However, these treatments hold much risk due to the invasiveness and potential for infection that surgery poses, as well as the fact that tPA is only successful if used within the first

few hours from the onset of symptoms [67]. Often the patients are left with lifelong impairments in their motor function and lose the ability to complete routine tasks such as reading, writing, and talking.

In order to combat central nervous system (CNS) damage it's important to gain a better understanding of the self-renewal ability and neurogenesis of neuronal stem cells. Past evidence has shown that human neurons naturally undergo neurogenesis within two areas of the brain: the hippocampal dentate gyrus and the anterior subventricular zone [68, 69]. Self-renewal of these cells is often limited to low amounts of healthy neurons that decrease with age and severity of brain injury [70]. The mechanism of neurogenesis is of interest within the regenerative biology and tissue engineering fields where healthy neuronal cells, molecules, and supporting structures are implanted into diseased tissue to promote neuron regeneration [71, 72]. The ability of embryonic stem cells (ESCs) and human mesenchymal stem cells (hMSCs) to grow and differentiate into multiple cells types, especially neuronal cells, make them an interesting candidate for stroke, traumatic brain injury, and PNS injury treatment [73, 74].

Human embryonic stem cells are multipotent cells derived from the undifferentiated germ layers found in early developing embryos, called blastocysts [75]. Mesenchymal stem cells are easily isolated from adult bone marrow tissue and, like hESCs, are multipotent and possess self-renewable properties [76]. Both cell types can be directed to differentiate into specific adult cell lineages depending on the cellular microenvironment for various cell therapy applications. To be a viable tissue regeneration option there needs to be a better understanding in the differentiation pathways and what role the environment plays in dictating the stem cell fate.

The extracellular matrix (ECM) is a three-dimensional network composed of proteins and macromolecules that physically support surrounding cells [77]. The ECM's biochemical

composition and surface play a major role in stem cells' ability to grow and differentiate into adult cell types [78]. The topography and spatial arrangement of features on artificial ECM surfaces has shown to guide stem cell attachment and differentiation into specific adult cell types [79]. Current artificial ECM materials are made from either natural or synthetic components. Natural components include both proteins (laminin, collagen, fibronectin, etc) and carbohydrates, primarily glycosaminoglycans (heparin, chondroitin sulfate, and hyaluronic acid) and polysaccharides (chitosan and cellulose) [80]. Although suitable, these materials are often difficult to isolate and purify making them expensive to culture cells in large quantities. Along with the cost, the natural materials can be easily degraded when exposed to cellular conditions for extended periods of time and are limited to two-dimensional networks [81].

Synthetic components typically consist of nanomaterials, hydrogels, membranes, and non-natural polymers. The advantages to using synthetic ECM mimics is that they are more consistent and customizable than naturally derived materials. There is less batch-to-batch variability and the chemistry and mechanical properties can be tuned to suit an individual application [82]. For years, polyglycolic acid (PGA), poly(L-Lactic acid) (PLLA), poly)lactic-co-glycolic acid) (PLGA), poly(anhydrides), and poly(orthoesters) have been used to fabricate synthetic ECMs [83]. These polymers possess excellent biocompatibility, the degradation rate can be tailored, and they can easily be molded and cast into desired shapes and sizes [84]. Most synthetic ECM materials do not directly mimic the in vivo cell environment and lack critical biomolecular signaling dynamics [85]. There is a need for a material that directly mimics the three-dimensional substrates found in neuronal networks to gain a better understanding of the effect of topographical cues on neuronal stem cell fate.

1.4 Peptoids (Poly-N-Substituted Glycines)

Naturally occurring peptides possess excellent biological properties that theoretically make them ideal candidates for biomedical applications. However, due to their susceptibility to *in vivo* proteolytic degradation they are actually limited in their functionality. Research efforts have focused on creating peptidomimetics, non-natural polymers that are designed to directly mimic peptides. Peptidomimetics are structurally and functionally similar to peptides but have improved stability against proteolysis and increased bioavailability [86]. Peptides often utilize their ability to assemble into complex three-dimensional secondary and tertiary structures. In order to mimic these advanced structures of peptides, specific peptidomimetics, called foldamers, also display well-defined secondary and tertiary structures [21].

Peptoids, or *N*-substituted glycines, are synthetic peptidomimetic oligomers that structurally resemble α-peptides but have side chains attached to the amide groups on the backbone instead of the α-carbon as in peptides (Figure 1.1) [23]. This structural modification generates an achiral backbone that eliminates the potential for hydrogen bonding, resulting in a protease-resistant polymer that exhibits good cell computability and protein binding characteristics resembling that of more "drug-like" molecules [87]. The small size and protease-resistance also makes peptoids biocompatible as they are unlikely to illicit an immune response.
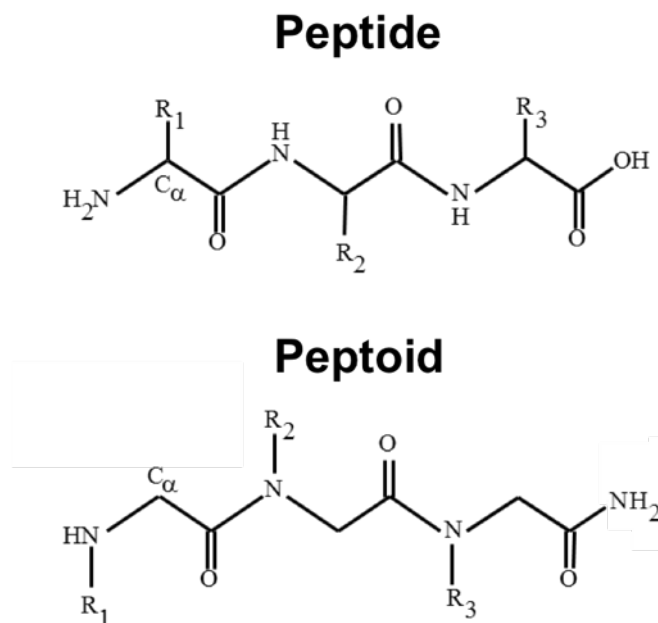
Peptide

Peptoid

Figure 1.1 Comparison of peptide and peptoid structures.

1.4.1   Peptoid Synthesis

The ease and efficiency of peptoid synthesis makes them an attractive peptidomimetic polymer. Peptoids can be produced via a sequence-specific, solid-phase synthesis method comparable to that of peptides [89]. Unlike peptide synthesis, where submonomers must be protected prior to addition, peptoid synthesis allows for the precise addition of unprotected submonomers greatly simplifying the process. The submonomer method is a highly efficient, low cost synthesis technique that allows for the addition of a wide variety of side chains as primary amines [89].
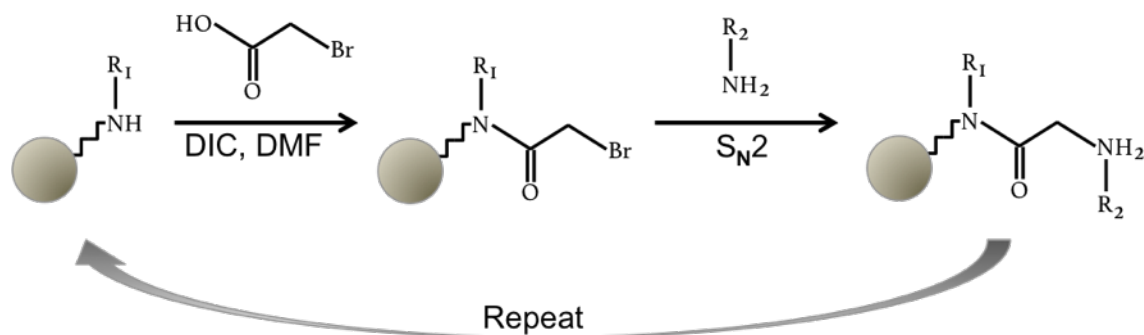
Figure 1.2 Illustration of peptoid submonomer solid-phase synthesis process [99].

Using a solid-phase support (ex: rink amide resin), submonomers are added from carboxylic to amine termini via a submonomer "cycle" made up of two-steps: (1) acylation and (2) amination (nucleophilic substitution) (Figure 1.2) [89]. The first reaction of the submonomer cycle, acylation, adds an activated carboxylic acid derivative onto a receptive amine generating a tertiary amide bond. In general, bromoacetic acid (BAA) and diisopropylcarbodiimide (DIC) are used for acylation. The BAA is activated by DIC separately, and then added to the solid-phase support [89]. The second step in the cycle, amination, involves the nucleophilic displacement of the halide (typically bromine) by a primary or N-terminal secondary amine (side chain). As the halide group is removed from the haloacetamide, the primary nitrogen submonomer attacks the alpha-carbon forming an ammonium salt. The halide ion then removes hydrogen from the ammonium salt producing hydrogen bromide. The amination step creates the molecular diversity that is present in peptoids due to the thousands of commercially available amine side-chains. Once synthesized, the peptoid molecule is cleaved from the resin and purified using preparative high-performance liquid chromatography.

1.4.2   Peptoid Microspheres

The backbone modification in peptoids eliminates the potential for hydrogen bonding, which is critical for secondary structure formation in peptides. However, including chiral side chains can induce secondary structures in peptoids such as turns, loops, and helices that allow for the formation of supramolecular assemblies [90, 21]. Peptoid helices are extremely robust as they are stabilized by steric hindrance and electrostatic repulsions between the side chains [90]. Peptoid homooligomers of (S)-methylbenzylamine as short as five monomers have shown polyproline type-I-like helices confirmed by circular dichroism (CD). The presence of minima at 207 nm and 2011 nm and a maximum at 190 nm resemble the spectrum for a peptide α-helix [92].

The Servoss lab has demonstrated that helical peptoids with partial water solubility self-assemble into microspheres in solution and can be cast onto a solid surface to form coatings. The peptoid of interest, P3, contains chiral, aromatic side chains that are positioned on two faces of the helix (Figure 3) to induce secondary structure and ultimately form microspheres (supramolecular structure) (Figure 4). The third face of the helix contains positively charged lysine-like side chains to enhance binding onto various substrates and incorporation of other adducts. The peptoid sequence and the effect that side chain placement (charge and bulk) along with the partial water solubility and helical content have been studied in detail [92, 93, 94]. Dissolving the peptoid in a 4:1 alcohol to water solution enables the formation of microspheres that can optimally be coated onto glass substrates. Further work has investigated the factors that affect the reproducible nature of microsphere coating formation including solvent effects, administration techniques, and drying conditions. These studies have shown that a 4:1 solution of

ethanol: water, drop-coating, and drying at 55% humidity produces optimal coatings that have excellent microsphere coverage.

Figure 1.3 Structure of P3 peptoid (MW=1919 Da).

Figure 1.4 Schematic representation of peptoid microsphere formation [93].

The peptoid microsphere coatings have excellent potential as drug delivery agents, biosensors, and artificial extracellular matrices. They are advantageous for the applications due to their topographical features, biocompatibility, and customizability. The spatial arrangement and contact angle of the microsphere coatings can be tuned for desired topographical properties. The positive surface charge of the microspheres can also be utilized in adding natural ECM components, such as laminin, collagen, heparin, and fibronectin, through polyelectrolyte multilayers.

1.5   Polyelectrolyte Multilayers

Polyelectrolyte coatings are rapidly gaining interest as biomaterials for various medical and pharmacology applications due to their ease and versatility [95]. Layer by layer (LbL) formation of polyelectrolyte multilayers (PEMs) is an intriguing method for surface modifications and nanoscale material synthesis. LbL utilizes the ionic attraction between opposite charges in alternating the adsorption of anionic and cationic polyelectrolytes [96]. The ability of PEMs to tune the chemical, physical, and topographical properties simply by altering the pH, ionic strength, number of layers, and layer thickness makes them ideal candidates for aECM substrates [97]. PEMs can be assembled by both naturally occurring and synthetic polymers where the library of potential polymers is endless. For example, PEMs constructed from naturally occurring polymers, heparin and collagen doped with IFN-γ, were able to promote enhanced cellular behaviors in human mesenchymal stem cells [98]. The tunability of PEM films make them interesting candidates as aECM substrates for neurogenesis in tissue engineering applications.

1.6   References

[1]   N. Huebsch and D. J. Mooney, "Inspiration and application in the evolution of biomaterials," *Nature,* vol. 462, no. 7272, pp. 426-432, 2009.

[2]   B. Ratner, A. Johnston and T. Lenk, "Biomaterial surfaces.," *Journal of Biomedical Materials Research,* vol. A1 Suppl, pp. 59-89, 1987.

[3]   D. Williams, "General Concepts of Biocompatibility," *Handbook of Biomaterial Properties,* pp. 481-489, 1987.

[4]   D. Williams, "Revisiting the definition of biocomptability," *Medical Device Technologies,* vol. 14, no. 8, pp. 10-3, 2003.

[5]   H. Liu, J. Ge, E. Ma and L. Yang, "10 - Advanced biomaterials for biosensor and theranostics," *A Biomaterials Approach,* pp. 213-255, 2019.

[6]   D. S. Kohane and R. Langer, "Polymeric Biomaterials in Tissue Engineering," *Biomaterials ,* vol. 63, pp. 487-491, 2008.

[7]   Y. K. Sung and S. W. Kim, "Recent advances in polymeric drug delivery systems," *Biomaterials Research,* vol. 24, no. 12, 2020.

[8]   A. Heller, "Integrated medical feedback systems for drug delivery," *AIChE Journal,* vol. 51, no. 4, pp. 1054-1066, 2005.

[9] D. D. Kiradzhiyska and R. D. Mantcheva, "Overview of Biocompatible Materials and Their Use in Medicine," *Folia Med (Plovdiv),* vol. 61, no. 1, pp. 34-40, 2019.

[10] M. Rahmati, E. A. Silva, J. E. Reseland, C. A. Heyward and H. J. Haugen, "Biological responses to physicochemical properties of biomaterial surface," *Chemical Society Reviews,* vol. 49, pp. 5178-5224, 2020.

[11] K. Prasad, O. Bazaka, M. Chua, M. Rochford, L. Fedrick, J. Spoor, R. Symes, M. Tieppo, C. Collins, A. Cao, D. Markwell, K. Ostrikov and K. Bazaka, "Metallic Biomaterials: Current Challenges and Opportunities," *Materials,* vol. 10, no. 8, p. 884, 2017.

[12] V. dos Santos, R. N. Brandalise and M. Savaris, "Ceramic Biomaterials," *Engineering of Biomaterials,* pp. 29-38, 2017.

[13] A. George, M. Sanjay, R. Srisuk, J. Parameswaranpillai and S. Siengchin, "A comprehensive review on chemical properties and applications of biopolymers and their composites," *International Journal of Biological Macromolecules,* vol. 151, pp. 329-338, 2020.

[14] A. A. Kaspar and J. M. Reichert, "Future directions for peptide therapeutics development," *Drug Discovery Today,* vol. 18, no. 17-18, pp. 807-817, 2013.

[15] A. K. Sato, M. Viswanathan, R. B. Kent and C. R. Wood, "Therapeutic peptides: technological advances driving peptides into development," *Current Opinions in Biotechnology,* vol. 17, no. 6, pp. 638-642, 2006.

[16] J. A. Patch and A. E. Barron, "Mimicry Of Bioactive Peptides via Non-Natural, Sequence-Specific Peptidomimetic Oligomers," *Current Opinion in Chemical Biology,* vol. 6, no. 6, p. 872–877, 2002.

[17] G. De Baets, L. Van Doorn, F. Rousseau and J. Schymkowitz, "Increased Aggregation Is More Frequently Associated to Human Disease-Associated Mutations Than to Neutral Polymorphisms," *PLoS Computational Biology,* vol. 11, no. 9, 2015.

[18] D. Seebach and J. L. Matthews, "β-Peptides: a surprise at every turn," *Chemistry Communication,* pp. 2015-2022, 1997.

[19] A. Grob, C. Hashimoto, H. Sticht and J. Eichler, "Synthetic Peptides as Protein Mimics," *Frontiers in Bioengineering and Biotechnology,* vol. 3, no. 211, 2015.

[20] D. H. Appella, L. A. Christianson, I. L. Karle, D. R. Powell and S. H. Gellman, "β-Peptide Foldamers: Robust Helix Formation In a New Family of β-Amino Acid Oligomers," *Journal of the American Chemical Society,* vol. 118, no. 51, p. 13071–13072, 1996.

[21] D. J. Hill, M. J. Mio, R. B. Prince, T. S. Hughes and J. S. Moore, "A Field Guide To Foldamers," *Chemical Reviews,* vol. 101, no. 12, p. 3893–4012, 2001.

[22] T. S. Burkoth, E. Beausoleil, S. Kaur, D. Tang, F. E. Cohen and R. N. Zuckermann, "Toward The Synthesis of Artificial Proteins," *Chemistry & Biology,* vol. 9, no. 5, p. 647–654, 2002.

[23] R. J. Simon, R. S. Kania, R. N. Zuckermann, V. D. Huebner, D. A. Jewell, S. Banville, S. Ng, L. Wang, S. Rosenberg and C. K. Marlowe, "Peptoids: a Modular Approach to Drug Discovery," *Proceedings of the National Academy of Sciences,* vol. 89, no. 20, p. 9367–9371 , 1992 .

[24] D. S. Pisal, M. P. Kosloski and S. V. Balu-lyer, "Delivery of therapeutic proteins," *Journal of Pharmaceutical Sciences,* vol. 99, no. 6, pp. 2557-2575, 2010.

[25] E. Koren, L. Zuckerman and A. Mire-Sluis, " Immune Responses to Therapeutic Proteins in Humans - Clinical Significance, Assessment and Prediction," *Current Pharmaceutical Biotechnology,* vol. 3, no. 4, pp. 349-360, 2002.

[26] R. I. Mahato, A. S. Narang, L. Thoma and D. D. Miller, "Emerging Trends in Oral Delivery of Peptide and Protein Drugs," *Critical Reviews in Therapeutic Drug Carrier Systems,* vol. 20, no. 2-3, pp. 153-214, 2003.

[27] A. K. Philip and B. Philip, "Colon Targeted Drug Delivery Systems: A Review on Primary and Novel Approaches," *Oman Medical Journal,* vol. 25, no. 2, pp. 79-87, 2010.

[28] V. Knepp, J. Hadgraft and R. Guy, "Transdermal drug delivery: problems and possibilities.," *Crit Rev Ther Drug Carrier Syst.,* vol. 4, no. 1, pp. 13-37, 1987.

[29] A. Fathallah, R. Bankert and S. Balu-lyer, "Immunogenecity of Subcutaneously Administered Therapeutic Proteins-a Mechanistic Perspective," *American Association of Pharmaceutical Scientists,* vol. 15, no. 4, pp. 897-900, 2013.

[30] Y. Chien and S. Chang, "Intranasal drug delivery for systemic medications.," *Critical Reviews in Therapeutic Drug Carrier Systems,* vol. 4, no. 2, pp. 67-194, 1987.

[31] M. Ugwoke, N. Verbeke and R. Kinget, "The biopharmaceutical aspects of nasal mucoadhesive drug delivery.," *The Journal of Pharmacy and Pharmacology,* vol. 53, no. 1, pp. 3-21, 2001.

[32] S. Gizurarson, "The Effect of Cilia and the Mucociliary Clearance on Successful Drug Delivery," *Biological and Pharmaceutical Bulletin,* vol. 38, no. 4, pp. 497-506, 2015.

[33] V. Filipe, A. Hawe and W. Jiskoot, "Critical Evaluation of Nanoparticle Tracking Analysis (NTA) by NanoSight for the Measurement of Nanoparticles and Protein Aggregates," *Pharmaceutical Research,* vol. 27, no. 5, pp. 796-810, 2010.

[34] T. M. Allen and P. R. Cullis, "Drug Delivery Systems: Entering the Mainstream," *Science,* vol. 303, no. 5665, pp. 1818-1822, 2004.

[35] F. Danhier, E. Ansorena, J. M. Silva, A. Le Breton and V. Preat, "PLGA-based nanoparticles: An overview of biomedical applications," *Journal of Controlled Release,* vol. 161, no. 2, pp. 505-522, 2012.

[36] A. S. Rosenberg, " Effects of Protein Aggregates: An Immunologic Perspective," *The AAPS Journal ,* vol. 8, no. 3, pp. 501-507, 2006.

[37] E. Frohlich, "The role of surface charge in cellular uptake and cytotoxicity of medical nanoparticles," *International Journal of Nanomedicine,* vol. 7, pp. 5577-5591, 2012.

[38] G. Gulati, N. Shafiq and S. Malhotra, "Drug-Loaded PLGA Nanoparticles for Oral Administration: Fundamental Issues and Challenges Ahead," *Critical Reviews in Therapeutic Drug Carrier Systems,* vol. 29, no. 2, pp. 149-182, 2012.

[39] D. Lasic, "The mechanism of vesicle formation.," *Biochemical Journal,* vol. 256, pp. 1-11, 1988.

[40] J. C. Kraft, J. P. Freeling and Z. H. R. J. Wang, "Emerging Research and Clinical Development Trends of Liposome and Lipid Nanoparticle Drug Delivery Systems," *Journal of Pharmaceutical Sciences,* vol. 103, no. 1, pp. 29-52, 2014.

[41] L. Sercombe, T. Veerati, F. Moheimani, S. Y. Wu, A. K. Sood and S. Hua, "Advances and Challenges of Liposome Assisted Drug Delivery," *Frontiers in Pharmacology,* vol. 6, no. 127, pp. 1-13, 2015.

[42] M. F. Ullah and M. Aatif, "The Footprints of Cancer Development: Cancer Biomarkers," *Cancer Treatment Reviews,* vol. 3, p. 193–200, 2009.

[43] A. C. Society, "Cancer Facts and Figures," American Cancer Society , 2021.

[44] W. Hamilton, "Cancer diagnosis in primary care," *British Journal of General Practice,* vol. 60, no. 571, pp. 121-128, 2010.

[45] R. Etzioni, N. Urban, S. Ramsey, M. Mcintosh, S. Schwartz, B. Reid, J. Radich, G. Anderson and L. Hartwell, "Early Detection: The Case for Early Detection," *Nature Reviews Cancer,* vol. 4, p. 243–252., 2003.

[46] M. A. Tainsky, "Genomic And Proteomic Biomarkers for Cancer: A Multitude of Opportunities.," *Biochimica et Biophysica Acta,* vol. 1796, no. 2, pp. 176-193, 2009.

[47] P. R. Srinivas, B. S. Kramer and S. Srivastava, "Trends In Biomarker Research for Cancer Detection," *The Lancet Oncology,* vol. 2, no. 11, pp. 698-704, 2001.

[48] J. DeRisi, L. Penland, P. Brown, M. Bittner, P. Meltzer, M. Ray, Y. Chen, Y. Su and J. Trent, "Use Of a CDNA Microarray to Analyse Gene Expression Patterns in Human Cancer," *Nature Genetics,* vol. 14, no. 4, pp. 457-460, 1996.

[49] M. Esteller, P. Corn, S. Baylin and J. Herman, "A Gene Hypermethylation Profile of Human Cancer," *Cancer Research,* vol. 61, no. 8, p. 3225–3229, 2001.

[50] N. L. Anderson, "The Human Plasma Proteome: History, Character, And Diagnostic Prospects," *Molecular & Cellular Proteomics,* vol. 1, no. 11, p. 845–867, 2002.

[51] C. A. Borrebaeck and C. Wingren, "Design Of High-Density Antibody Microarrays for Disease Proteomics: Key Technological Issues," *Journal of Proteomics,* vol. 72, no. 6, pp. 928-935, 2009.

[52] C. A. Borrebaeck and C. Wingren, "High-Throughput Proteomics Using Antibody Microarrays: an Update," *Expert Review of Molecular Diagnostics,* vol. 7, no. 5, p. 673–686, 2007.

[53] R. Ekins and F. W. Chu, "Microarrays: Their Origins and Applications," *Trends in Biotechnology,* vol. 17, no. 6, p. 217–218, 1999.

[54] P. Saviranta, "Evaluating Sandwich Immunoassays In Microarray Format in Terms of the Ambient Analyte Regime.," *Clinical Chemistry,* vol. 50, no. 10, p. 1907–1920, 2004.

[55] R. C. Zangar, D. S. Daly and A. M. White, "ELISA Microarray Technology as a High-Throughput System for Cancer Biomarker Validation," *Expert Review of Proteomics,* vol. 3, no. 1, pp. 37-44, 2006.

[56] P. Angenendt, J. Glökler, D. Murphy, H. Lehrach and D. J. Cahill, "Toward Optimized Antibody Microarrays: a Comparison of Current Microarray Support Materials," *Analytical Biochemistry,* vol. 309, no. 2, p. 253–260, 2002.

[57] S. L. Servoss, A. White, C. Baird, K. Rodland and R. Zangar, "Evaluation Of Surface Chemistries For Antibody Microarrays," *Analytical Biochemistry,* vol. 371, p. 105–115, 2007.

[58] W. Kusnezow and J. D. Hoheisel, "Solid Supports for Microarray Immunoassays," *Journal of Molecular Recognition,* vol. 4, pp. 165-176, 2003.

[59] P. Angenendt, "Progress In Protein and Antibody Microarray Technology," *Drug Discovery Today,* vol. 10, no. 7, p. 503–511, 2005.

[60] M. J. Taussig and U. Landegren, "Progress In Antibody Arrays," *Targets,* vol. 2, no. 4, p. 169–176, 2003.

[61] W. Kusnezow, V. Banzon, C. Schröder, R. Schaal, J. D. Hoheisel, S. Rüffer, P. Luft, A. Duschl and Y. V. Syagailo, "Antibody Microarray-Based Profiling of Complex Specimens: Systematic Evaluation of Labeling Strategies," *Proteomics,* vol. 7, no. 11, pp. 1786-1799, 2007.

[62] C. Wingren, J. Ingvarsson, L. Dexlin, D. Szul and C. A. Borrebaeck, "Design Of Recombinant Antibody Microarrays for Complex Proteome Analysis: Choice of Sample Labeling-Tag and Solid Support," *Proteomics,* vol. 7, no. 17, p. 3055–3065, 2007.

[63] O. Blixt, S. Head, T. Mondala, C. Scanlan, M. E. Huflejt, R. Alvarez, M. C. Bryan, F. Fazio, D. Calarese, J. Stevens, N. Razi, D. J. Stevens, J. J. Skehel, I. V. Die, D. Burton, I. A. Wilson, R. Cummings, N. Bovin, C. Wong and J. Paulson, "Printed Covalent Glycan Array for Ligand Profiling of Diverse Glycan Binding Proteins," *Proceedings of the National Academy of Sciences,* vol. 101, no. 49, p. 17033–17038, 2004.

[64] J. Ingvarsson, A. Larsson, A. G. Sjöholm, L. Truedsson, B. Jansson, C. A. K. Borrebaeck and C. Wingren, "Design Of Recombinant Antibody Microarrays for Serum Protein Profiling: Targeting of Complement Proteins," *Journal of Proteome Research,* vol. 6, no. 9, p. 3527–3536, 2007.

[65] E. Benjamin, "Heart Disease and Stroke Statistics—2019 Update: A Report From the American Heart Association," *American Heart Association,* vol. 139, no. 10, 2019.

[66] J. Gomes and A. Wachsman, "Types of Stroke BT- Handbook of Clinical Nutrition and Stroke,"," *Humana Press,* pp. 15-31, 2013.

[67] S. Gurav and e. al, "Problems and limitations in thrombolysis of acute stroke patients at a tertiary care center," *Indian Journal of Critical Care Medicine,* vol. 19, no. 5, pp. 265-269, 2015.

[68] M. Gotz and W. Huttner, "The cell biology of neurogenesis," *National Review of Molecular Cell Biology,* vol. 6, no. 10, pp. 777-778, 2005.

[69] A. Bedard and A. Parent, "Evidence of newly generated neurons in the human olfactory bulb," *Dev Brain Res,* vol. 151, no. 1, pp. 159-168, 2004.

[70] V. Galvan and K. Jin, "Neurogenesis in the aging brain," *Clin Interv. Aging,* vol. 2, no. 4, pp. 605-610, 2007.

[71] T. El Tal, R. El Sibai, S. Mondello and F. Kobeissy, "Neural-Tissue Engineering Interventions for Traumatic Brain Injury," *Tissue Engineering for Artificial Organs,* no. 655-657, 2017.

[72] M. Modo, "Bioscaffold-Induced Brain Tissue Regeneration," *Frontiers of Neuroscience,* vol. 13, p. 1156, 2019.

[73] Y. Zhou, A. Shao, W. Xu, H. Wu and Y. Deng, "Advance of Stem Cell Treatment for Traumatic Brain Injury," *Frontiers of Cellular Neuroscience,* vol. 13, p. 301, 2019.

[74] P. Dharmasaroja, "Bone marrow-derived mesenchymal stem cells for the treatment of ischemic stroke," *Journal of Clinical Neuroscience,* vol. 16, no. 1, pp. 12-20, 2009.

[75] C. Cowan and e. al, "Derivation of Embryonic Stem-Cell Lines from Human Blastocysts," *New England Journal of Medicine,* vol. 350, no. 13, pp. 1353-1356, 2009.

[76] K. e. a. Baghaei, "Isolation, differentiation, and characterization of mesenchymal stem cells from human bone marrow," *Gastroentrol. Hepatol. from bed to bench,* vol. 10, no. 3, pp. 208-213, 2017.

[77] T. Rozario and D. DeSimone, "The extracellular matrix in development and morphogenesis: a dynamic view," *Dev. Biol,* vol. 341, no. 1, pp. 126-140, 2010.

[78] I. Kazanis, "Extracellular matrix and the neural stem cell nmiche," *Dev. Neurobiol.,* vol. 71, no. 11, pp. 1006-1017, 2011.

[79] C. Czeisler and e. al, "Surface topography during neural stem cell differentiation regulates cell migration and cell morphology," *J. Comp. Neurol,* vol. 524, no. 17, pp. 3485-3502, 2016.

[80] C. Frantz, K. Stewart and V. Weaver, "The extracellular matrix at a glance," *Journal of Cell Science,* vol. 123, no. 24, pp. 4195-4200, 2010.

[81] S. Lopresti and B. Brown, "Chapter 4- Host Response to Naturally Derived Biomaterials," *Ed. Oxford: Academic Press,* pp. 53-79, 2015.

[82] R. Wade and J. Burdick, "Engineering ECM signals into biomaterials," *Materials Today,* vol. 15, no. 10, pp. 454-459, 2012.

[83] G. Albertini and e. al, "Organization of Extracellular Matrix Fibers Within Polyglycolic Acid-Polylactic Acid Scaffolds Analyzed Using X-Ray Synchotron-Radiation Phase-Contrast Micro Computed Tomography," *Tissue Engineering Part C Methods,* vol. 15, no. 3, pp. 403-411, 2009.

[84] Y. Zhang and e. al, "Synthetic Polymers Provide a Robust Substrate for Functional Neuron Culture," *Adv. Healthc. Mater.,* vol. 9, no. 4, pp. 1-7, 2020.

[85] M. Lutolf and J. Hubbell, "Synthetic biomaterials as instructive extracellular microenvironments for morphogenesis in tissue engineering," *Nat. Biotechnol.,* vol. 23, no. 1, pp. 47-55, 2005.

[86] J. Vagner, H. Qu and V. J. Hruby, "Peptidomimetics, a synthetic tool of drug discovery," *Curr Opin Chem Biol,* vol. 12, no. 3, pp. 292-296, 2008.

[87] K. Kirshenbaum, A. E. Barron, R. A. Goldsmith, P. Armand, E. K. Bradley, K. T. V. Truong, K. A. Dill, F. E. Cohen and R. N. Zuckermann, "Sequence-Specific Polypeptoids: A Diverse Family of Heteropolymers with Stable Secondary Structure," *Proceedings of the National Academy of Sciences ,* vol. 95, no. 8, p. 4303–4308, 1998.

[88] R. N. Zuckermann, J. M. Kerr, S. B. H. Kent and W. H. Moos, "Efficient Method for the Preparation of Peptoids [Oligo(N-Substituted Glycines)] by Submonomer Solid-Phase Synthesis," *J. Am. Chem. Soc.,* vol. 114, no. 26, p. 10646–10647, 1992.

[89] G. Figliozzi, R. Goldsmith, S. Ng, S. Banville and R. Zuckermann, "Synthesis of N-substituted glycine peptoid libraries," *Combinatorial Chemistry,* vol. 267, no. 437-447, 1996.

[90] C. W. Wu, T. J. Sanborn, K. Huang, R. N. Zuckermann and A. E. Barron, "Peptoid Oligomers With α-Chiral, Aromatic Side Chains: Sequence Requirements for the Formation of Stable Peptoid Helices," *J. Am. Chem. Soc.,* vol. 123, no. 28, p. 6778–6784, 2001.

[91] J. A. Patch, K. Kirshenbaum, S. L. Seurynck, R. N. Zuckermann and A. E. Barron, "Versatile Oligo(N-Substituted) Glycines: The Many Roles Of Peptoids in Drug Discovery," *Pseudo-Peptides in Drug Development,* p. 1–31, 2005.

[92] M. Hebert, D. Shah, P. Blake and S. Servoss, "Uniform And Robust Peptoid Microsphere Coatings," *Coatings,* vol. 3, no. 2, p. 98–107, 2013.

[93] M. L. Hebert, D. S. Shah, P. Blake, J. P. Turner and S. L. Servoss, "Tunable Peptoid Microspheres: Effects of Side Chain Chemistry and Sequence," *Organic & Biomolecular Chemistry,* vol. 11, no. 27, p. 4459, 2013.

[94] G. Perez Bakovic, J. Roberts, B. Colford, M. Joyce and S. Servoss, "Peptoid microsphere coatings: The effects of helicity, temperature, pH, and ionic strengths," *Biopolymers,* vol. 110, no. 6, 2019.

[95] S. Pahal, R. Gakhar, A. Raichur and M. Varma, "Polyelectrolyte multilayers for bio-applications: recent advancements," *IET nanobiotechnology,* vol. 11, no. 8, pp. 903-908, 2017.

[96] K. Tang and N. Besseling, "Formation of polyelectrolyte multilayers: ionic strengths and growth regimes," *Soft Matter,* vol. 12, no. 4, pp. 1032-1040, 2016.

[97] S. Zhang, M. Xing and B. Li, "Biomimetic Layer-by-Layer Self-Assembly of Nanofilms, Nanocoatings, and 3D Scaffols for Tissue Engineering," *Int. J. Mol. Sci,* vol. 19, no. 6, p. 1641, 2018.

[98] D. Castilla-Casadiego, J. Garcia, A. Garcia and J. Almodovar, "Heparin/Collagen Coatings Improve Human Mesenchymal Stromal Cell Response to Interferon Gamme," *ACS Biomaterial Science Eng,* vol. 5, no. 6, pp. 2793-2803.

2. Research Rationale

   This dissertation is focused on developing and characterizing peptoid microspheres (Chapter 3) as suitable substrates for biosensing (Chapter 4), LbL fabrication (Chapter 5), and tissue engineering applications (Chapter 6). It supports work done by Jesse Roberts and Dr. Shannon Servoss to assemble a novel, three-dimensional peptoid substrate for biosensing and tissue engineering applications. The peptoid microspheres provide potential to be a more biocompatible and customizable substrate than commercially available polymer-based substrates. The peptoid microspheres possess the ability to attach other naturally occurring biopolymers (laminin, collagen, heparin, etc.) through polymeric multilayer fabrication methods to combine the topography and surface chemistry that the stem cells favor.

3. Peptoid Microsphere Coatings: The Effects of Helicity, pH, and Ionic Strength

German R. Perez Bakovic, Jesse L. Roberts, Bryce Colford, Myles Joyce, and Shannon L. Servoss

Ralph E. Martin Department of Chemical Engineering, University of Arkansas Fayetteville

Abstract

Peptoids are peptidomimetic oligomers that predominantly harness similarities to peptides for biomimetic functionality. They have potential for use in biomedical applications and biosensors due to resistance to proteolytic degradation and low immunogenicity. The incorporation of chiral, aromatic side chains in the peptoid sequence allows for the formation of distinct secondary structures and self-assembly into supramolecular assemblies, including microspheres. Peptoid microspheres can be coated onto substrates for potential use in biosensor technologies, tissue engineering platforms, and drug-delivery systems. In order to be useful for these applications, the peptoid coatings must be robust under physiological conditions. In this study we report the effects of various conditions on the peptoid microsphere coatings, including (i) helicity, (ii) temperature (iii) pH, and (iv) ionic strength. These studies show that microsphere size decreases with increasing peptoid helicity and the positively charged side chains are positioned on the outside of the microspheres. The peptoid microsphere coatings are robust under physiological conditions but degrade in acidic conditions (pH < 7) and at low ionic strengths (< 150 μM).

3.1   Introduction

Natural polymers, such as proteins and peptides, have inspired the development of synthetic materials that mimic the fundamental molecular features, and are therefore also able to mimic the function. [1] While proteins and peptides have a myriad of unique functional properties, as biomaterials they are limited due to proteolytic degradation and as a result are restricted in their potential for use in biomedical and therapeutic applications. [2] Efforts to overcome these limitations have led to the design and development of innovative peptidomimetic oligomers. [3, 4, 5, 6, 7, 8] These synthetic oligomer analogs largely exploit structural similarities to allow for bioactive functionalities. Some bioactive roles are determined by the unique ability of proteins and peptides to self-assemble into complex, sequence-specific secondary and supramolecular structures. [9] Specific peptidomimetic oligomers, commonly referred to as foldamers [10], display well-defined secondary structures, and are therefore of great interest for use in biomaterials.

One class of foldamers, peptoids or poly-N-substituted glycines, closely resemble peptides, with the side chains attached to the backbone amide nitrogen rather than the backbone α-carbon as in peptides. This seemingly minor modification to the backbone has important implications to peptoid structure and function, including reduced proteolytic degradation that makes them a promising alternative to peptides for therapeutic applications where proteolysis is of major concern. The backbone modification also prevents hydrogen bonding within the backbone, which is critical for the formation of secondary structure in peptides. However, including specific side chains can induce the formation of peptoid secondary structures such as turns [11, 12], loops [13], and helices [14, 15, 16, 17, 18] that allow for the formation of supramolecular assemblies. [19, 20, 21, 22, 23, 24] For peptoid homooligomers of (S)-methylbenzylamine, stable helices

are formed with as few as five monomer units and full helicity is reached at 13 monomer units. [9] The circular dichroism (CD) spectra strongly resembles that for protein α-helices [9] and NMR confirms a helical structure similar to protein polyproline type-I helices, with a periodicity of three residues per turn and a helical pitch of ~6 Å. [16] Like peptides, peptoids are constructed via solid-phase synthesis, but following a submonomer method that provides a robust and highly efficient synthesis platform with precise sequence control. [25] Side chains are introduced by the incorporation of commercially available primary amines, enabling access to more than 300 side chain chemistries. [1]

Previous work has focused on the effects of peptoid water solubility, helical content, charge placement, and side chain bulk on self-assembly into microspheres. [24] Both peptoid helicity and partial water solubility were found to be crucial for microsphere formation. The microspheres (0.3 – 3.6 μm) are orders of magnitude larger than the length of a single peptoid helix (~24 Angstrom), suggesting that larger peptoid groupings are formed by stacking of the chiral aromatic groups. [24] Aromatic stacking has been observed in similar types of supramolecular assemblies for both peptides and peptoids. [26, 22,27,28,29] Further, peptoid sequences with alternating positive and negative charges on one face of the helix produce smaller microspheres (~0.3 μm) as compared to those with alternating positive and neutral charges on one face of the helix (~1.5 μm). It is believed that the opposite charges interact to form tighter helices, resulting in smaller microspheres. [24] Further work in the Servoss lab investigated the factors that affect the reproducible formation of microsphere coatings including solvent effects, administration technique, and drying conditions. [30] These studies showed that reproducible coatings were formed by solubilizing the peptoid in an aqueous solution of protic solvent, completely covering the surface with solution, and allowing it to dry at room temperature with

60% humidity.

Potential applications for peptoid microspheres include biosensors, artificial extracellular matrices, and drug delivery systems. The customizability of the microsphere chemistry allows for the fine-tuning based on application or environment. The work reported here shows the effect of peptoid length (and in turn helicity) on microsphere size, as well as the effects of temperature, pH, and ionic strength on the robustness of peptoid microsphere coatings. The surface charge and phase transition temperatures of the different peptoid lengths were measured using zeta potential and differential scanning calorimetry (DSC), respectively. Scanning electron microscopy (SEM) and ImageJ processing show that as peptoid chain length, or helicity, is increased microsphere size decreases and the size distribution increases. Zeta potential proved that there is a positive charge located on the outer surface of the peptoid microspheres, and DSC showed that the melting temperatures ranged from 78-83°C for the various peptoid lengths. Furthermore, SEM confirmed that the microsphere coatings are extremely robust under physiological conditions, however they degraded in low ionic strength and low pH solutions.

3.2   Materials and Method

3.2.1   Materials

(S)-methylbenzylamine and 4-methoxybenzylamine were purchased from Acros Organics (Pittsburgh, PA). *tert*-butyl N-(4-aminobutyl)carbamate was purchased from CNH Technologies Inc. (Woburn, MA). MBHA rink amide resin was purchased from NovaBiochem (Gibbstown, NJ). Piperidine was purchased from Sigma-Aldrich (St. Louis, MO). Ultra clean glass microarray slides, and disuccinimidyl suberate (DSS) were purchased from Thermo Scientific (Pittsburgh, PA). All other reagents were purchased from VWR (Radnor, PA). All chemicals were used without further modifications unless otherwise specified.

3.2.2 Peptoid Synthesis, Purification, and Characterization

Peptoids were synthesized following a submonomer, solid-phase method on rink amide resin, as previously described.[25, 31] Synthesis follows a carboxy to amino direction and the submonomer method includes two steps: acylation to extend the backbone and nucleophilic substitution to incorporate the side chain. [32] Briefly, the resin was swelled with dimethylformamide (DMF), and the Fmoc protecting group was removed using a 20% solution of piperidine in DMF. The resin-bound secondary amine was acylated with 0.4 M bromoacetic acid in DMF in the presence of N,N'-diisopropyl carbodiimide, mixing for 1 minute. Amine submonomers were incorporated via an S_N2 nucleophilic substitution reaction with 0.5 M primary amine in DMF, mixing for 2 minutes. The two-step acylation and nucleophilic substitution cycle was repeated until the desired sequence was obtained. The peptoid was cleaved from the resin using a mixture of 95% trifluoroacetic acid (TFA), 2.5% water, and 2.5% triisopropylsilane.

Peptoids were purified using a Waters Delta 600 preparative high-performance liquid chromatography (HPLC) instrument (Milford, MA) with a Duragel G C18 150 × 20 mm column (Peeke Scientific, Novato, CA) and a linear gradient of 35-95% solvent B (acetonitrile, 5% water, 0.1% TFA) in A (water, 5% acetonitrile, 0.1% TFA), over 60 minutes. Peptoids were confirmed to be >98% pure via analytical HPLC (Waters Alliance) with a Duragel G C18 150 × 2.1 mm column (Peeke Scientific) using a linear gradient of 35-95% solvent D (acetonitrile, 0.1% TFA) in C (water, 0.1% TFA), over 30 minutes. Presence of the desired sequence was confirmed via matrix assisted laser desorption/ionization time of flight (MALDI-TOF) mass spectrometry (Bruker, Billerica, MA). Purified peptoid fractions were lyophilized and stored as a powder at -20 °C.

3.2.3 Circular Dichroism

Peptoid secondary structure was confirmed via circular dichroism (CD) spectroscopy using a Jasco J-715 instrument (Easton, MD). The peptoids were dissolved in methanol at a concentration of 60 μM. Data was collected at room temperature with a scanning speed of 20 nm/min in a cuvette with a path length of 0.2 mm. Each spectrum was the average of twenty accumulations.

3.2.4 Peptoid Microsphere Coatings

Peptoid microspheres were prepared by dissolving the peptoid in a 4:1 ethanol/water (v/v) solution at a concentration of 5 mg/mL. The peptoid solution was applied to glass substrates using a pipette and allowed to dry at room temperature and 60% relative humidity for one hour. Coating morphology was imaged using a Phillips XL-30 environmental scanning electron microscope (SEM; FEI, Hillsboro, OR).

3.2.5 Microsphere Size Analysis

Particle size analysis was performed using ImageJ software (National Institute of Health, MD). Noise reduction was completed with a fast Fourier transform (FFT) band-pass filter normalization, eliminating low- and high-spatial frequencies and transforming the original SEM images to a two-dimensional representation of the frequency. The images were converted to 8-bit grayscale and binarized adjusting the white and black threshold to optimize particle contrast with the background. Greater than 200 particles were manually evaluated for each experimental condition and plotted using Origin2018.

3.2.6 Surface Charge Measurements

The surface charge of the peptoid microspheres was measured in terms of zeta potential using a Beckman Coulter Delsa NanoHC instrument (Brea, CA). A flat cell was employed for

determination of the zeta potential of the peptoid microspheres. The peptoid microsphere coatings were submerged in the feed solution that was set at a neutral pH of 7.0 and the measurements were taken.

3.2.7 Differential Scanning Calorimetry

The melting temperature and phase transition properties of the peptoid microspheres were measured using a TA Instruments Differential Scanning Calorimeter Model 25 (New Castle, DE). The peptoid microspheres were formed by dissolving peptoid in a 4:1 ethanol/water (v/v) solution at a concentration of 3 mg/mL. The peptoid microspheres were deposited onto a TA Instruments Tzero aluminum pan at a constant volume of 60 μL. The pan was set in a holding vessel where a lid was hermetically sealed using a specialized Tzero Press. Individual sample masses were taken and documented in the DSC control software, TRIOS v4.4, where after temperature equilibration at 0 °C, an isothermal period of ten minutes was completed. The ramping period of 20 °C per minute up to a maximum temperature of 200-240 °C was used to determine the phase transition and melting temperature of the peptoid microspheres. Upon conclusion, the plot of normalized heat flow (W/g) versus temperature (°C) was analyzed and the peak integration function within TRIOS resulted in the normalized enthalpy (J/g) and peak temperature (°C) for phase change.

3.2.8 Coating Robustness Under Biological Assay Conditions

The robustness of the peptoid microsphere coatings was assessed by incubation in solutions common to bioanalytical assays that have various values of pH and ionic strengths. Specifically, the coatings were incubated in 10 mg/mL casein in phosphate-buffered saline (PBS; pH 7.3, ionic strength 150 mM) for one hour, 0.05% Tween in PBS (PBS-T; pH 7.3, ionic strength 150 mM) for 12 hours, 0.003% hydrogen peroxide in 0.1M sodium borate (pH 8.2, ionic

strength 600 mM) for 10 minutes, and nanopure water (pH ~7, ionic strength ~0 mM) for up to 30 minutes.

3.2.9 Effect of Temperature, pH, and Ionic Strength on Coating

The ability of the peptoid microsphere coatings to withstand temperature, pH, and ionic strength was assessed through incubation in various solutions. The effect of temperature was evaluated by incubating the peptoid microsphere coatings in PBS and water at 37 °C. The temperature of both PBS and nanopure water was preheated and kept constant at 37 °C using a covered incubation chamber and hot plate. The pH and ionic strength robustness studies were assessed by incubating the peptoid microsphere coatings in solutions ranging from pH 3-11 and ionic strength of 0-500 mM at room temperature (25°C). The solution pH was adjusted by adding a stock hydrochloric acid or sodium hydroxide solution drop-wise until the desired pH was attained. The coatings were incubated in solutions of different pH values (pH = 3, 4, 5, 6, 7, 8, 9, 10, 11) for one hour. The ionic strength of water and PBS was adjusted using a stock potassium chloride solution until the desired ionic strengths were obtained. The coatings were incubated in solutions of different ionic strength values (ionic strength = 0, 50, 100, 150, 250, 500 mM) for one hour. The robustness of the peptoid microsphere coatings was assessed via SEM by analyzing microsphere morphology and surface coverage.

3.3 Results

3.3.1 Peptoid Sequence and Characterization

The peptoid sequences used in this study (Figure 3.1A) are based on that of a helical and partially water soluble 12mer that was previously reported to form microspheres. [24] Helical secondary structure is induced by including two-thirds chiral, aromatic side chains (Nspe) such that two faces of the helix contain Nspe side chains (Figure 3.1B). This configuration allows for

interactions between the benzene rings on different peptoid molecules. The third face of the peptoid helix contains alternating side chains with amine and methoxybenzyl groups to increase water solubility, as well as facilitate attachment to glass substrates. In this study, the length of the peptoid was varied by repeating the same six monomer unit for final lengths of 6, 12, 18, and 24 monomers (Figure 3.1A).
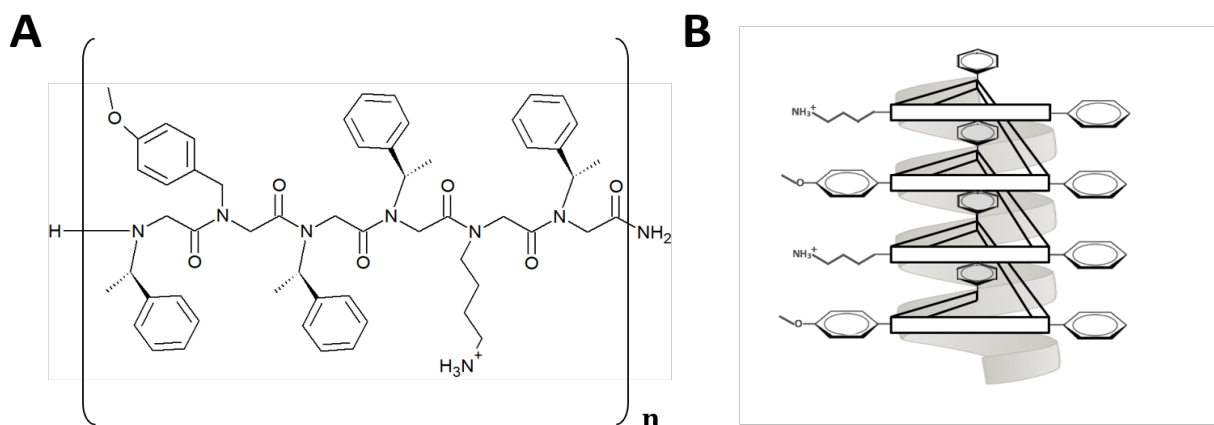
Figure 3.1 (A) Linear peptoid sequence. Four peptoids were studied: 6mer (n=1, MW=968), 12mer (n=2, MW=1919), 18mer (n=3, MW=2870), and 24mer (n=4, MW=3821). (B) Representation of the 12mer peptoid helix.

Peptoid helicity was assessed by CD spectroscopy (Figure 3.2). The 12mer, 18mer, and 24mer peptoids exhibit a maximum near 193 nm and two minima near 208 and 222 nm, indicative of polyproline type-I-like peptoid helices. [32] The 6mer also displayed a maximum near 193 nm and a minima near 222 nm; however, a second minima at 200 nm indicates both random coil and polyproline type-I-like peptoid helix secondary structures. [33] The relative helicity increases with peptoid length, as evidenced by the increasing intensity of the minimum peak at 222 nm. [34] This corresponds to previous studies, which have shown that peptoid helicity increases with peptoid length. [9] This is further corroborated by molecular simulations. [35] These studies, which were validated by NMR experiments, show that peptoid helix formation is a function of temperature and chain length; ultimately, proving that as chain length increases

helicity increases and peptoid helix formation is thermodynamically favorable. [35, 36]
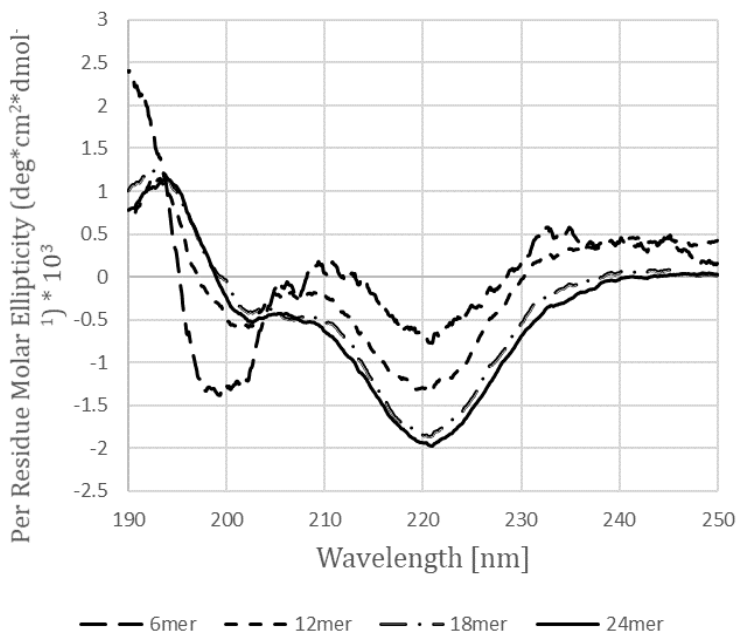

Figure 3.2 Circular dichroism spectra for 6mer, 12mer, 18mer, and 24mer peptoid in methanol at 60 μM.

3.3.2   Effect of Helicity on Microsphere Size and Distribution

It is desirable to tune the size of microspheres for different applications. Based on our previous results, [30] we hypothesized that peptoids with tighter helicity would form smaller microspheres. The formation of microspheres by peptoids with different helicities (6mer, 12mer, 18mer, and 24mer) was tested. The peptoids were solubilized in 4:1 ethanol:water and dried on glass substrates to form the microsphere coatings. Microsphere size was visually assessed by SEM and measured using ImageJ software. The 6mer peptoid did not form microspheres (Figure S3.1 in Supplemental Information), likely due to decreased helicity, increased water solubility, and the limited number of aromatic side chains to induce stacking. The 12mer, 18mer, and 24mer peptoids all formed microspheres of different sizes (Figures 3.3A, 3.3B, and 3.3C, respectively). As expected, microsphere diameter decreased with increasing helicity, with average diameters of 2.26 μm, 1.91 μm, and 1.24 μm for the 12mer, 18mer, and 24mer peptoids, respectively.

The decrease in size is likely due to the increased interactions between the peptoids that have higher helical content, and therefore closer packing in the microspheres. Conversely, peptoids with more loose helical structure are not able to pack as tightly and form larger microspheres. In addition, there is a direct relationship between peptoid length and microsphere size distribution, with the most uniform size distribution observed for the 12mer peptoid (Figures 3.3A and 3.3D) and the most disperse sizes observed for the 24mer peptoid (Figures 3.3C and 3.3F).

Like the peptoid microspheres, peptide foldamers use their molecular interactions to form distinct secondary structures that can be tailored into self-assembling supramolecular structures (spherical micelles [37], worm-like micelles [38], lamellar sheets [39], vesicles [40], nanotubes [41], and fibrils [42]). The size of spherical micelles formed from thermally responsive elastin-like peptides can be tuned through the secondary structure by altering the total chain length and the hydrophilic-hydrophobic chain ratio in the peptide. [37] Peptide nanotubes can be formed by incorporated cyclic peptides with D- and L- amino acids that self-assemble through antiparallel hydrogen bonding and stereochemical interactions of the peptide backbone. [43] By strategically assembling the peptide entities at specific ratios and altering the number of amino acids, the overall length and size of the peptide nanotube can be controlled for desirable end-product formation. [44] These supramolecular structures prove that the overall size is a function of secondary structure and intermolecular interactions, like the helicity of the peptoid microspheres.
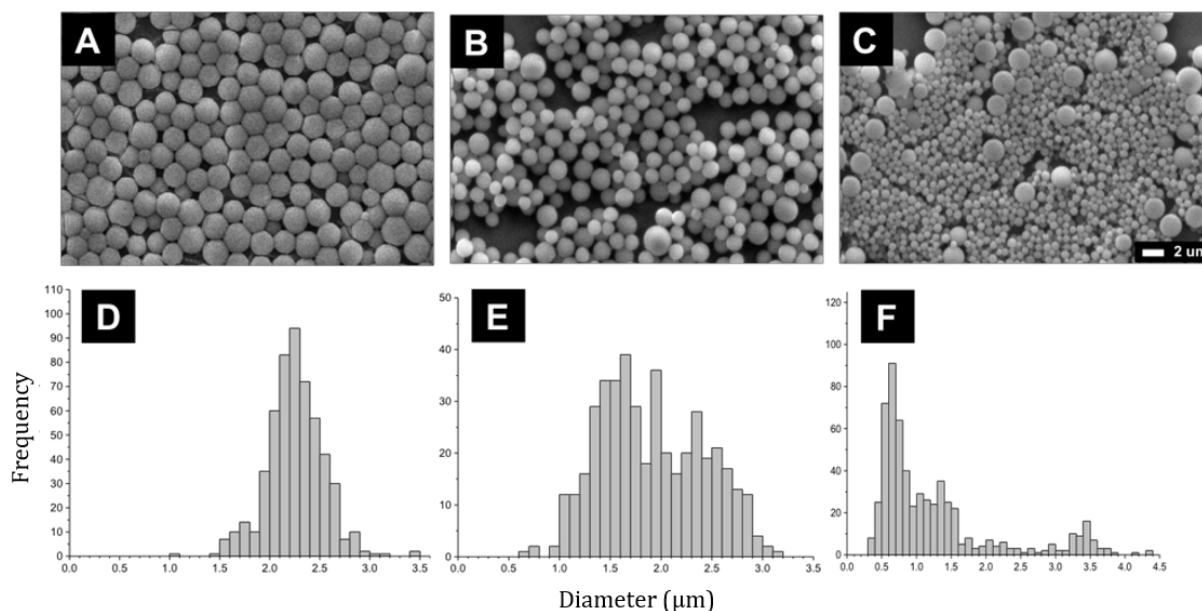
Figure 3.3 SEM images of (A) 12mer, (B) 18mer, and (C) 24mer peptoid microspheres. The size distribution for (D) 12mer, (E) 18mer, and (F) 24mer was evaluated using ImageJ software.

3.3.3   Surface Charge of Peptoid Microspheres

The surface charge, or zeta potential, of the different length peptoids was obtained using electrophoretic light scattering (ELS). The zeta potential gives the potential difference between the solid-liquid interface of the charged particle and the liquid media. It is hypothesized that the positively charged side chains are located on the outside of the microspheres due to the stacking of the aromatic groups, as well as the ability of the peptoid microspheres to robustly attach glass surfaces that have a relative negative charge. The surface zeta potential of the peptoid microspheres showed a drastic increase as compared to the ultraclean glass (Figure 3.4). The difference between the unmodified surface and peptoid-coated substrate indicates that the surface of the peptoid microspheres are positively charged. Although aqueous feed at neutral pH was used (~7.0), the amine side chain can be protonated ($-NH_3^+$) resulting in a net positive charge. [45] An increase in zeta potential as the peptoid chain length increases (12mer = +11.85, 18mer = +28.79, 24mer = +41.64) is potentially due to an increase in the number of cationic side chains,

along with the increase in the total number of spheres on the substrate that forms from the tighter helicity.
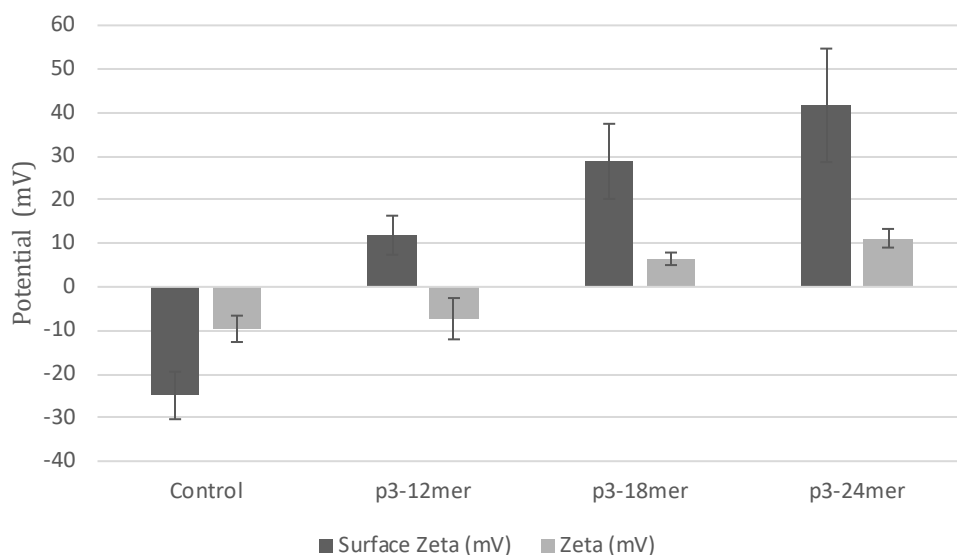
Figure 3.4 Zeta potential measurements for control (4:1 ethanol:water), 12mer, 18mer, and 24mer peptoid microsphere coatings.

3.3.4 Differential Scanning Calorimetry Measurements

The thermal behavior of the peptoid microspheres was examined by differential scanning calorimetry (DSC) to measure the excess heat capacity as a function of temperature. DSC was run in solid state for the 12mer, 18mer, and 24mer peptoid microspheres to determine the thermodynamic properties of thermally induced phase transitions such as melting temperature (T_m), enthalpy in terms of endothermic vs. exothermic peptoid degradation, and the polymorphic nature of the material. As expected, the heat flow was negative for all three peptoid samples, suggesting that the peptoid microsphere degradation occurs endothermically as the peptoid microspheres require heat to break the interactions and bonds during phase transition. [46, 47] The phase transition temperature increases as peptoid chain length increases, indicating a correlation between peptoid helicity and thermal stability (Figure 3.5). The 24mer peptoid microspheres had

the highest melting temperature on average at 82.94 ± 0.3845 °C, while the 12mer and 18mer

peptoid microspheres were similar at 74.00 ± 4.121 °C and 75.22 ± 4.121 °C, respectively. The

broadness in the DSC peaks indicate that the samples are forming polymorphic structures,

similar to many common polymers and other microspheres, and at the melting temperature, over

50% of the sample has undergone a phase transition. [48, 49]
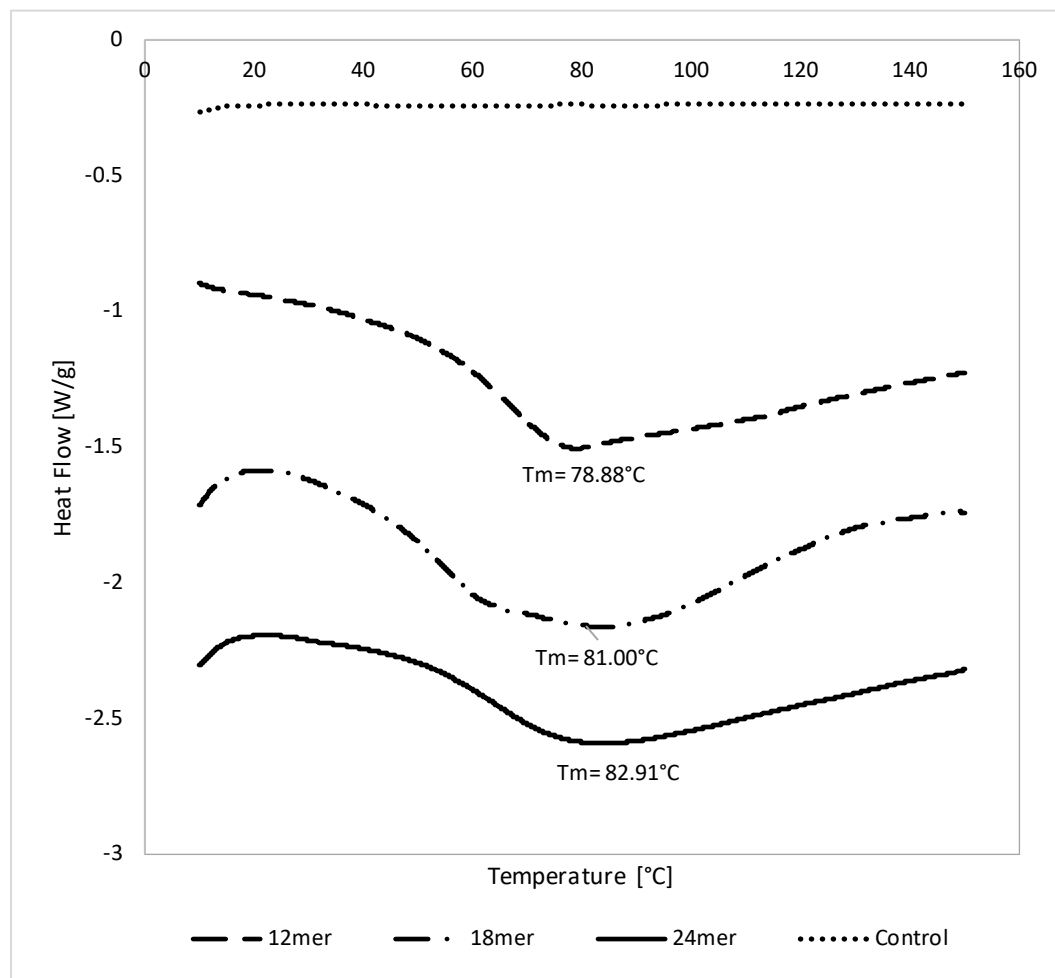

Figure 3.5 Differential Scanning Calorimetry measurements for control (4:1 ethanol:water), 12mer, 18mer, and 24mer peptoid microsphere coatings.

3.3.5   Coating Robustness under Biological Assay Conditions

In order to be practical in biomedical applications, the 12mer peptoid microsphere

coatings must be robust under various conditions. It was previously observed that the

microsphere coatings degrade when exposed to ultrapure water for 24 hours [30], therefore a thorough investigation was completed to determine whether pH, ionic concentration, or a combination of the two were responsible. The robustness of 12mer peptoid microsphere coatings was assessed by incubating the coatings in solutions with varying values of pH and ionic strength, including casein in PBS for 1 hour, 0.05% Tween in PBS for 12 hours, 0.003% hydrogen peroxide in 0.1M sodium borate for 10 minutes, and nanopure water for 10 minutes. The microsphere coatings showed minimum degradation, as assessed by morphology and surface coverage, in all solutions except water (Figure 3.6A-C and Figure S3.2 in Supplemental Information). After exposure to water for 30 minutes the microspheres appeared to disintegrate and lift from the surface. Despite the instability of the peptoid microspheres in water, they are robust in PBS for up to 2 months (Figure S3.3 in Supplemental Information). Based on these preliminary findings, the effects of pH and ionic strength on peptoid microsphere coating robustness has been thoroughly investigated.
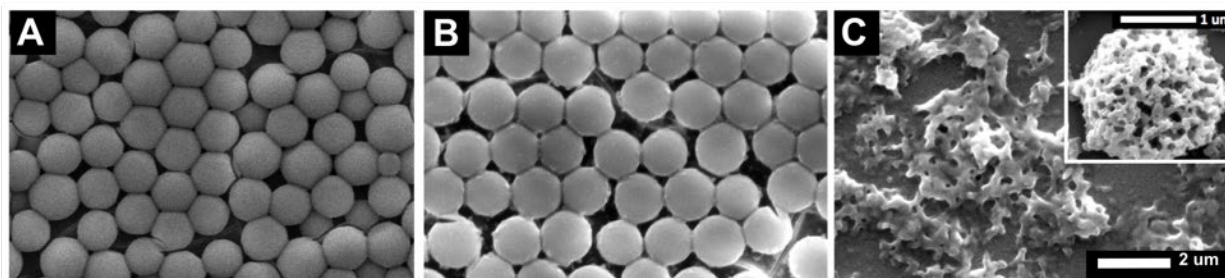
Figure 3.6 SEM images of the peptoid microspheres coatings (A) before incubation, (B) after 24 hour incubation in PBS, and (C) after 30 minute incubation in water with inset showing a high magnification peptoid microsphere.

3.3.6 Effect of Temperature on Coating Robustness

The effect of temperature on the 12mer peptoid microsphere coating robustness was assessed by visually analyzing the coating morphology following incubation in PBS and nanopure water at a physiological temperature of 37 °C for 30 minutes (Figure 3.7). At this

temperature, the peptoid microsphere coatings withstood degradation in all solutions except water. In PBS at 37 °C a small salt layer began forming due to the evaporation and deposition of PBS salts on the glass substrate, but the overall sphere morphology was maintained. After 30 minutes of incubating in water at 37°C, the microspheres began swelling and lifting from the surface and overall surface coverage was diminished.
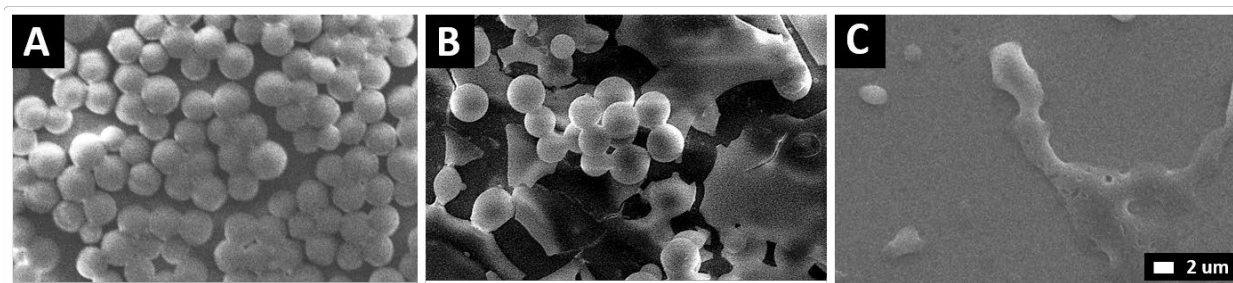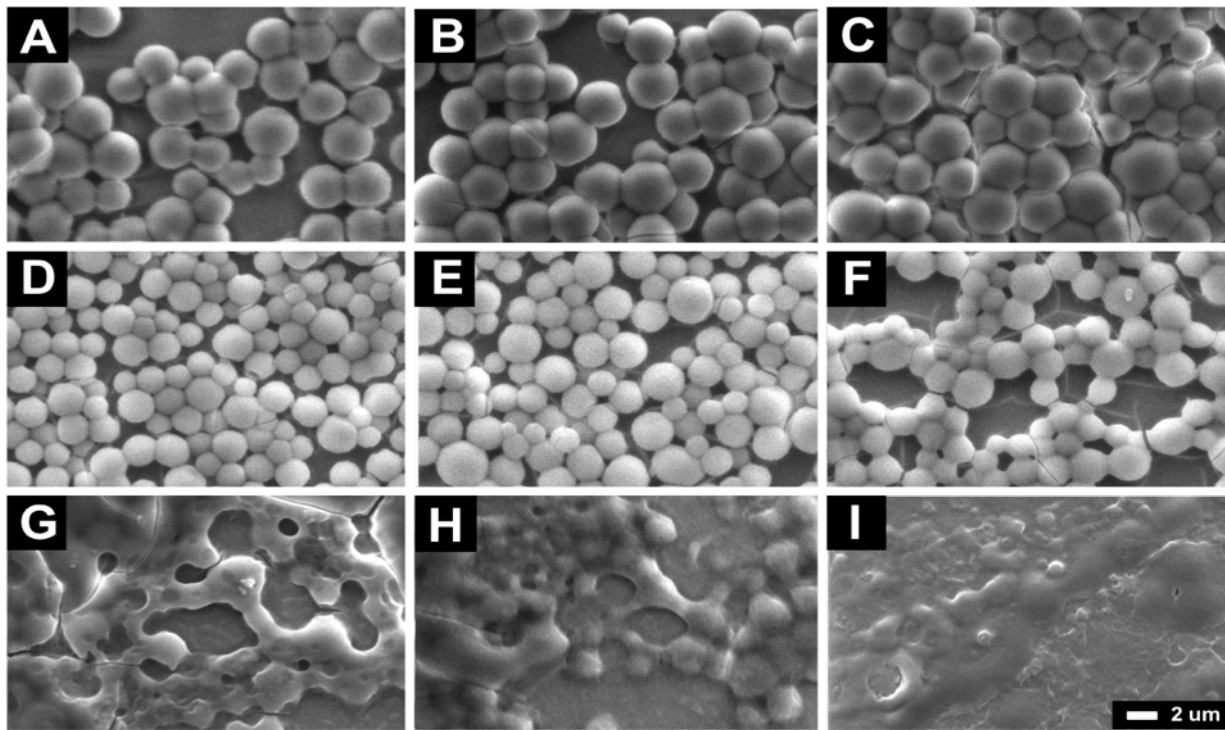

Figure 3.7 SEM images of 12mer peptoid microsphere coatings (A) before incubation (B) after 30 minute incubation in PBS at 37 °C, and (C) after 30 minute incubation in nanopore water at 37 °C.

3.3.7   Effect of pH on Coating Robustness

The effect of solvent pH on the 12mer peptoid microsphere coating robustness was studied by assessment of coating morphology and coverage following incubation in PBS (Figure 3.8) with varying pH. Coatings exposed to solutions with pH of 7 or greater are robust, with no significant differences in microsphere morphology or coating coverage (Figures 3.8A-8E). As the solvent starts to approach acidic conditions (pH less than 7), the microsphere morphology and coating coverage deteriorate (Figures 3.8F-8I). These observations are consistent in both PBS and water solutions at similar pH values. These studies were confirmed with water-based solutions (Figure S3.4 in Supplemental Information). While we do not anticipate changes in pH of the solvent to change the charge state of the peptoids, solubility is increased under acidic conditions. [50] Peptoids with ionizable side chains have been demonstrated to destabilize in

response to pH-dependent changes in aqueous solvents. [11, 51] In aqueous solvents, the supramolecular structure of the peptoid is ultimately determined by interactions between the side chains and water. In general, polar and charged groups are located on the outside surface due to their stabilization with water, while the hydrophobic residues tend to favor the inside of the structure. [52] The charged and polar residues, specifically lysine in the case of the peptoids studied here, help maintain the solvation necessary to form specific supramolecular structures. Therefore, at higher pH values the pKa of the lysine-like side chain is stabilized by being unprotonated or neutrally charged, maintaining an optimal solvation effect allowing the peptoid microspheres to be robust or less soluble under basic conditions.[53] At low pH (>7) the lysine side chains are below the isoelectric point resulting in a protonated amine group. The protonation forms an energetically less favorable charge solvation structure that results in the destabilization and increased solubility ultimately leading to the deterioration of the peptoid microspheres. [54]

Figure 3.8 SEM images of 12mer peptoid microsphere morphology after 30 minutes in PBS with pH values of (A) 11, (B) 10, (C) 9, (D) 8, (E) 7, (F) 6, (G) 5, (H) 4, or (I) 3.

3.3.8 Effect of Ionic Strength on Coating Robustness

The effect of ionic strength on 12mer peptoid microsphere coating robustness was visually assessed by SEM following incubation in various ionic strength solutions (0-500 mM) at pH 6.7 (Figure 3.9). SEM images demonstrate there is no considerable effect on microsphere morphology at ionic strengths greater than 150 mM (Figures 3.9A-9C). For ionic strength less than 150 mM, microsphere morphology and coverage showed signs of degradation (Figures 3.9D-9F). Specifically, the microspheres appear to fuse together and detach from the surface at ionic strengths less than 100 mM.
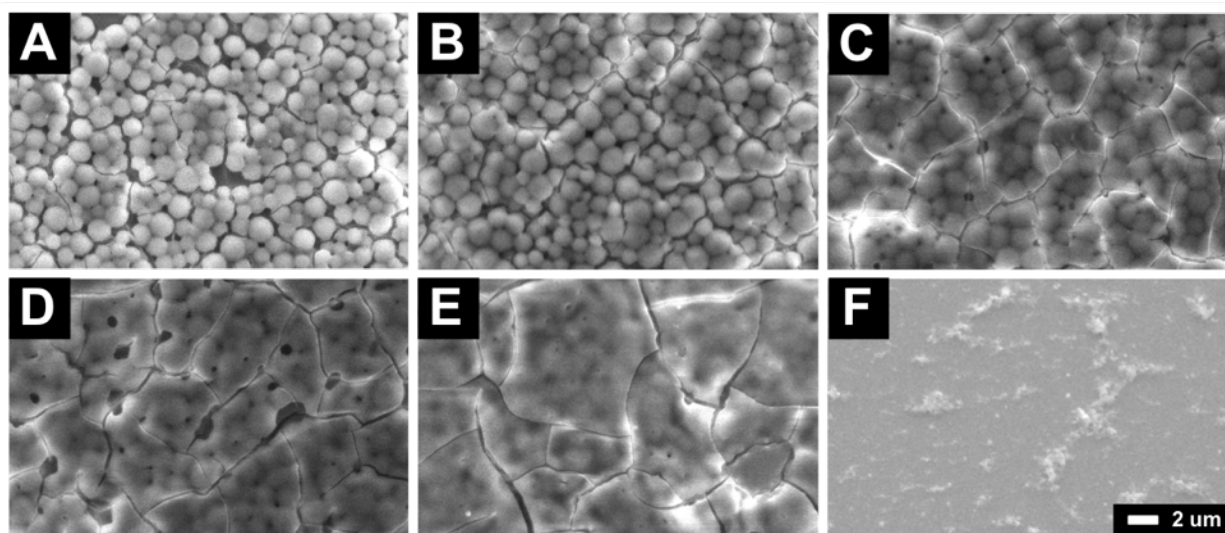
Figure 3.9 SEM images demonstrating the effect of ionic strength on sphere morphology after 30 minutes incubation in water solutions with ionic strengths of (A) 500 mM, (B) 250 mM, (C) 150 mM, (D) 100 mM, (E) 50 mM, and (F) 0 mM.

As compared to peptide helices, peptoid helices are much more stable when under harsh conditions. As a result, helical peptoids have been demonstrated to be less susceptible to degradation when exposed to various solvent environments (e.g. 2,2,2-trifluorethanol, methanol, and concentrated urea) and high temperatures. [18] However, increasing the ionic strength of the solvent has been demonstrated to stabilize secondary structure for a variety of ionic polypeptides due to screening the electrostatic repulsion between side chains. [55, 56, 57] Strongly charged helical peptides are completely destabilized in low ionic strength environments. [58] A similar dependence has been observed in high-ionic strength solutions for peptoids. [18, 51] It is hypothesized that the screening of charge-charge repulsive interactions at higher ionic strengths preserves the helical secondary structure that is crucial for microsphere formation. The Hofmeister series claims that based on the presence of specific ionic compounds there can be a salting "in" or "out" effect that changes the hydrophobicity of the solvent composition, ultimately changing the macromolecules' optical activity and secondary structure. [59, 60, 61]

3.4 Conclusion

In this study we have shown for the first time that peptoid relative helicity affects the size of microspheres formed, the relative charge location on the microspheres, as well as evaluated the effects of temperature, pH, and ionic strength on the robustness of microsphere coatings. Peptoid microsphere size can be tuned by varying relative helicity, or peptoid chain length (increased length leads to increased helicity). Increased relative helicity leads to smaller peptoid microspheres due to the tight helical secondary structures. Conversely, peptoids with looser helical structures form larger microspheres. The chain length, related to size, also effects the surface charge, as increased chain length had a higher surface zeta potential than the shorter chains. The phase transition temperature for the microsphere coatings increased as the peptoid chain length increased, pointing towards a stability conundrum between helicity and degradative resistance. Future studies will be performed to determine the overall number of peptoid molecules per microsphere, or packing density, using Small Angle X-ray Scattering and Small Angle Neutron Scattering. These current studies have proven that the peptoid microsphere coatings are robust at physiological conditions, as well as high pH and ionic strength solutions. However, under acidic conditions or at low ionic strengths the coatings deteriorate. The ability to tune peptoid microsphere size, as well as stability at physiological conditions, make peptoid coatings promising for use in biosensors and other biomedical applications.

3.5 Acknowledgments

3.6 References

[1] T. S. Burkoth, E. Beausoleil, S. Kaur, D. Tang, F. E. Cohen and R. N. Zuckermann, "Toward The Synthesis of Artificial Proteins," *Chemistry & Biology,* vol. 9, no. 5, p. 647–654, 2002.

[2] J. A. Patch and A. E. Barron, "Mimicry Of Bioactive Peptides via Non-Natural, Sequence-Specific Peptidomimetic Oligomers," *Current Opinion in Chemical Biology,* vol. 6, no. 6, p. 872–877, 2002.

[3] R. J. Simon, R. S. Kania, R. N. Zuckermann, V. D. Huebner, D. A. Jewell, S. Banville, S. Ng, L. Wang, S. Rosenberg and C. K. Marlowe, "Peptoids: a Modular Approach to Drug Discovery," *Proceedings of the National Academy of Sciences,* vol. 89, no. 20, p. 9367–9371 , 1992 .

[4] M. Hagihara, N. J. Anthony, T. J. Stout, J. Clardy and S. L. V. Schreiber, "Polypeptides: an Alternative Peptide Backbone," *Journal of the American Chemical Society,* vol. 114, no. 16, p. 6568–6570, 1992.

[5] K. Burgess, H. Shin and D. S. Linthicum, "Solid-Phase Syntheses Of Unnatural Biopolymers Containing Repeating Urea Units," *Angewandte Chemie International Edition in English Angew,* vol. 34, no. 8, pp. 907-909, 1995.

[6] A. B. Smith, D. A. Favor, P. A. Sprengeler, M. C. Guzman, P. J. Carroll, G. T. Furst and R. Hirschmann, "Molecular Modeling, Synthesis, and Structures of N-Methylated 3,5-Linked Pyrrolin-4-Ones toward the Creation of a Privileged Nonpeptide Scaffold," *Bioorganic & Medicinal Chemistry,* vol. 7, no. 1, pp. 9-22, 1999.

[7] D. H. Appella, L. A. Christianson, I. L. Karle, D. R. Powell and S. H. Gellman, "β-Peptide Foldamers: Robust Helix Formation In a New Family of β-Amino Acid Oligomers," *Journal of the American Chemical Society,* vol. 118, no. 51, p. 13071–13072, 1996.

[8] S. Hanessian, X. Luo and R. Schaum, "Synthesis And Folding Preferences of γ-Amino Acid Oligopeptides: Stereochemical Control in the Formation of a Reverse Turn and a Helix," *Tetrahedron Letters,* vol. 40, no. 27, p. 4925–4929, 1999.

[9] C. W. Wu, T. J. Sanborn, R. N. Zuckermann and A. E. Barron, "Peptoid Oligomers With α-Chiral, Aromatic Side Chains: Effects of Chain Length on Secondary Structure," *Journal of the American Chemical Society,* vol. 123, no. 13, p. 2958–2963, 2001.

[10] S. H. Gellman, "Foldamers: A Manifesto," *Accounts of Chemical Research,* vol. 31, no. 4, p. 173–180, 1998.

[11] J. R. Stringer, J. A. Crapster, I. A. Guzei and B. H. E., "Construction of Peptoids with All Trans-Amide Backbones and Peptoid Reverse Turns via the Tactical Incorporation of N-Aryl Side Chains Capable of Hydrogen Bonding," *J. Org. Chem.,* vol. 75, p. 6068–6078, 2010.

[12] S. B. Shin, B. Yoo, L. J. Todaro and K. Kirshenbaum, "Cyclic Peptoids," *J. Am. Chem. Soc.,* vol. 129, p. 3218–3225, 2007.

[13] K. Huang, C. W. Wu, T. J. Sanborn, J. A. Patch, K. Kirshenbaum, R. N. Zuckermann, A. E. Barron and I. Radhakrishnan, "A Threaded Loop Conformation Adopted by a Family of Peptoid Nonamers," *J. Am. Chem. Soc.,* vol. 128, p. 1733–1738, 2006.

[14] P. Armand, K. Kirshenbaum, A. Falicov, R. L. Dunbrack Jr, K. A. Dill, R. N. Zuckermann and F. E. Cohen, "Chiral N-Substituted Glycines Can Form Stable Helical Conformations," *Fold. Des. ,* vol. 2, p. 369–375, 1997.

[15] K. Kirshenbaum, A. E. Barron, R. A. Goldsmith, P. Armand, E. K. Bradley, K. T. V. Truong, K. A. Dill, F. E. Cohen and R. N. Zuckermann, "Sequence-Specific Polypeptoids: A Diverse Family of Heteropolymers with Stable Secondary Structure," *Proceedings of the National Academy of Sciences ,* vol. 95, no. 8, p. 4303–4308, 1998.

[16] P. Armand, K. Kirshenbaum, R. A. Goldsmith, S. Farr-Jones, A. E. Barron, K. T. V. Truong, K. A. Dill, D. F. Mierke, F. E. Cohen, R. N. Zuckermann and E. K. Bradley, "NMR Determination of the Major Solution Conformation of a Peptoid Pentamer with Chiral Side Chains," *Proceedings of the National Academy of Sciences,* vol. 95, no. 8, p. 4309–4314, 1998.

[17] C. W. Wu, T. J. Sanborn, K. Huang, R. N. Zuckermann and A. E. Barron, "Peptoid Oligomers With α-Chiral, Aromatic Side Chains: Sequence Requirements for the Formation of Stable Peptoid Helices," *J. Am. Chem. Soc.,* vol. 123, no. 28, p. 6778–6784, 2001.

[18] T. J. Sanborn, C. W. Wu, R. N. Zuckermann and A. E. Barron, "Extreme Stability of Helices Formed by Water-Soluble Poly-N-Substituted Glycines (Polypeptoids) with α - Chiral Side Chains," *Biopolymers,* vol. 63, no. 1, pp. 12-20, 2001.

[19] H. Murnen, A. Rosales, J. Jaworski, R. Segalman and R. Zuckermann, "Hierarchical self-assembly of a biomimetic diblock copolypeptoid into homochiral superhelices," *J. Am. Chem. Soc.,* vol. 132, p. 16112–16119, 2010.

[20] J. Nam, J. Johnson and J. A. S. Lannutti, "Modulation Of Embryonic Mesenchymal Progenitor Cell Differentiation Via Control Over Pure Mechanical Modulus In Electrospun Nanofibers," *Acta Biomater.,* vol. 7, p. 1516–1524, 2001.

[21] X. Chen, K. Ding and N. Ayres, "Investigation Into Fiber Formation In N-Alkyl Urea Peptoid Oligomers And The Synthesis Of A Water-Soluble PEG/N-Alkyl Urea Peptoid Oligomer Conjugate," *Polym. Chem. ,* vol. 2, p. 2635–2642, 2011.

[22] B. Sanii, R. Kudirka, A. Cho, N. Venkateswaran, G. K. Olivier, A. M. Olson, H. Tran, R. M. Harada, L. Tan and R. N. Zuckermann, "Shaken, Not Stirred: Collapsing a Peptoid Monolayer To Produce Free-Floating, Stable Nanosheets," *Journal of the American Chemical Society,* vol. 133, no. 51, p. 20808–20815, 2011.

[23] E. Robertson, A. P. C. Battigelli, R. Mannige, T. Haxton, L. Yun, S. Whitelam and R. Zuckermann, "Design, Synthesis, Assembly, and Engineering of Peptoid Nanosheets," *Acc. Chem. Res.,* vol. 49, no. 3, p. 379–389, 2016.

[24] M. L. Hebert, D. S. Shah, P. Blake, J. P. Turner and S. L. Servoss, "Tunable Peptoid Microspheres: Effects of Side Chain Chemistry and Sequence," *Organic & Biomolecular Chemistry,* vol. 11, no. 27, p. 4459, 2013.

[25] R. N. Zuckermann, J. M. Kerr, S. B. H. Kent and W. H. Moos, "Efficient Method for the Preparation of Peptoids [Oligo(N-Substituted Glycines)] by Submonomer Solid-Phase Synthesis," *J. Am. Chem. Soc.,* vol. 114, no. 26, p. 10646–10647, 1992.

[26] K. T. Nam, S. A. Shelby, P. H. Choi, A. B. Marciel, R. Chen, L. Tan, T. K. Chu, R. A. Mesch, B.-C. Lee, M. D. Connolly, C. Kisielowski and R. N. Zuckermann, "Free-Floating Ultrathin Two-Dimensional Crystals from Sequence-Specific Peptoid Polymers," *Nature Materials,* vol. 9, no. 5, p. 454–460, 2010.

[27] M. L. Waters, "Aromatic Interactions in Model Systems," *Current Opinion in Chemical Biology,* vol. 6, no. 6, p. 736–741, 2002.

[28] A. S. Shetty, J. Zhang and J. S. Moore, "Aromatic π-Stacking In Solution as Revealed through the Aggregation of Phenylacetylene Macrocycles," *Journal of the American Chemical Society,* vol. 118, no. 5, p. 1019–1027, 1996.

[29] C. G. Claessens and J. F. Stoddart, "Interactions In Self-Assembly," *Journal of Physical Organic Chemistry,* vol. 10, no. 5, p. 254–272, 1997.

[30] M. Hebert, D. Shah, P. Blake and S. Servoss, "Uniform And Robust Peptoid Microsphere Coatings," *Coatings,* vol. 3, no. 2, p. 98–107, 2013.

[31] N. Mahmoudi, L. Reed, A. Moix, N. Alshammari, J. Hestekin and S. L. Servoss, "PEG-mimetic peptoid reduces protein fouling of polysulfone hollow fibers," *Colloids and Surfaces B: Biointerfaces,* vol. 149, pp. 23-29, 2017.

[32] J. A. Patch, K. Kirshenbaum, S. L. Seurynck, R. N. Zuckermann and A. E. Barron, "Versatile Oligo(N-Substituted) Glycines: The Many Roles Of Peptoids in Drug Discovery," *Pseudo-Peptides in Drug Development,* p. 1–31, 2005.

[33] I. Gokce, R. W. Woody, G. Anderluh and J. H. Lakey, "Single Peptide Bonds Exhibit Poly(Pro)II ("Random Coil") Circular Dichroism Spectra," *Journal of American Chemical Society,* vol. 127, no. 27, pp. 9700-9701, 2005.

[34] Y. Wei, A. Thyparambil and R. Latour, "Protein Helical Structure Determination Using CD Spectroscopy for Solutions with Strong Background Absorbance from 190-230 nm," *Biochim Biophys Acta,* vol. 1844, no. 12, p. 2331–2337, 2014.

[35] S. Mukherjee, G. Zhou, C. Michel and V. A. Voelz, "Insights into Peptoid Helix Folding Cooperativity from an Improved Backbone Potential," *The Journal of Physical Chemistry,* vol. 119, no. 50, pp. 15407-15417, 2015.

[36] L. J. Weiser and E. E. Santiso, "Molecular modeling studies of peptoid polymers," *AIMS Materials Science,* vol. 4, no. 5, pp. 1029-1051, 2017.

[37] M. R. Dreher, A. J. Simnick, K. Fischer, R. J. Smith, A. Patel, M. Schmidt and A. Chilkoti, "Temperature Triggered Self-Assembly of Polypeptides into Multivalent Spherical Micelles," *Journal of The American Chemical Society,* vol. 130, no. 2, pp. 687-694, 2008.

[38] T. Shimada, S. Lee, F. S. Bates, A. Hotta and M. Tirrell, "Wormlike Micelle Formation in Peptide-Lipid Conjugates Driven by Secondary Structure Transformation of the Headgroups†," *The Journal of Physical Chemistry,* vol. 113, no. 42, pp. 13711-13714, 2009.

[39] K. Kornmueller, B. Lehofer, G. Leitinger, H. Amenitsch and R. Prassl, "Peptide self-assembly into lamellar phases and the formation of lipid-peptide nanostructures," *Nano Research,* vol. 11, no. 2, pp. 913-928, 2018.

[40] S. Gudlur, P. Sukhankar, J. Gao, L. A. Avila, Y. Hiromasa, J. Che, T. Iwamoto and J. M. Tomish, "Peptide Nanovesicles Formed by the Self-Assembly of Branched Amphiphilic Peptides," *PLoS ONE,* vol. 7, no. 9, 2012.

[41] S. Vauthey, S. Santoso, H. Gong, N. Watson and S. Zhang, "Molecular self-assembly of surfactant-like peptides to form nanotubes and nanovesicles," *Proceedings of the National Academy of Sciences of the United States of America,* vol. 99, no. 8, pp. 5355-5360, 2002.

[42] J. D. Hartgerink, E. Beniash and S. I. Stupp, "Self-Assembly and Mineralization of Peptide-Amphiphile Nanofibers," *Science,* vol. 294, no. 5547, pp. 1684-1688, 2001.

[43] J. D. Hartgerink, J. R. Granja, R. A. Milligan and M. R. Ghadiri, "Self-assembling Peptide Nanotubes," *Journal of The American Chemical Society,* vol. 118, no. 1, pp. 43-50, 1996.

[44] L. Adier-Abramovich, P. Marco, Z. A. Arnon, R. C. Creasey, T. C. Michaels, A. Levin, D. J. Scurr, C. J. Roberts, T. P. Knowles, S. J. Tendler and E. Gazit, "Controlling the Physical Dimensions of Peptide Nanotubes by Supramolecular Polymer Coassembly," *ACS NANO,* vol. 10, no. 8, pp. 7436-7442, 2016.

[45] Y.-H. Chiao, A. Sengupta, S.-T. Chen, S.-H. Huang, C.-C. Hu, W.-S. Hung, Y. Chang, X. Qian, S. Wickramasinghe, K.-R. Lee and J.-Y. Lai, "Zwitterion augmented polyamide membrane for improved forward osmosis performance with significant antifouling characteristics," *Separation and Purification Technology,* vol. 212, pp. 316-325, 2019.

[46] M. H. Chiu and E. J. Prenner, "Differential scanning calorimetry: An invaluable tool for a detailed thermodynamic characterization of macromolecules and their interactions," *Journal of Pharmacy BioAllied Sciences,* vol. 3, no. 1, pp. 39-59, 2011.

[47] D. Giron, "Applications of Thermal Analysis and Coupled Techniques in Pharmaceutical Industry," *Journal of Thermal Analysis and Calorimetry,* vol. 68, no. 2, pp. 335-357, 2002.

[48] B. Sauer, W. Kampert, E. N. Blanchard, S. Threefoot and B. Hsiao, "Temperature modulated DSC studies of melting and recrystallization in polymers exhibiting multiple endotherms," *Polymer,* vol. 41, no. 3, pp. 1099-1108, 2000.

[49] V. Maravajhala, N. Dasari, A. Sepuri and S. Joginapalli, "Design and Evaluation of Niacin Microspheres," *Indian Journal of Pharmaceutical Sciences,* vol. 71, no. 6, pp. 663-669, 2009.

[50] L. Malavolta, M. R. Pinto, J. H. Cuvero and C. R. Nakaie, "Interpretation of the dissolution of insoluble peptide sequences based on the acid-base properties of the solvent," *Protein Science,* vol. 15, no. 6, pp. 1476-1488, 2006.

[51] S. Shin and K. Kirshenbaum, "Conformational Rearrangements by Water-Soluble Peptoid Foldamers," *Organic Letters,* vol. 9, no. 24, pp. 5003-5006, 2007.

[52] J. Kim, J. Mao and M. Gunner, "https://www.sciencedirect.com/science/article/pii/S0022283605003311," *Journal of Molecular Biology,* vol. 348, pp. 1283-1298, 2005.

[53] D. Bashford, "Macroscopic Electrostatic Models For Protonation States in Proteins," *Frontiers in Bioscience,* vol. 9, pp. 1082-1999, 2004.

[54] J. Dwyer, A. Gittis, D. Karp, E. Lattman, D. Spencer, Stites, W.E. and B. Garcia-Moreno, "High apparent dielectric constants in the interior of a protein reflect water penetration.," *Biophysical Journal,* vol. 79, no. 3, pp. 1610-1620, 2000.

[55] M. van der Graaf and M. Hemminga, "Conformational Studies on a Peptide Fragment Representing the RNA-Binding N-terminus of a Viral Coat Protein Using Circular Dichroism and NMR Spectroscopy," *The FEBS Journal,* vol. 201, no. 2, pp. 489-494, 1991.

[56] W. Kohn, C. Kay and R. Hodges, "Protein Destabilization by Electrostatic Repulsions in the Two-Stranded α-Helical Coiled-Coil/Leucine Zipper," *Protein Sci ,* vol. 4, p. 237–250., 1995.

[57] I. Jelesarov, E. Durr, R. Thoma and H. Bosshard, "Salt Effects on Hydrophobic Interaction and Charge Screening in the Folding of a Negatively Charged Peptide to a Coiled Coil (Leucine Zipper)," *Biochemistry,* vol. 37, p. 7539 –7550, 1998.

[58] M. Hoshino, N. Yumoto, S. Yoshikawa and Y. Goto, "Design And Characterization f the Anion-Sensitive Coiled-Coil Peptide.," *Protein Sci.,* vol. 6, no. 7, p. 1396–1404, 1997.

[59] H. I. Okur, J. Hladilkova, Rembert, K. B., Y. Cho, J. Heyda, J. Dzubiella, P. S. Cremer and P. Jungwirth, "Beyond the Hofmeister Series: Ion-Specific Effects on Proteins and Their Biological Functions," *The Journal of Physical Chemistry,* vol. 121, no. 9, pp. 1997-2014, 2017.

[60] A. H. Crevenna, N. Naredi-Rainer, D. C. Lamb, R. Wedlich-soldner and J. Dzubiella, "Effects of Hofmeister Ions on the α-Helical Structure of Proteins," *Biophysical Journal,* vol. 102, no. 4, pp. 907-915, 2012.

[61] Y. Zhang and P. S. Cremer, "Interactions between macromolecules and ions: The Hofmeister series.," *Current Opinion in Chemical Biology,* vol. 10, no. 6, pp. 658-663, 2006.

4. Peptoid Microsphere Coatings to Improve Performance in Sandwich ELISA Microarrays

Jesse L. Roberts,[1] German R. Perez Bakovic,[1] and Shannon L. Servoss[1, *]

[1] University of Arkansas, Ralph E. Martin Department of Chemical Engineering, 3202 Bell Engineering Center, 1 University of Arkansas, Fayetteville, AR 72701

*Corresponding Author

Abstract

Enzyme-linked immunosorbent assay (ELISA) microarray performance is limited by low assay sensitivity and dynamic range. Increasing the surface area for reagent binding can help to improve performance, but standard techniques such as roughening the surface or adding a polymer coating lead to increased non-specific fluorescence and do not have reproducibly improved performance. Another approach to increase surface area is adding a microsphere coating on the surface. Poly-N-substituted glycine (peptoid) microspheres are ideal for this application due to low immunogenicity, protease-resistance, and biocompatibility. Peptoids are polymers with a backbone similar to peptides, but with the side chains appended to nitrogen rather than the alpha carbon. A variety of side chain chemistries can be incorporated into peptoids through a solid-phase, sequence-specific synthesis protocol. Here we report the development of sandwich ELISA microarray on peptoid microsphere coated glass slides. Coating morphology was evaluated via SEM and efficacy was assessed by ELISA microarray performance. Peptoid microsphere coated glass slides exhibit an increase in signal intensity and dynamic range as compared to commercially available microarray slides. These studies show the potential for peptoid microspheres as coatings for ELISA microarray slides, as well as for use in other biosensor applications.

Keywords

peptoid; ELISA; microarray; microspheres

Abbreviations

ELISA – enzyme-linked immunosorbent assay

DSS – Disuccinimidyl suberate

BS^3 – bis[sulfosuccinimidyl] suberate

PBS – phosphate-buffered saline

TSA – Tyramide Signal Amplification

DMF – dimethylformamide

TFA – trifluoroacetic acid

HPLC – high-performance liquid chromatography

MALDI-TOF – matrix assisted laser desorption/ionization time of flight mass spectrometry

SEM – scanning electron microscope

PBS-T – PBS containing 0.05% Tween-20

4.1　Introduction

Over the last several decades there have been numerous publications focused on the development of sensitive, disease-specific assays to assist in therapeutic decisions [76, 77, 78, 79, 80]. Early disease detection decreases economic costs, improves treatment options, and reduces mortality [6]. Biomarker-based technologies, including enzyme-linked immunosorbent assay (ELISA) microarray and bead-based immunoassay, offer platforms for sensitive and specific disease detection [7]. Multiplex bead array assays (MBAA) such as Luminex, xMap [8], Smartbead UltraPlex [9], and flow cytometry technologies [10] offer promising, high-throughput methods of detecting cytokines and other analytes in serum and plasma samples. MBAAs make it possible to perform immunoassays in a multiplexed design to independently and qualitatively analyze multiple samples at one time. For instance, the xMAP technique utilizes hundreds of uniquely colored beads, ranging from much larger magnetic beads (6.5 μm) to smaller non-magnetic beads (~1 μm), created by two different fluorescent dyes to simultaneously identify multiple analytes [8]. However, a key concern in the viability of MBAAs is the potential for interference between analyte samples. The antibodies on each bead may cross-react with other antibodies, cross-species antibodies, and molecules, ultimately reducing the efficacy of the MBAA techniques and requiring additional testing to ensure no cross-reacting has occurred [11].

ELISA microarray technology has emerged as a strong platform for the analysis of biomarkers due to its ability to quantify low-abundance proteins in complex biological fluids over large concentration ranges [12,2]. ELISA microarray eliminates the cross-reactivity that is commonly seen in MBAAs by focusing on a single analyte at a time. The use of matched high-affinity antibody pairs to target a single antigen results in unmatched sensitivity and specificity. The miniature scale of the platform allows for cost-effective and efficient parallel screening of

small sample volumes in a high-throughput manner [12]. The slide chemistry and morphology is crucial for optimal performance of ELISA microarray, as is evident by the large number of slide chemistries commercially available [13, 14, 15, 16, 17, 18, 4]. The slides must allow antibodies to be immobilized in a manner that maintains protein binding affinity while retaining high binding capacities, high signal-to-noise ratios, and high reproducibility [19]. Additionally, the high-throughput nature of the platform requires substrates to be robust and retain high levels of specificity and sensitivity through rigorous processing conditions and prolonged storage periods. While poly-L-lysine slides have emerged as promising slide chemistry due to strong antibody attachment via adsorption and high signal-to-noise ratio [20, 21], ELISA microarray performance can be further improved by increasing the surface area for antibody attachment. In theory, increasing the surface area for antibody attachment should enhance the microarray results by providing more sites of attachment to increase signal intensity and the dynamic range. Polymer-based surfaces that increase surface area such as polyacrylamide [5, 22], agarose [23], and nitrocellulose [24, 25, 26, 27, 28] suffer from low signal-to-noise ratios due to absorption of protein in the porous coating [20, 21].

Poly-*N*-substituted glycines (peptoids) are promising as coatings for microarray slides due to their low immunogenicity, ease of synthesis, variety of available side chain chemistries, and the ability to form supramolecular structures that can increase surface area [29]. Peptoids are bioinspired, peptidomimetic polymers with a backbone structure closely resembling that of peptides, but with the side chains appended to the amide groups rather than the alpha-carbons. This structural modification prevents proteolytic degradation, making peptoids attractive as biocompatible materials. However, this modification also removes the presence of backbone amide hydrogens, which are critical for the formation of the hydrogen bond linkages that

stabilize beta sheets and helices in peptides. Introduction of steric hindrance through side chain chemistry allows for the formation of secondary structures including turns [30, 31], loops [32], and helices [33, 34, 35, 36, 37], as well as supramolecular assemblies such as superhelices [38], nanosheets [39], nanotubes [40], and microspheres [41].

Our lab has previously shown that partially water-soluble, helical peptoids self-assemble into microspheres [37] and can form uniform surface coatings [44]. The peptoid sequence, referred to as P3 (Figure 4.1), includes chiral, aromatic side chains on two faces of the helix to induce the formation of helical secondary structure [41]. The third face of the helix, which offers considerable flexibility of design, contains methoxy and amine groups to increase water solubility. The amine groups enable covalent linkage to and electrostatic interactions with the slide surface. The secondary structure of P3 was determined by circular dichroism, which confirms polyproline type-I-like secondary structure [35].
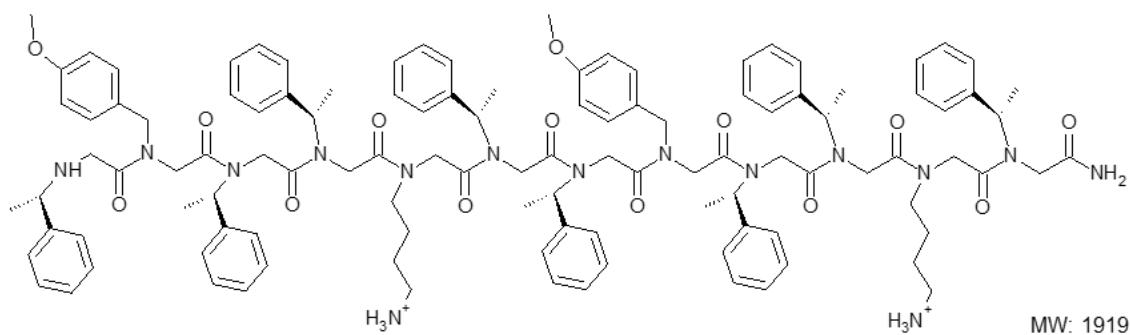
Figure 4.1 Peptoid structure for the P3 sequence.

In this study, we report the development of peptoid microsphere coated glass substrates for use in sandwich ELISA microarray. The morphology and uniformity of the coatings was evaluated by SEM and the coating efficacy was analyzed by ELISA microarray with known antibody pairs. The peptoid microsphere coated surfaces were found to exhibit higher signal intensity and dynamic range as compared to commercially available microarray slides.

4.2 Materials and Methods

4.2.1 Materials

4-methoxybenzylamine and (S)-methylbenzylamine were purchased from Acros Organics (Pittsburgh, PA). *tert*-butyl N-(4-aminobutyl) carbamate was purchased from CNH Technologies Inc. (Woburn, MA). MBHA rink amide resin was purchased from NovaBiochem (Gibbstown, NJ). Piperidine was purchased from Sigma-Aldrich (St. Louis, MO). Test grade silicon wafers were purchased from University Wafer (South Boston, MA). Poly-L-lysine and ultra clean glass microarray slides were purchased from Thermo Scientific (Pittsburgh, PA). Disuccinimidyl suberate (DSS) and bis[sulfosuccinimidyl] suberate (BS^3) were purchased from Pierce (Rockford, IL, USA). Purified antibodies and antigens were purchased from R&D Systems (Minneapolis, MN, USA). Blocking solution containing 10 mg/ml casein in phosphate-buffered saline, pH 7.2 (PBS) was purchased from Bio Rad Laboratories (Hercules, CA, USA). Tyramide Signal Amplification (TSA) system, including streptavidin-conjugated horseradish peroxidase, amplification diluent, and biotinyl tyramide, was purchased from Perkin Elmer (Wellesley, MA, USA). Alexa647-conjugated streptavidin was purchased from Invitrogen Life Technologies (Gaithersburg, MD). All other reagents were purchased from VWR (Radnor, PA). Chemicals were used without further modifications unless otherwise specified.

4.2.2 Peptoid Synthesis

Peptoids were synthesized via the submonomer solid-phase method on rink amide resin, as previously described [42]. Briefly, the resin was swelled with dimethylformamide (DMF) and the Fmoc protecting group was removed using a 20% solution of piperidine in DMF. The resin-bound secondary amine was acylated with 0.4

M bromoacetic acid in DMF in the presence of N,N'-diisopropyl carbodiimide. Amine submonomers were incorporated via an S_N2 nucleophilic substitution reaction with primary amine in DMF. The two-step bromoacetylation and nucleophilic substitution cycle was repeated until all desired side chains were incorporated. The peptoid was cleaved from the resin using a mixture of 95% trifluoroacetic acid (TFA), 2.5% water, and 2.5% triisopropylsilane, and the acid was removed using a Heidolph Laborota 4001 rotary evaporator (Elk Grove Village, IL). The peptoid was lyophilized to a powder using a Labconco lyophilizer (Kansas City, MO) and diluted to a concentration of ~3 mg/ml in a 50:50 acetonitrile-water solution.

4.2.3   Peptoid Purification

Peptoids were purified using a Waters Delta 600 preparative high-performance liquid chromatography (HPLC) instrument (Milford, MA) with a Duragel G C18 150 × 20 mm column (Peeke Scientific, Novato, CA) and a linear gradient of 35-95% solvent B (acetonitrile, 5% water, 0.1% TFA) in A (water, 5% acetonitrile, 0.1% TFA) over 60 minutes. Peptoids were confirmed to be >98% pure via analytical HPLC (Waters Alliance, Milford, MA) with a Duragel G C18 150 × 2.1 mm column (Peeke Scientific) using a linear gradient of 35 to 95% solvent D (acetonitrile, 0.1% TFA) in C (water, 0.1% TFA) over 30 minutes. Purified peptoid fractions were lyophilized and stored as a powder at -20 °C.

4.2.4   Peptoid Characterization

Synthesis of the desired peptoid sequence was confirmed via matrix assisted laser desorption/ionization time of flight mass spectrometry (MALDI-TOF; Bruker, Billerica, MA). Secondary structure was confirmed via CD spectrometry using a Jasco J-715 instrument (Easton, MD) at room temperature with a scanning speed of 20 nm/min and a

path length of 0.1 mm. The peptoid was dissolved in methanol at a concentration of 120 µM. Each spectrum was the average of twenty accumulations.

4.2.5   Peptoid Microsphere Coatings

Peptoid microspheres were prepared by dissolving the peptoid in a 4:1 (v/v) ethanol/water solution at a concentration of 5 mg/ml, as previously described [41]. Glass slides (Erie Scientific, Portsmouth, NH) were outlined with an 8 x 2 array pattern using a Barnstead Thermolyne microarray slide imprinter (Dubuque, IA) to create a hydrophobic barrier for processing 16 wells per slide. The peptoid solution was applied to the glass surfaces and allowed to dry at room temperature and 60% relative humidity. Coating morphologies were visually assessed using a Phillips XL-30 scanning electron microscope (SEM; FEI, Hillsboro, OR).

4.2.6   Microsphere Surface Density Distribution

Microsphere surface density distribution of the microsphere coatings was calculated using ImageJ software (National Institute of Health, MD). Noise reduction was completed with a fast Fourier transform (FFT) band-pass filter normalization, eliminating low- and high-spatial frequencies and transforming the original SEM images to a two-dimensional representation of the frequency. The images were converted to 8-bit grayscale and binarized adjusting the white and black threshold to optimize particle contrast with the background. Particle analysis was completed on the adjusted images to give an area percentage for the microsphere particles.

4.2.7   Microarray Printing

ELISA microarray printing was performed at room temperature and 60% relative humidity as previously described [20]. Briefly, a GeSiM NanoPlotter 2.1 non-contact microarray printer with humidity control (Quantum Analytics, Foster City, CA, USA)

was used to spot the antibodies. Prior to spotting, the microsphere coated surfaces, and in some cases the poly-L-lyisne slides, were treated with a 0.3 mg/ml solution of the homo-bifunctional cross-linker BS[3] in PBS for 20 minutes to create a reactive site for covalent attachment of antibodies via the amine groups. After incubation, the slides were rinsed in nanopure water and dried in a centrifuge. Capture antibodies were suspended in PBS to a concentration of 0.8 mg/ml and ~400 picoliters per spot were printed 500 μm apart in quintuplicate on each array. Upon completion, the antibodies were allowed to dry for an additional hour at 60% relative humidity. The slides were blocked with 10 mg/ml casein in PBS and processed immediately.

4.2.8 ELISA Microarray

ELISA microarray was performed as previously described [20]. Briefly, all incubation steps were performed at room temperature in a closed, dark, humid chamber, with gentle mixing on an orbital shaker (Belly Dancer, Stovall Life Science, Greensboro, NC). A two-step wash procedure between processing steps was performed by submerging the slides twice into PBS containing 0.05% Tween-20 (PBS-T). The slides were incubated with a mixture of antigen standards in 1 mg/ml casein in PBS overnight. Standard curves were created using a three-fold dilution series of the antigen mix along with an antigen-free blank for twelve total dilutions. Following a wash cycle, the slides were incubated with biotinylated detection antibody at 25 ng/ml in 1 mg/ml casein in PBS. The biotin signal was amplified using the TSA system following manufacturer instructions, and incubated with 1 μg/ml Alexa647-conjugated streptavidin in PBS-T. The slides were rinsed twice in PBS-T followed by deionized water.

A GenePix Autoloader 4200AL laser scanner (Molecular Devices, CA) was used to image the Alexa 647 fluorescence signal. The spot fluorescence intensity from the

scanned slide images was quantified using GenePix Pro 3.0 software. Standard curves were created using ProMAT, a software program specifically developed for the analysis of ELISA microarray data based on a four-parameter logistic curves model [43]. The values for the lower limits of detection are calculated as the median concentration of the antigen-free blank plus three standard deviations [45]. In order to provide a value that is representative of all assays for comparisons, a relative limit of detection value was calculated using the median value for all assay replicates on each surface, as previously described [20]. Unless noted otherwise, results shown encompass three replicate experiments performed using slides that were coated, printed, and processed on independent occasions.

4.3   Results and Discussion

### 4.3.1   Coating Characterization

The formation of uniform peptoid microsphere coatings is essential to reduce variability in ELISA microarray. Coating morphology is directly linked to evaporation rate, requiring careful monitoring of drying conditions to ensure uniform sphere distribution and reproducible coatings. One issue observed in the formation of peptoid coatings is perimetral intensive deposition, often referred to as the "coffee ring effect," in which denser coverage is observed at the perimeter of the coatings as compared to the center. Previous studies have shown that this effect is reduced when samples are evaporated at a constant contact area, which can be achieved by including surfactant in the microsphere solution [46]. The addition of Tween-20 to the peptoid microsphere solution results in improved coating uniformity, lessening perimetral microsphere deposition and allowing for an even distribution of microspheres on the surface (Figure 4.2). At concentrations >0.1%, Tween-20 disrupts microspheres formation and alters

microsphere size distribution (Figure S4.1 in Supplemental Information). Previous work

in our lab has focused on the reproducibility of the coatings, the physical properties of the

microspheres, and their ability to withstand various conditions (pH, ionic strength,

solvents) [36][47]. Using ImageJ particle analysis of SEM images, the average local

microsphere surface density (n=10) on the glass slides was 87% (s=2.59%) covered

(Figure S4.2 in Supplemental Information).
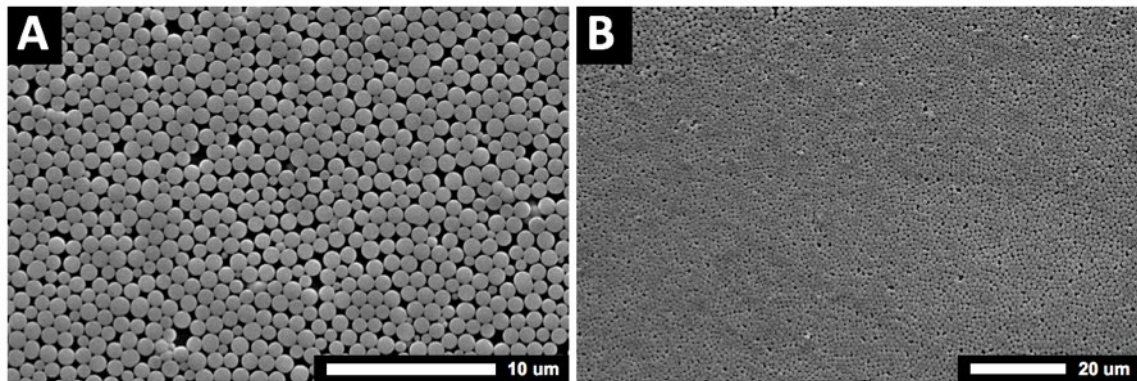
Figure 4.2 Peptoid microsphere coated glass surfaces at (A) 3500x and (B) 1000x
magnifications. Peptoids were dissolved in a 4:1 (v/v) ethanol/water solution at a
concentration of 5 mg/ml. The peptoid solution was applied to the glass surfaces and
allowed to dry at room temperature and 60% relative humidity.

When antibodies were spotted directly on the peptoid microsphere coated slides,

faint fluorescent signals were observed indicating weak adsorption of the antibodies to

the surface. The homobifunctional linker, BS^3, was used to covalently attach the

antibodies to the peptoid microsphere coated slides (Figure 4.3A). ELISA microarray

results were reproducible for the slides with covalently attached antibodies. It should be

noted that antibodies were not covalently attached to the poly-L-lysine surfaces because

both our results (Figure 4.3B) and findings by others [20] show no significant difference

in ELISA microarray performance between adsorbed and covalently attached antibodies.
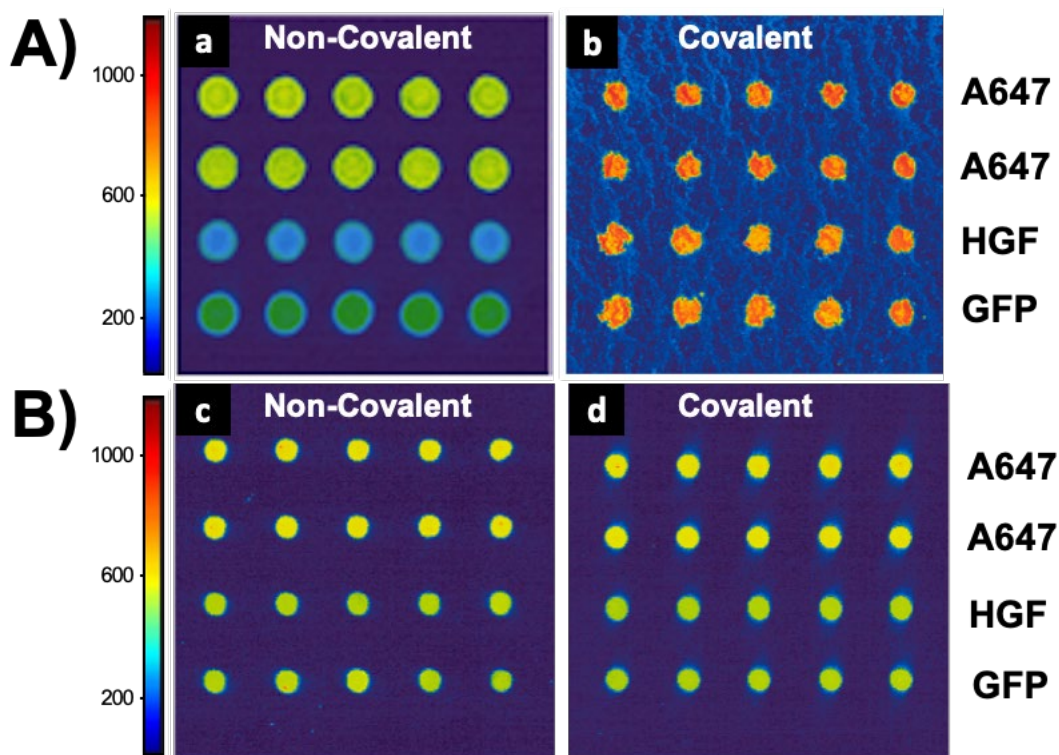
Figure 4.3 (A) Images of fluorescence for GFP and HGF on peptoid microsphere coated glass surfaces with (a) non-covalent treated and (b) BS^3 treated covalent surfaces. (B) Images of fluorescence for GFP and HGF on uncoated poly-L-lysine slides with (a) non-covalent treated and (b) BS^3 treated covalent slides.

4.3.2 Coating Efficacy for ELISA Microarray

The efficacy of the peptoid microsphere coatings was evaluated by ELISA microarray with four antibody assays (Table 4.1) that were previously shown to have good assay sensitivity and specificity, as well as low cross-reactivity, in multiplexed ELISA microarray [3]. The performance of the surfaces was evaluated based on spot morphology, signal to noise ratio, limit of detection, and standard curve dynamic range. Signal intensities were evaluated by comparing single concentration assays on peptoid microsphere coated blocks with poly-L-lysine surfaces. Single point antigen concentrations correspond to the third dilution of the three-fold standard curve dilution series (i.e., approximately 11% of the maximal concentration), which has previously been

shown to provide a strong signal intensity near saturation and in the upper usable range of the standard curve [3].

Table 4.1 Summary of the results detailing the maximal concentration of antigens, lower and upper bound, dynamic range concentrations, and single point signal intensities (11% of the maximal concentration) for the 'uncoated' poly-L-lysine surfaces and peptoid-based microsphere coated surfaces antigens for all 4 different assays: CD14 (cluster of differentiation 14), GFP (green fluorescent protein), HGF (hepatocyte growth factor), and RANTES (regulated on activation normal T cell expressed and secreted).

Assay	Max Conc. (pg/mL)	Limit of Detection (pg/mL)		Dynamic Range (pg/mL)		Signal/Noise Ratio	
		Uncoated	Coated	Uncoated	Coated	Uncoated	Coated
CD14	2500	1.9	2.0	527.8	530.2	21.4	21.3
GFP	500	0.2	0.7	80.0	97.0	17.8	30.5
HGF	1000	0.3	2.7	135.3	492.8	20.7	30.6
RANTES	500	0.4	0.3	64.6	264.2	15.8	16.8

Spot morphology is dependent on the characteristics of the surface, and as such the increased topographical complexity of peptoid microsphere coated surfaces presents challenges. Although the spot morphology on peptoid microspheres is not as crisp as those on the two-dimensional poly-L-lysine surfaces (Figure 4.3A), they are greatly improved over other three-dimensional surfaces [20]. The shape of the spots is still detected and analyzed by the GenePix software without any issues.

As expected, peptoid microsphere coated surfaces consistently displayed stronger signal intensities as compared to poly-L-lysine slides (Figure 4.3C and Table 4.1). This observation is consistent for all assays independent of whether the comparisons are based on a single concentration point (Figure 4.3C) or over the full standard curve (Figure 4.4). However, as is the case with other three-dimensional slide surfaces, the peptoid microsphere coated surface exhibits higher background fluorescence as compared to the

poly-L-lysine surface (Figure 4.3B). Despite the increased background signal, the signal-to-noise ratio for the peptoid microsphere coating is the same as or higher than the poly-L-lysine coating (Table 4.1). More specifically, the signal-to-noise ratio is higher on the peptoid microsphere coated slides for three of the four assays tested. These data support the hypothesis that the use of peptoid microsphere coatings to increase surface area leads to improved ELISA microarray properties.
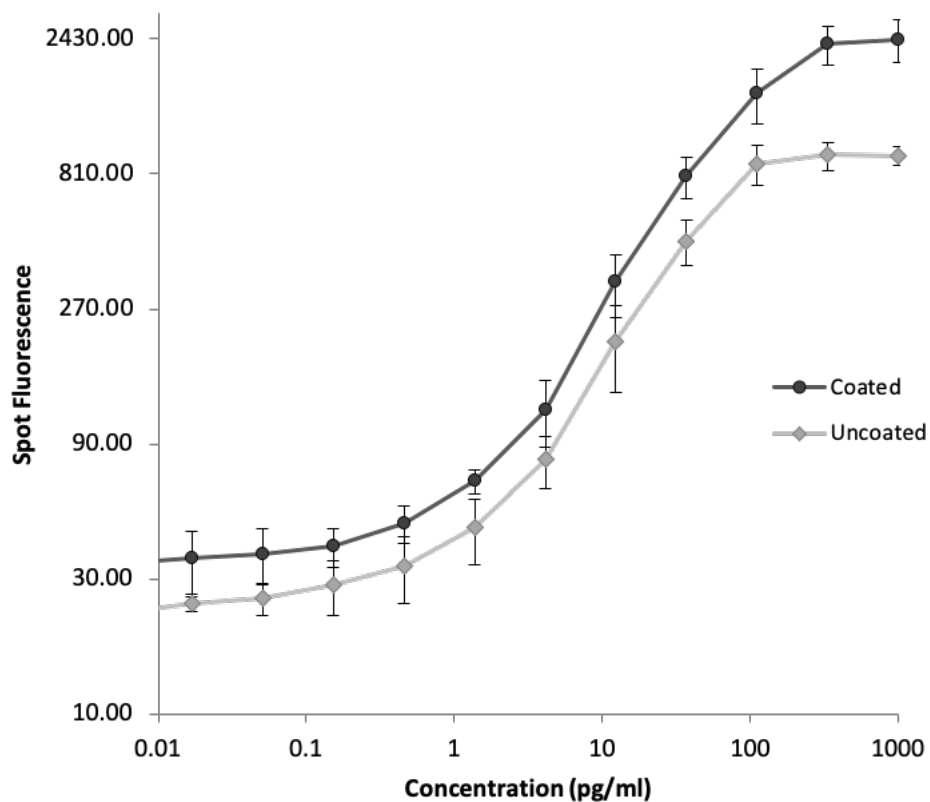
Figure 4.4 Standard curves for HGF on uncoated poly-L-lysine slides and peptoid microsphere coated surfaces. Results are representative of the trends observed across all antibody assays (see Figure S3 in Supplemental Information). Data points and cross-bars represent the means and standard deviations, respectively. The standard curves encompass data from all three replicate experiments performed using slides that were coated, printed, and processed on independent occasions.

The limit of detection is defined as the lowest concentration that can be reliably detected and is a direct assessment of assay sensitivity. Evaluation of surface

performance is based on previously published methods, where relative limit of detection below 2 is 'superior', between 2 and 4 is 'normal', and above 4 is 'poor' [20]. Despite the larger standard deviation observed at low antigen concentration for the peptoid microsphere coatings, they are rated in the superior category with a score of 0.9 ± 0.5 as compared to a score of 0.8 ± 0.3 for poly-L-lysine slides in our study. These values are comparable to published values for commercially available slides including poly-L-lysine (0.7 ± 0.1), aminosilane (1.3 ± 0.6), aldehyde silane (1.1 ± 0.4), epoxysilane (1.2 ± 0.6), Slide E (0.8 ± 0.4), and Full Moon (1 ± 0.7) [87].

ProMAT interprets the useful range of the standard curves as that between the lower limit of detection and upper concentration bound. As the standard curve for HGF in Figure 4 demonstrates, and Table 1 details for all assays, the dynamic range observed for the peptoid microsphere coated surfaces is increased as compared to poly-L-lysine surfaces (2.4 pg/ml for CD14, 17 pg/ml for GFP, 357.5 pg/ml for HGF, and 199.6 pg/ml for RANTES).

4.4 Conclusion

Disease detection requires high-throughput assessment of multiple proteins within small sample volumes. The use of ELISA microarray and biosensors for disease detection will require the development of optimized support surfaces that allow for more generally applicable and direct immobilization procedures. While high binding affinities are imperative to prevent antibody loss and ensure robust attachment, the challenge lies in designing a microarray support that accommodates proteins of varying characteristics and provides an environment that preserves the active form of the protein. The use of peptoid microsphere coatings as a novel surface for the improvement of sandwich ELISA microarray has been evaluated. This peptoid-based, three-dimensional coating offers a

customizable, robust, biocompatible interface that increases the surface area available for binding. The efficacy of the coating was assessed in terms of its overall ELISA microarray performance as compared to commercially available poly-L-lysine surfaces. The peptoid microsphere coated surfaces allowed for strong covalent antibody attachment and performed well in terms of spot morphology, signal to noise ratio, limit of detection, and standard curve dynamic range. The increase in surface area enables higher protein binding capacities as compared to poly-L-lysine surfaces, and although the peptoid microsphere coatings displayed higher background fluorescence and coefficients of variation the signal-to-noise ratios were higher as compared to poly-L-lysine surfaces. Furthermore, the limits of detection were comparable to the poly-L-lysine surfaces and an improvement in dynamic range was observed for all assays tested.

The peptoid microsphere coatings provide an exciting new interface for a wide range of biosensor applications. Results suggest that commonly used biosensor protocols and procedures can be readily applied to peptoid microsphere coatings, and that the coatings outperform state-of-the art surfaces such as poly-L-lysine. The robust peptoid microsphere coated surface provides a versatile platform that can be easily customizable to allow for various surface chemistries and incorporate different attachment sites. It offers the benefits that come with an increased surface area for binding, while at the same time allow for use of familiar chemistries that are established for both protein microarray and biosensor applications.

4.5   Acknowledgments

consultation regarding SEM, and Dr. Suresh Kumar for use of and consultation regarding

CD.

4.6 Funding

4.7 References

[1] Ullah, M. F.; Aatif, M. The Footprints of Cancer Development: Cancer Biomarkers. *Cancer Treatment Reviews* **2009**, 35 (3), 193–200.

[2] Etzioni, R.; Urban, N.; Ramsey, S.; Mcintosh, M.; Schwartz, S.; Reid, B.; Radich, J.; Anderson, G.; Hartwell, L. Early Detection: The Case for Early Detection. *Nature Reviews Cancer* **2003**, 3 (4), 243–252.

[3] Kiviat, N. B.; Critchlow, C. W. Novel Approaches To Identification of Biomarkers for Detection of Early Stage Cancer. *Disease Markers* **2002**, 18 (2), 73–81.

[4] Tainsky, M. A. Genomic And Proteomic Biomarkers for Cancer: A Multitude of Opportunities. *Biochimica et Biophysica Acta* **2009**, 1796 (2), 176–193.

[5] Rai, A. J.; Chan, D. W. Cancer Proteomics: New Developments In Clinical Chemistry. *Laboratoriums Medizin* **2001**, *25* (9-10), 399–403.

[6] DeRisi, J.; Penland, L.; Brown, P.O.; Bittner, M.L.; Meltzer, P.S.; Ray, M.; Chen, Y.; Su, Y.A; Trent, J.M. Use Of a CDNA Microarray to Analyse Gene Expression Patterns in Human Cancer. *Nature Genetics* **1996**, *14* (4), 457–460.

[7] Esteller, M.; Corn, P.G.; Baylin, S.B.; Herman, J.G. A Gene Hypermethylation Profile of Human Cancer, *Cancer Research* **2001**, 61(8), 3225–3229.

[8] B. Houser, "Bio-Rad's Bio-Plex® suspension array system, xMAP technology overview," *The Journal of Metabolic Diseases,* vol. 118, no. 4, pp. 192-196, 2012.

[9] J. Smith, D. Onley, C. Garey, S. Crowther, N. Cahir, A. Johanson, S. Painter, G. Harradence, R. Davis and P. Swarbrick, "Determination of ANA Specificity Using the UltraPlex™ Platform," *Annals of The New York Academy of Sciences,* vol. 1050, no. 1, 2006.

[10] A. Spiro, M. Lowe and D. Brown, "A Bead-Based Method for Multiplexed Identification and Quantitation of DNA Sequences Using Flow Cytometry," *Applied and Environmental Microbiology,* vol. 66, no. 10, pp. 4258-4265, 2000.

[11] M. F. Elshal and J. P. McCoy Jr., "Multiplex Bead Array Assays: Performance Evaluation and Comparison of Sensitivity to ELISA," *Methods,* vol. 38, no. 4, pp. 317-323, 2006.

[12] Borrebaeck, C. A.; Wingren, C. Design Of High-Density Antibody Microarrays for Disease Proteomics: Key Technological Issues. *Journal of Proteomics* **2009**, *72* (6), 928–935.

[13] Haab, B. B. Applications Of Antibody Array Platforms. *Current Opinion in Biotechnology* **2006**, *17* (4), 415–421.

[14] Borrebaeck, C. A.; Wingren, C. High-Throughput Proteomics Using Antibody Microarrays: an Update. *Expert Review of Molecular Diagnostics* **2007**, *7* (5), 673–686.

[15] Kingsmore, S. F. Multiplexed Protein Measurement: Technologies and Applications of Protein and Antibody Arrays. *Nature Reviews Drug Discovery* **2006**, *5* (4), 310–321.

[16] Pavlickova, P.; Schneider, E.; Hug, H. Advances In Recombinant Antibody Microarrays. *Clinica Chimica Acta* **2004**, *343* (1-2), 17–35.

[17] Ingvarsson, J.; Larsson, A.; Sjöholm, A. G.; Truedsson, L.; Jansson, B.; Borrebaeck, C. A. K.; Wingren, C. Design Of Recombinant Antibody Microarrays for Serum Protein Profiling: Targeting of Complement Proteins. *Journal of Proteome Research* **2007**, *6* (9), 3527–3536.

[18] Kusnezow, W.; Banzon, V.; Schröder, C.; Schaal, R.; Hoheisel, J. D.; Rüffer, S.; Luft, P.; Duschl, A.; Syagailo, Y. V. Antibody Microarray-Based Profiling of Complex Specimens: Systematic Evaluation of Labeling Strategies. *Proteomics* **2007**, *7* (11), 1786–1799.

[19] Wingren, C.; Ingvarsson, J.; Dexlin, L.; Szul, D.; Borrebaeck, C. A. K. Design Of Recombinant Antibody Microarrays for Complex Proteome Analysis: Choice of Sample Labeling-Tag and Solid Support. *Proteomics* **2007**, *7* (17), 3055–3065.

[20] Angenendt, P. Progress In Protein and Antibody Microarray Technology. *Drug Discovery Today* **2005**, *10* (7), 503–511.

[21] Sanchez-Carbayo, M. Antibody Arrays: Technical Considerations And Clinical Applications in Cancer. *Clinical Chemistry* **2006**, *52* (9), 1651–1659.

[22] Anderson, N. L. The Human Plasma Proteome: History, Character, And Diagnostic Prospects. *Molecular & Cellular Proteomics* **2002**, *1* (11), 845–867.

[23] Haab, B.B.; Dunham, M.J. ; Brown, P.O. Protein Microarrays For Highly Parallel Detection And Quantitation Of Specific Proteins And Antibodies In Complex Solutions. *Genome Biology* **2001**, 2 (2).

[24] Zangar, R. C.; Daly, D. S.; White, A. M. ELISA Microarray Technology as a High-Throughput System for Cancer Biomarker Validation. *Expert Review of Proteomics* **2006**, *3* (1), 37–44.

[25] Angenendt, P.; Glökler, J.; Murphy, D.; Lehrach, H.; Cahill, D. J. Toward Optimized Antibody Microarrays: a Comparison of Current Microarray Support Materials. *Analytical Biochemistry* **2002**, *309* (2), 253–260.

[26] Xu, Q.; Miyamoto, S.; Lam, K. S. A Novel Approach To Chemical Microarray Using Ketone-Modified Macromolecular Scaffolds: Application In Micro Cell-Adhesion Assay. *Molecular Diversity* **2004**, *8*, 301–310. ⌈SEP⌉

[27] Lee, M.; Shin, I. Fabrication of Chemical Microarrays by Efficient Immobilization of Hydrazide-Linked Substances on Epoxide-Coated Glass Surfaces *Angew. Chem.* **2005**, *44*, 2881–2884. ⌈SEP⌉

[28] Kusnezow, W.; Hoheisel, J. D. Solid Supports for Microarray Immunoassays. *Journal of Molecular Recognition* **2003**, *16* (4), 165–176.

[29] Peluso, P.; Wilson, D. S.; Do, D.; Tran, H.; Venkatasubbaiah, M.; Quincy, D.; Heidecker, B.; Poindexter, K.; Tolani, N.; Phelan, M.; Witte, K.; Jung, L. S.; Wagner, P.; Nock, S. Optimizing Antibody Immobilization Strategies for the Construction of Protein Microarrays. *Analytical Biochemistry* **2003**, *312* (2), 113–124.

[30] Bradner, J. E.; Mcpherson, O. M.; Koehler, A. N. A Method for the Covalent Capture and Screening of Diverse Small Molecules in a Microarray Format. *Nat Protoc Nature Protocols* **2006**, *1* (5), 2344–2352.

[31] Bradner, J. E.; Mcpherson, O. M.; Mazitschek, R.; Barnes-Seeman, D.; Shen, J. P.; Dhaliwal, J.; Stevenson, K. E.; Duffner, J. L.; Park, S. B.; Neuberg, D. S.; Nghiem, P.; Schreiber, S. L.; Koehler, A. N. A Robust Small-Molecule Microarray Platform For Screening Cell Lysates. *Chemistry & Biology* **2006**, *13* (5), 493–504.

[32] Servoss, S. L.; White, A.M.; Baird, C.L.; Rodland, K.D.; Zangar, R.C. Evaluation Of Surface Chemistries For Antibody Microarrays. *Analytical Biochemistry* **2007**, 371, 105–115.

[33] Hill, D. J.; Mio, M. J.; Prince, R. B.; Hughes, T. S.; Moore, J. S. A Field Guide To Foldamers. *Chemical Reviews* **2001**, *101* (12), 3893–4012.

[34] Hebert, M. L.; Shah, D. S.; Blake, P.; Turner, J. P.; Servoss, S. L. Tunable Peptoid Microspheres: Effects of Side Chain Chemistry and Sequence. *Organic & Biomolecular Chemistry Org. Biomol. Chem.* **2013**, *11* (27), 4459.

[35] Patch, J. A.; Kirshenbaum, K.; Seurynck, S. L.; Zuckermann, R. N.; Barron, A. E. Versatile Oligo(N-Substituted) Glycines: The Many Roles Of Peptoids in Drug Discovery. *Nielsen: Pseudo-Peptides O-BK Pseudo-Peptides in Drug Development* **2005**, 1–31.

[36] Hebert, M.; Shah, D.; Blake, P.; Servoss, S. Uniform And Robust Peptoid Microsphere Coatings. *Coatings* **2013**, *3* (2), 98–107.

[37] Seurynck-Servoss, S. L; Baird, C.L.; Miller, K.D.; Pefaur, N.B.; Gonzalez, R.M.; Apiyo, D.O.; Engelmann, H.E.; Srivastava, S.; Kagan, J.; Rodland K.D.; Zangar, R.C. Immobilization Strategies For Single-Chain Antibody Microarrays. *Proteomics* **2008**, *8,* 2199–2210.

[38] White, A.M.; Daly, D.S.; Varnum, S.M.; Anderson, K.K.; Bollinger, N.; Zangar, R.C. Promat: Protein Microarray Analysis Tool. *Bioinformatics* **2006**, 22, 1278–1279.

[39] Armand, P.; Kirshenbaum, K.; Goldsmith, R. A.; Farr-Jones, S.; Barron, A. E.; Truong, K. T. V.; Dill, K. A.; Mierke, D. F.; Cohen, F. E.; Zuckermann, R. N.; Bradley, E. K. NMR Determination of the Major Solution Conformation of a Peptoid Pentamer with Chiral Side Chains. *Proceedings of the National Academy of Sciences* **1998**, *95* (8), 4309–4314.

[40] Wu, C. W.; Sanborn, T. J.; Zuckermann, R. N.; Barron, A. E. Peptoid Oligomers With α-Chiral, Aromatic Side Chains: Effects of Chain Length on Secondary Structure. *J. Am. Chem. Soc. Journal of the American Chemical Society* **2001**, *123* (13), 2958–2963.

[41] Nam, K. T.; Shelby, S. A.; Choi, P. H.; Marciel, A. B.; Chen, R.; Tan, L.; Chu, T. K.; Mesch, R. A.; Lee, B.-C.; Connolly, M. D.; Kisielowski, C.; Zuckermann, R. N. Free-Floating Ultrathin Two-Dimensional Crystals from Sequence-Specific Peptoid Polymers. *Nature Materials Nat Mater* **2010**, *9* (5), 454–460.

[42] Sanii, B.; Kudirka, R.; Cho, A.; Venkateswaran, N.; Olivier, G. K.; Olson, A. M.; Tran, H.; Harada, R. M.; Tan, L.; Zuckermann, R. N. Shaken, Not Stirred: Collapsing a Peptoid Monolayer To Produce Free-Floating, Stable Nanosheets. *J. Am. Chem. Soc. Journal of the American Chemical Society* **2011**, *133* (51), 20808–20815.

[43] Waters, M. L. Aromatic Interactions in Model Systems. *Current Opinion in Chemical Biology* **2002**, *6* (6), 736–741.

[44] Shetty, A. S.; Zhang, J.; Moore, J. S. Aromatic π-Stacking In Solution as Revealed through the Aggregation of Phenylacetylene Macrocycles. *J. Am. Chem. Soc. Journal of the American Chemical Society* **1996**, *118* (5), 1019–1027.

[45] Selvarajah, S.; Negm, O.H.; Hamed, M.R.; Tubby, C.; Todd, I.; Tighe, P.J.; Harrison, T.; Fairclough, L.C. Development and Validation of Protein

Microarray Technology for Simultaneous Inflammatory Mediator Detection in Human Sera. *Mediators of Inflammation* **2014**, 2014, 1-12.

[46] Claessens, C. G.; Stoddart, J. F. π-π Interactions In Self-Assembly. *Journal of Physical Organic Chemistry J. Phys. Org. Chem.* **1997**, *10* (5), 254–272.

[47] Perez Bakovic, G.R.; Roberts, J.L.; Colford, B.; Joyce, M.; Servoss, S.L. Peptoid microsphere coatings: The effects of helicity, temperature, pH, and ionic strength. *Biopolymers.* **2019**, *110* (6).

Supplemental Information
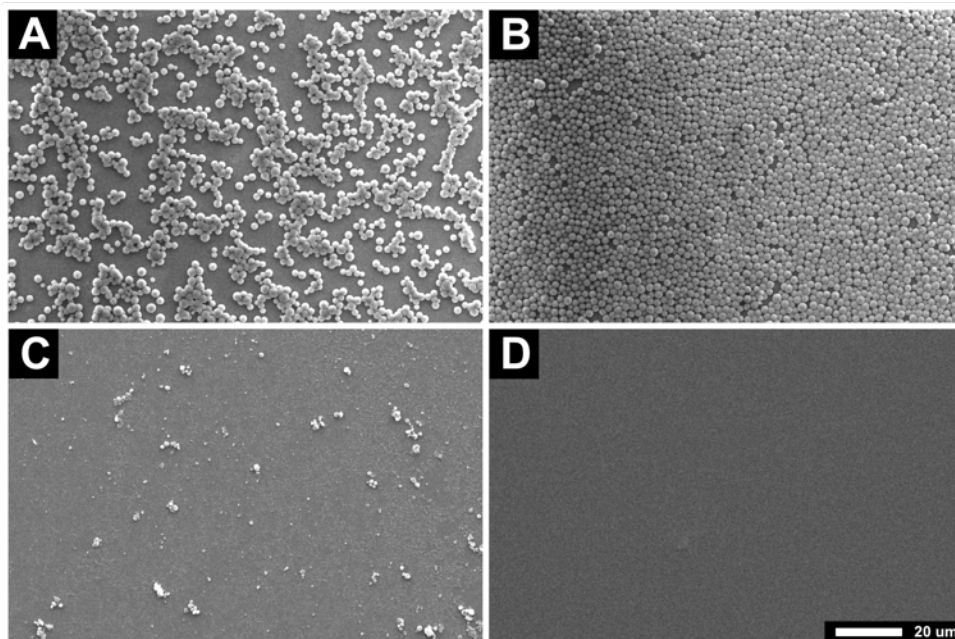
Figure S4.1 Effects of Tween-20 on microsphere coatings: A) 0.001%, B) 0.01%, C) 0.1%, and D) 1% by volume.
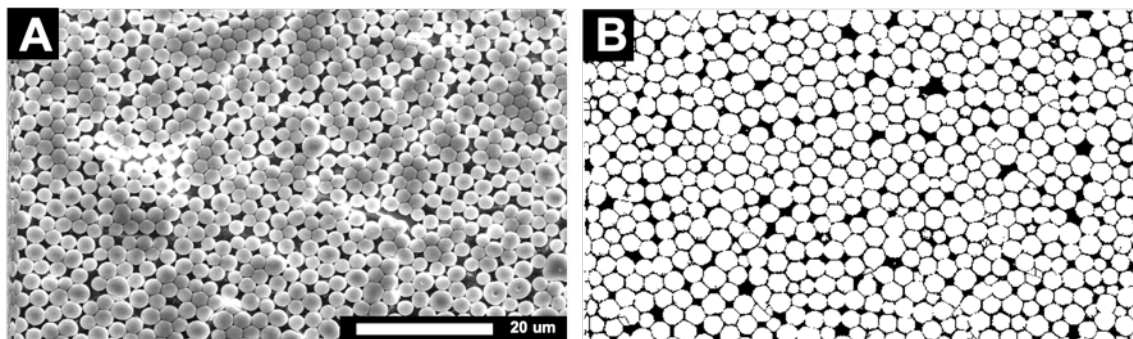
Figure S4.2 The surface coverage density was calculated using ImageJ particle analysis of A) SEM images of peptoid microsphere coatings and B) processed 8-bit binary grayscale image.
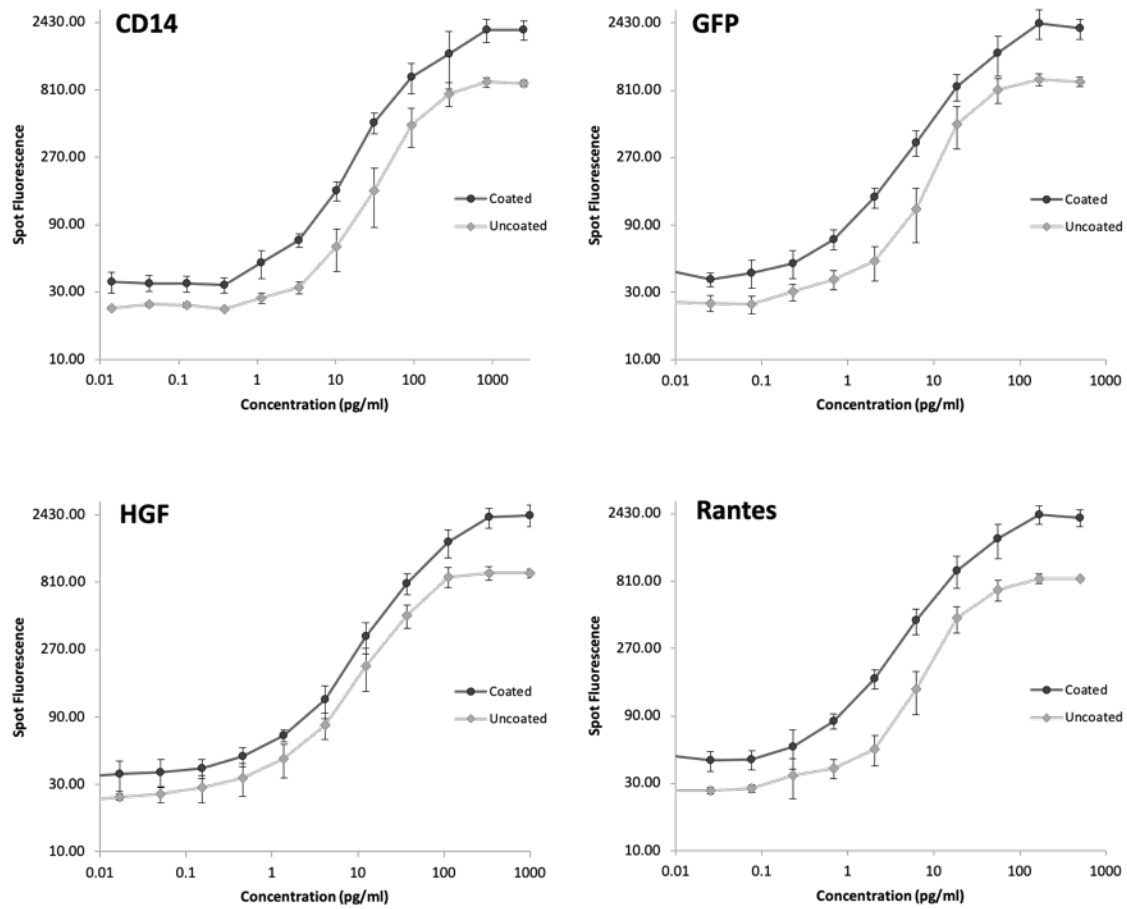
Figure S4.3 Standard curves for all 4 antibody assays (CD14, GFP, HGF, and RANTES) on 'uncoated' poly-L-lysine slides and the peptoid-based microspheres coated glass surfaces.

5. Peptoid Microsphere and Polyelectrolyte Multilayer Fabrication for Cell Culture Applications

5.1 Introduction

Naturally occurring polymers, specifically proteins and peptides, have beneficial fundamental features that make them ideal candidates for biomedical applications [1]. However, these proteins and peptides are susceptible to proteolytic degradation and often have low bioavailability [161, 19]. Researchers are increasingly turning to synthetic polymers, or peptidomimetic oligomers, that emulate the function of naturally occurring polymers, but have increased resistance to enzymatic degradation [161, 87]. One class of peptidomimetic oligomers, peptoids or poly-N-substituted glycines, closely resemble the structure of peptides with the side chains attached to the backbone amide groups rather than the alpha-carbon as in peptides [162]. This structural modification creates an achiral backbone and eliminates the hydrogen bond donors, both of which are necessary for forming secondary structures. By including chiral, aromatic side chains to the peptoid sequence a helical secondary structure can be induced. Peptoid synthesis involves using a solid phase "sub-monomer" method that allows for the precise construction of a diverse polypeptoid sequence library [163]. Thus, making peptoids an attractive candidate for biomaterial development and therapeutic applications.

Biomimetics have gained traction for use as artificial extracellular matrix (aECM) components in tissue engineering. The natural extracellular matrix is a complicated network of various biomacromolecules that includes proteins, polysaccharides, and glycoproteins [7]. The goal for these biomimetic materials is to generate scaffolds that directly mimic the natural tissue's biomechanical and chemical properties to incite cellular adhesion, growth, and survival for potential in tissue repair and disease treatment.

The aECM scaffolds must be three-dimensional to fully mimic the complicated ECM network [8]. Nevertheless, little is known on the direct effect that the topography and spatial arrangement of aECM structural features have on stem cell fate.

The layer-by-layer (LbL) formation of polyelectrolyte multilayers (PEMs) utilizes the ionic attraction between oppositely charged materials to alternate the adsorption of anionic and cationic polyelectrolytes [9]. The ability to tune the chemical, physical, and topographical properties of the LbL deposition by altering the pH, ionic strength, number of layers, and layer thickness makes them ideal candidates for tissue engineering, biosensors, and drug delivery applications [10]. LbL films can be assembled using naturally occurring and synthetic polymers, creating a vast library of potential polymers [11]. For example, heparin is an essential polysaccharide found in the ECM and has been utilized in LbL depositions for enhanced cellular activity. Heparin is known to regulate cell proliferation, cellular adhesion, matrix assembly, and would healing [12, 13]. Poly-L-lysine (PLL) is a cationic, homopolypeptide consisting of repeated positively charged L-lysine residues. PLL solutions are commonly coated on cell culturing substrates to help enhance cell adherence and cell viability [14]. Therefore, LbL films constructed from heparin and PLL layers makes an interesting candidate as a bioactive substrate for stem cell culturing.

Our lab has previously shown that partially water-soluble, helical peptoids self-assemble into microspheres [15] and can form uniform surface coatings [16]. The peptoid sequence (Figure 1.3) includes chiral, aromatic side chains on two faces of the helix to induce the formation of helical secondary structure. The third face of the helix offers customizability, contains methoxy and amine groups to increase water solubility. The amine groups provide a positive surface charge to the microspheres allowing for

attachment to glass slides and other adducts. The positive charge can serve as an anchor for LbL development to build thin films of polymers across the surface of the peptoid microspheres. The customizability of the microsphere chemistry allows for fine-tuning based on the desired application.

Figure 1.3 Structure of P3 peptoid (MW=1919 Da).

In this study, we discuss the addition of heparin and poly-L-lysine LbL films to the peptoid microspheres for potential applications as an aECM substrate. The morphology and uniformity of the coatings were evaluated by SEM and 3D Laser Scanning Microscopy. The chemical composition of the coatings was analyzed by FTIR. The peptoid microsphere and HEP/PLL coated surfaces were found to be biocompatible and non-cytotoxic with primary cortical rat astrocytes.

5.2   Materials and Methods

5.2.1   Materials

(S)-methylbenzylamine and 4-methoxybenzylamine were purchased from Acros Organics (Pittsburgh, PA). *tert*-butyl N-(4-aminobutyl)carbamate was purchased from CNH Technologies Inc. (Woburn, MA). MBHA rink amide resin was purchased from NovaBiochem (Gibbstown, NJ). Piperidine, N-(3-Dimethylaminopropyl)-N'-ethylcarbodiimide hydrochloride (EDC), and N-hydroxysulfosuccinimide sodium salt (Sulfo-NHS), and poly-L-lysine hydrobromide (mol wt 30,000-70,000) was purchased from Millipore-Sigma (St. Louis, MO). Ultra clean glass microarray slides and disuccinimidyl suberate (DSS) were purchased from Fisher Scientific (Pittsburgh, PA). All other reagents were purchased from VWR (Radnor, PA). All chemicals were used without further modifications unless otherwise specified.

5.2.2   Peptoid Synthesis, Purification, and Characterization

The peptoid was synthesized following a submonomer, solid-phase method on rink amide resin at room temperature [163]. The synthesis follows two steps: (1) acylation, which adds an activated carboxylic acid derivative onto a receptive amine generating the backbone of the peptoid, and (2) amination, the nucleophilic displacement by a primary or N-terminal secondary amine (side chain). The Fmoc-protection group was removed from the resin using 20% piperidine/DMF for 12 minutes creating a resin-bound amine. The resin was acylated with 0.4 M bromoacetic acid in DMF (4.25 mL) and N,N'-diisopropyl carbodiimide (0.8 mL), mixing for 1 minute. The amine submonomers were added to the resin at a concentration of 1.0 M via a nucleophilic substitution reaction for a period of 2 minutes. The two-step acylation and nucleophilic substitution cycle was repeated until the desired sequence was obtained. The resin was washed with DMF (4 x 5mL) after each step and with dicholoromethane (DCM) (3 x 5 mL)

after the last submononer was added. The peptoid was cleaved from the resin using a mixture of 95% trifluoroacetic acid (TFA), 2.5% water, and 2.5% triisopropylsilane for 10 minutes prior to evaporating the acid off using a Heidolph Laborota 4001 rotating evaporator (Elk Grove Village, IL).

The peptoid was dissolved in a 3 mg/mL solution of acetonitrile and water. The peptoid was purified using a Waters Delta 600 preparative high-performance liquid chromatography (HPLC) instrument (Milford, MA) with a Duragel G C18 150 × 20 mm column (Peeke Scientific, Novato, CA) and a linear gradient of 35-95% solvent B (acetonitrile, 5% water, 0.1% TFA) in A (water, 5% acetonitrile, 0.1% TFA), over 60 minutes. Peptoids were confirmed to be >98% pure via analytical HPLC (Waters Alliance) with a Duragel G C18 150 × 2.1 mm column (Peeke Scientific) using a linear gradient of 5-95% solvent B (acetonitrile, 0.1% TFA) in A (water, 0.1% TFA), over 30 minutes. Presence of the desired sequence was confirmed via matrix assisted laser desorption/ionization time of flight (MALDI-TOF) mass spectrometry (Bruker, Billerica, MA). Purified peptoid fractions were lyophilized and stored as a powder at -20 °C.

5.2.3   Peptoid Microsphere Coatings

In order to create a covalent binding site on the ultraclean glass slides, they were pretreated with the homo-bifunctional cross-linker, disuccinimidyl suberate (DSS). The DSS (30 mg) was dissolved in DMF (1 mL) and diluted with HPLC-grade methanol (150 mL) to form a final concentration of 0.2 mg/mL. The DSS solution was applied to the ultraclean glass slides for 5 minutes at room temperature by dipping the slides in the solution using a slide rack and incubation chamber. The glass slides were rinsed twice with methanol and dried using a centrifuge at 500 RPM for 30 seconds. Peptoid microspheres were prepared by dissolving the peptoid in a 4:1 ethanol/water (v/v) solution at a concentration of 3 mg/mL. The peptoid

microsphere solution was drop casted onto the DSS treated glass slides using a pipette and allowed to dry at room temperature and 60% relative humidity for 1 hour. The coating morphology was characterized using a Phillips XL-30 environmental scanning electron microscope (SEM; FEI, Hillsboro, OR).

5.2.4 Preparation of Polymeric Multilayers on Peptoid Microspheres

HEP and PLL were used to prepare polymeric multilayers on ultraclean glass slides and peptoid microsphere coated substrates using the LbL technique. The HEP/PLL multilayers were deposited on the substrates for a combination of 0.5, 1.0, 3.0, and 3.5 bilayers. The ultraclean glass substrates were treated with poly(ethylenimine) (PEI) dissolved in HEPES buffer (pH 7.4) for 15 minutes to provide an anchor, or strongly positive layer on the surface. The positive surface charge of the peptoid microsphere coatings was utilized in applying the first anionic heparin layer. Both HEP and PLL polymers were dissolved to 1 mg mL^{-1} in HEPES buffer (pH 7.4), which was also used as the washing solution. We evaluated layers of HEP/PLL ending in either HEP or PLL for a combination of 0.5 (HEP only), 1.0, 3.0, and 3.5 bilayers. HEP and PLL were deposited on the glass or peptoid microsphere substrate by pipetting the polymer solution onto the substrate and incubating for 5 minutes per layer with a 3-minute wash in HEPES buffer in between. After the desired number of layers was achieved, the substrates were washed with HEPES for 5 minutes and centrifuged at 500 RPM for 30 seconds to dry. To promote cellular adhesion, the PEMs were cross-linked overnight with EDC at 10 mg/mL and Sulfo-NHS at 11 mg/mL dissolved in HEPES buffer. After 24 hours, the samples were washed with HEPES buffer three times and dried using the centrifuge at 500 RPM for 30 seconds. The PEM samples were stored at 4°C until needed.

5.2.5   Coating Morphology and Uniformity

The surface topographies of the peptoid microsphere and HEP/PLL coatings were investigated using a Keyence VK-X260K 3D laser scanning confocal microscope. This microscope allows for the three-dimensional analysis of the surface without harming the samples. The images were taken using a 100x objective lens and a surface map was created by scanning the surface of our samples.

The morphology of the peptoid microsphere and HEP/PLL surfaces was analyzed using a Phillips XL-30 scanning electron microscope (SEM; FEI, Hillsboro, OR). The peptoid microsphere coatings were imaged to ensure successful coating of the microspheres prior to applying the LbL films. Once fabricated, the peptoid microsphere and HEP/PLL coatings were analyzed using SEM. The samples were sputter-coated with gold prior to imaging to remove charged electrons from the material and decrease the signal-to-noise ratio allowing for higher quality images to be captured.

5.2.6   Astrocyte Culturing

Primary cortical rat astrocytes were previously isolated and expanded from 1-day old neonatal rats and were cryopreserved for future testing [17]. For use in cell viability studies, the cryopreserved astrocytes were thawed, plated onto tissue culture treated flasks, and expanded to desired growth numbers in cell growth media consisting of Dulbecco's Modified Eagle Medium F12 Formulation (DMEM/F12) supplemented with 10% fetal bovine serum (FBS). The astrocytes were incubated at 37 °C, 95% humidity, and 5% CO_2. Prior to seeding, the peptoid microsphere, LbL, glass control, and fibronectin controls were prepared and transferred to a 12 well plate for testing. The glass for the control samples was sterilized and prepped by sonicating the ultraclean glass slides in ethanol for 5 minutes, drying in the oven at 70 °C, and treating with

UV/ozone for 30 minutes. The positive control sample was prepared by adding 50 µL of a 40 µg/µL fibronectin in sterile distilled water solution. The expanded astrocytes were detached from the culture surface using trypsin supplemented with EDTA (0.25%), counted with the hemocytometer, and seeded on the substrates at a cell density of 1×10^5 cells per sample. The astrocyte seeded substrates were incubated for 72 hours to facilitate astrocyte attachment and growth.

5.2.7   Cell Viability Assay

The cell viability was assessed using a Live/Dead® Viability/Cytotoxicity Kit that utilizes green-fluorescent calcein-AM and red-fluorescent ethidium homodimer-1. After 72 hours of culturing, the media was removed from the cell cultures and the samples were washed with Dulbecco's phosphate-buffered saline (D-PBS). A solution of 2 µM calcein and 4 µM ethidium homodimer-1 in D-PBS was added to the samples for 30 minutes. The live/dead stains were removed and the cells were imaged with a fluorescence microscope. The live cells were observed with a fluorescein isothiocyanate (FITC) filter and the dead cells were observed with a tetramethylrhodamine isothiocyanate (TRITC) filter. The live and dead images were overlaid and analyzed using ImageJ software.

5.3   Results and Discussion

5.3.1   Coating Characterization

SEM confirmed the uniformity and morphology of the peptoid microsphere coatings on the glass surfaces (Figure 5.1). From a previous study, the average local microsphere surface density (n=10) on the glass slides was 87% (s=2.59%) covered. The LbL films were then deposited on the peptoid microsphere coated glass slides for 0.5, 1.0, 3.0, and 3.5 bilayers of heparin and poly-L-lysine. SEM confirmed that the peptoid microsphere morphology was

maintained and the LbL films were successfully deposited on the microsphere surface. Figure 5.2 shows the SEM images for the peptoid microspheres and 0.5 LbL (Figure 5.2A), 1.0 LbL (5.2B), 3.0 LbL (5.2C), and 3.5 LbL (5.2D). The LbL films are visible on top of the peptoid microspheres and the overall coating coverage is maintained. The topography of the microsphere coatings is maintained after HEP/PLL depositions are applied to the top of the microspheres. These topographical features are from the three-dimensional spherical morphology that the peptoid microspheres create on the surface of the substrates. Overall, the contact angle between microspheres is important in creating the topography needed for aECM development.
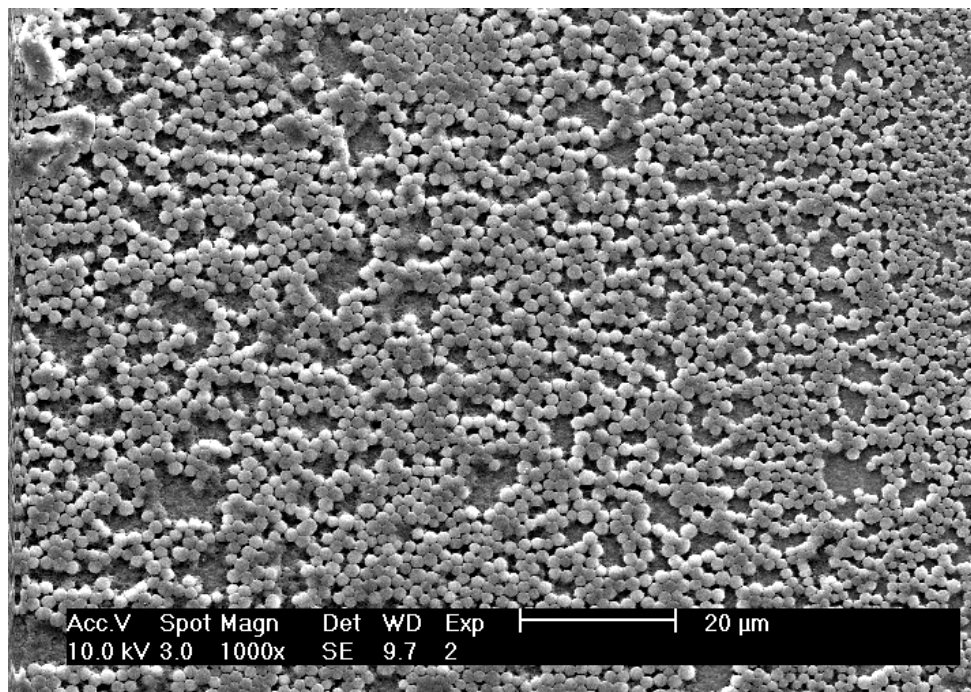

Figure 5.1 SEM image for peptoid microsphere coatings on a DSS treated glass slide.
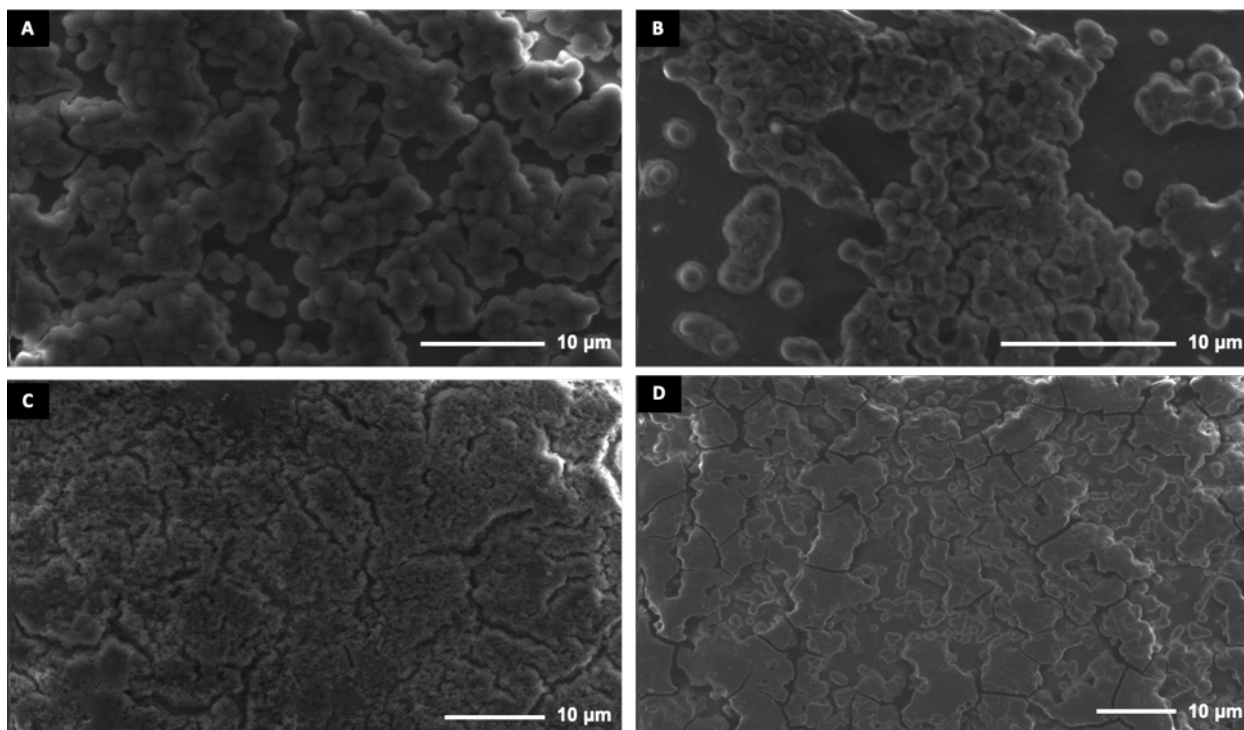
Figure 5.2 SEM images for peptoid microsphere coatings with (A) 0.5 layer (Heparin only), (B) 1.0 bilayers (Hep/PLL)$_{1.0}$, (C) 3.0 bilayers (Hep/PLL)$_{3.0}$, and (D) 3.5 bilayers (Hep/PLL)$_{3.5}$.

Although SEM is useful in generating high-resolution images of object morphology and spatial arrangements, it is limited to two-dimensional characterization. The Keyence 3D Laser Scanning Optical Microscope (3D LSM) allows for three-dimensional scans of a sample to better characterization the surface topography and coating uniformity [18]. The 3D LSM utilizes both optical and laser settings to analyze the surface and depth of a material. The peptoid microsphere and HEP/PLL films were imaged with the 3D LSM to provide a surface analysis and 3D height map of our samples (Figure 5.3). For all of the peptoid microsphere and LbL coatings, the 3D LSM images confirmed the presence of both microspheres and HEP/PLL films. The peptoid microsphere and 0.5 LbL (HEP)$_{0.5}$ (Figure 5.3A) and 3.0 LbL (HEP/PLL)$_{3.0}$ coatings had the best surface coverage and were the most uniform. The heat maps for all peptoid microsphere and LbL coatings displayed an increase in height as compared to the peptoid microspheres alone. Due to

the low sensitivity of the instrument, the height measurement was inconsistent across experimental replicates. There was an increase in the height with added layers, but the starting height measurement varied across samples causing the height values given by the 3D scan to be inaccurate. Overall, the HEP/PLL films were successfully covered the peptoid microspheres without eliminating the desired spherical topography that is created by the microsphere coating.
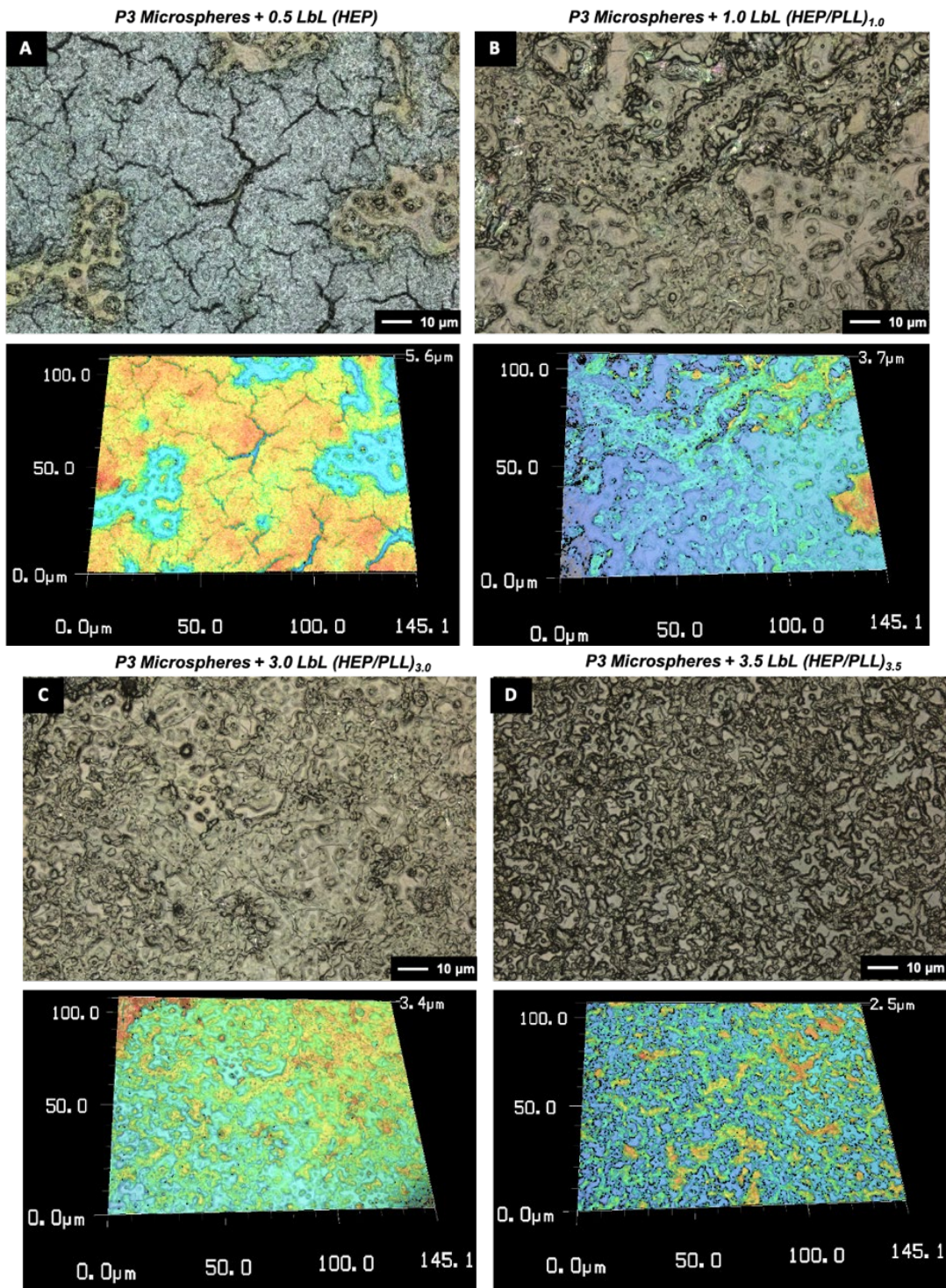
Figure 5.3 3D Laser Scanning Microscope images for (A) 0.5 layer (Heparin only), (B) 1.0 bilayers (Hep/PLL)$_{1.0}$, (C) 3.0 bilayers (Hep/PLL)$_{3.0}$, and (D) 3.5 bilayers (Hep/PLL)$_{3.5}$.

5.3.2 Chemical Composition Analysis

Fourier transform infrared (FTIR) spectroscopy reveals information on the molecular nature of chemical compounds and is useful for the characterization of various biopolymers. FTIR was used to analyze the presence of specific functional groups on our peptoid microsphere and HEP/PLL coatings (Figure 5.4). The peptoid sequence is composed of a repetitive peptide-like backbone that includes multiple carboxyl and amine groups. The prominent functional groups for the peptoid side chains include hydroxyl (-OH) groups on the hydroxybenzylamine side chains and a primary amine groups ($-NH_3^+$) on the lysine-like side chains. The carboxyl group from the peptoid backbone had an intense adsorption peak at 1650 cm^{-1} (Figure 5.4A). The 1650 cm^{-1} peak was present for all of the peptoid microsphere and HEP/PLL coatings, but as more bilayers were added the intensity of the peak decreased (Figure 5.4B-D). The number of bilayers for this study was increased to 6.0 bilayers of HEP/PLL to increase the coating thickness. For 6.0 bilayers, the intensity of the 1650 cm^{-1} peak drastically decreased by over 50%. The chemical structure of poly-L-lysine has an abundance of positively charged primary amines. The broad peak at 3,000-3,500 cm^{-1} for the 6.0 bilayer sample (Figure 5.4D) indicates the presence of amine bonds (N-H) found in the poly-L-lysine polymer [19]. The FTIR peaks at 1650^{-1} and the band at 3,000-3,500^{-1} confirm the presence of the HEP/PLL films on top of our peptoid microsphere coatings.
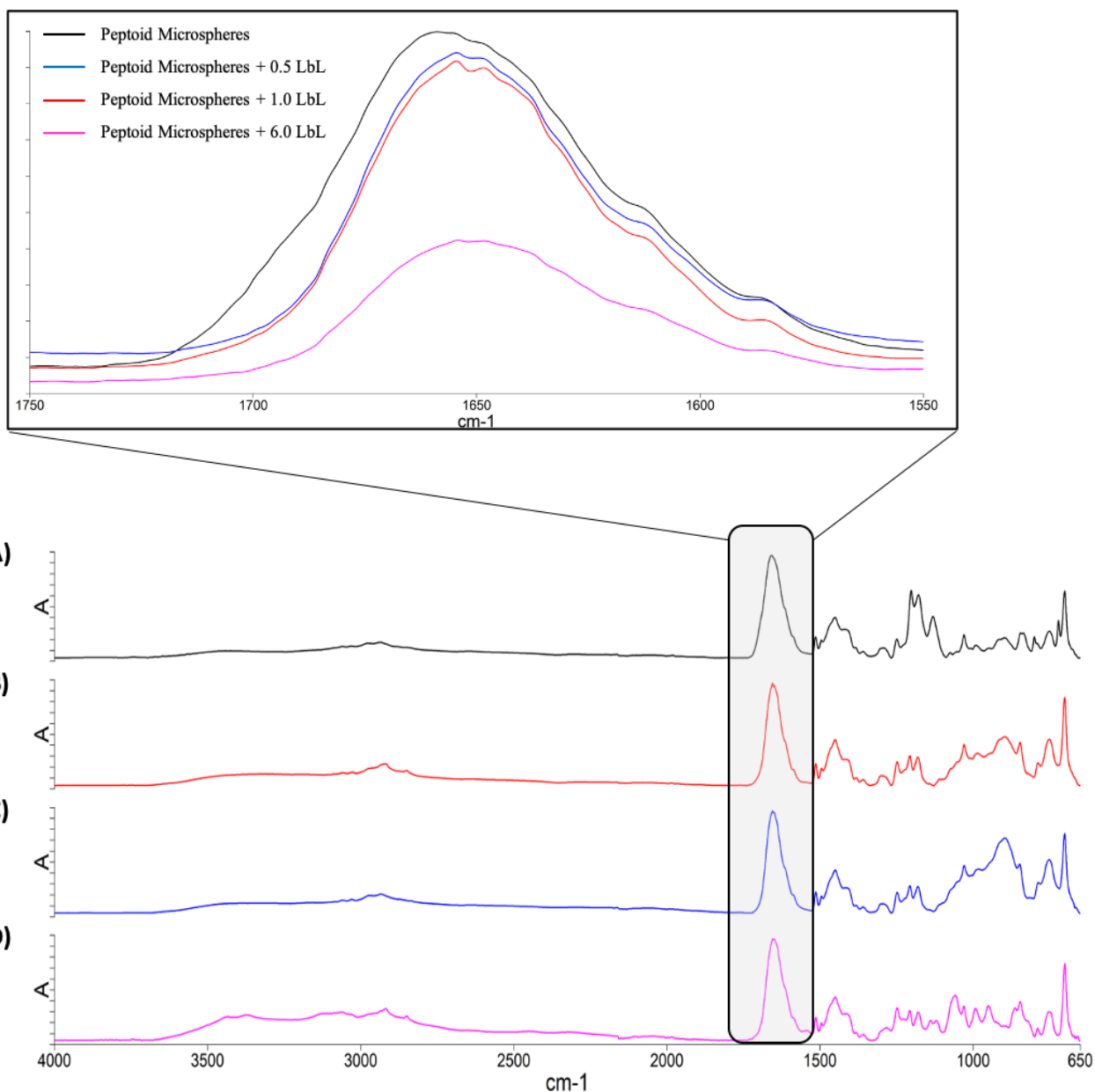
Figure 5.4 FTIR results for glass slides coated with (A) peptoid microspheres, (B) 0.5 layer (Heparin only), (C) 1.0 bilayers $(Hep/PLL)_1$, (D) 6.0 bilayers $(Hep/PLL)_6$. The inset focused on the main peaks at 1650 cm-1 are representative of the carbonyl (C=O) bond that is common in the peptoid and heparin structures.

5.3.3 Cytotoxicity/Viability Assay

Cell viability is determined by the number of live cells on the surface and the overall cell morphology. Cells that are alive and spread out on the surface are considered to have high cell viability. Healthy astrocyte cells will begin developing cellular networks with neighboring cells

[22]. Primary cortical rat astrocytes (passage 6-8) that were isolated from 1-day old neonatal rat pups were used to assess the toxicity of our peptoid and LbL surfaces. The cells were grown on laminin coated cell culture flasks to confluency and plated on the substrates at 100,000 cells/cm^2. The samples consisted of uncoated ultraclean glass and ultraclean glass coated with fibronectin (positive control), peptoid monomer, peptoid microspheres, peptoid microspheres and 0.5 bilayers (heparin only), peptoid microspheres and 1.0 bilayers (HEP/PLL)$_{1.0}$, peptoid microspheres and 3.0 bilayers (HEP/PLL)$_{3.0}$, peptoid microspheres and 3.5 bilayers (HEP/PLL)$_{3.5}$, 0.5 LbL (HEP), and 1.0 LbL (HEP/PLL)$_{1.0}$. The cells were grown for 3 days prior to staining with a Live/Dead® Viability/Cytotoxicity Kit that utilizes green-fluorescent calcein-AM to indicate intercellular esterase activity and red-fluorescent ethidium homodimer-1 to indicate the loss of plasma membrane integrity in dead cells. The ethidium homodimer-1 is a nucleic acid stain that enters dead cells through the disintegrated membrane, while the calcein-AM stains all metabolically active cells [170, 171].

The cytotoxicity of the fabricated surfaces was analyzed using the live/dead stains and imaging with a fluorescent microscope at 10x magnification. The uncoated glass and glass coated with fibronectin (+ control), 1.0 LbL (HEP/PLL)$_{1.0}$, and 3.0 LbL (HEP/PLL)$_{3.0}$ (Figure 5.5) were tested in comparison to the peptoid-based surfaces (Figure 5.6). Overall, the only surfaces to have a cell survival rate of less than 97% were the uncoated glass slide (33%) (Figure 5A), peptoid monomer coating (0%) (Figure 6A), and peptoid microsphere coating (0%) (Figure 6B). The cells did not fully adhere to the plain glass surface and had the poorest cell viability as compared to the fibronectin (Figure 5B) and HEP/PLL coated glass (Figure 5C-D). Fibronectin was used as the positive control since it is well studied for promoting cellular adhesion and proliferation. With the rat astrocytes, the fibronectin surface promoted the best cell adhesion,

proliferation, and viability. The glass and LbL surfaces had good cell adhesion, but less cells were observed on the surface and they did not branch out compared to those on the fibronectin sample. The peptoid monomer (Figure 6A) and microsphere (Figure 6B) coatings facilitated cell adhesion, but all the cells were dead after XX time. Just a single layer of heparin added to the peptoid microsphere coating (Figure 6C) resulted in increased cell viability with similar cell morphology to the fibronectin surface. Similar results were observed for the other peptoid microsphere and LbL coatings (Figure 6D-F). There was no difference in cytotoxicity and cell viability between the peptoid microsphere and LbL coatings ending in heparin or poly-L-lysine, where both showed efficacy in promoting cellular adhesion and expansion.
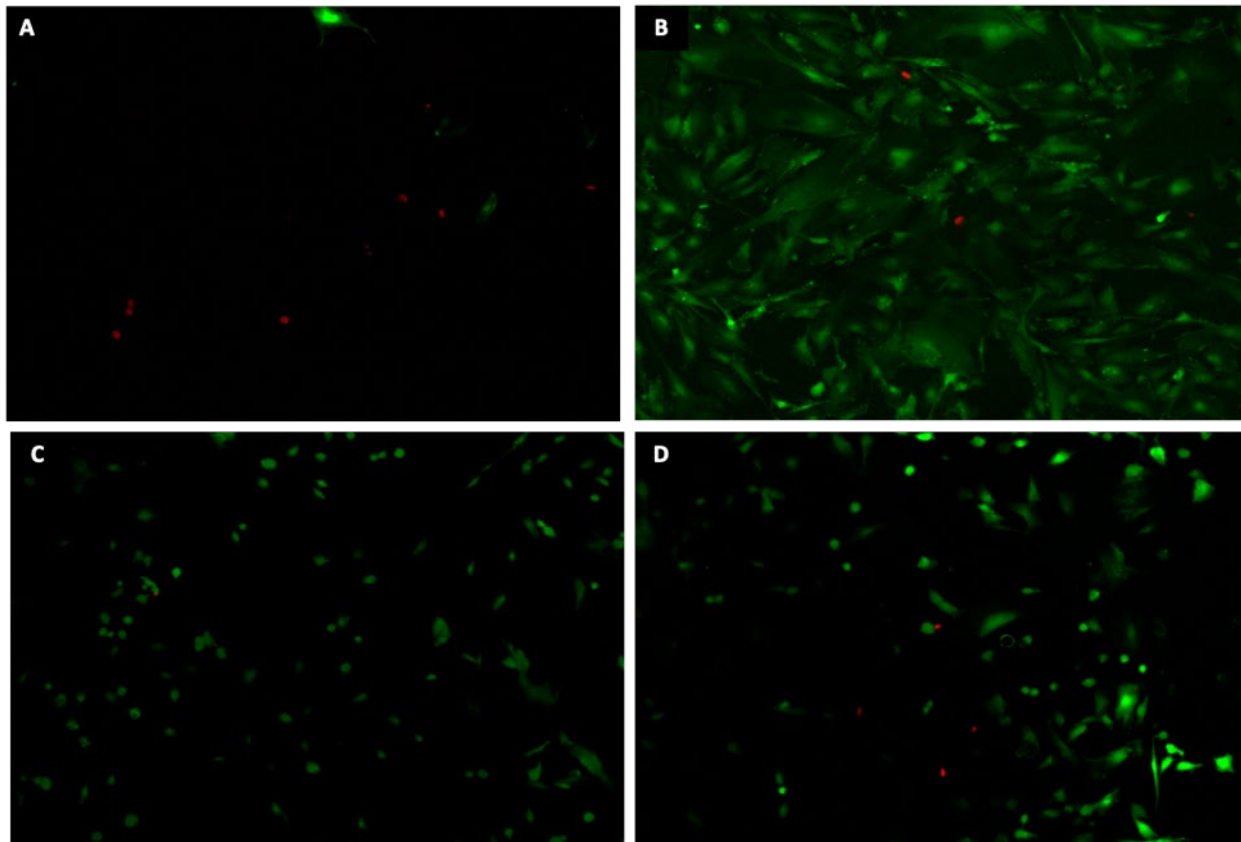
Figure 5.5 Fluorescent microscopy images of rat astrocytes stained with a live/dead assay on (A) ultraclean glass, (B) fibronectin coated glass, (C) 1.0 LbL $(HEP/PLL)_{1.0}$, and (D) 3.0 LbL $(HEP/PLL)_{3.0}$
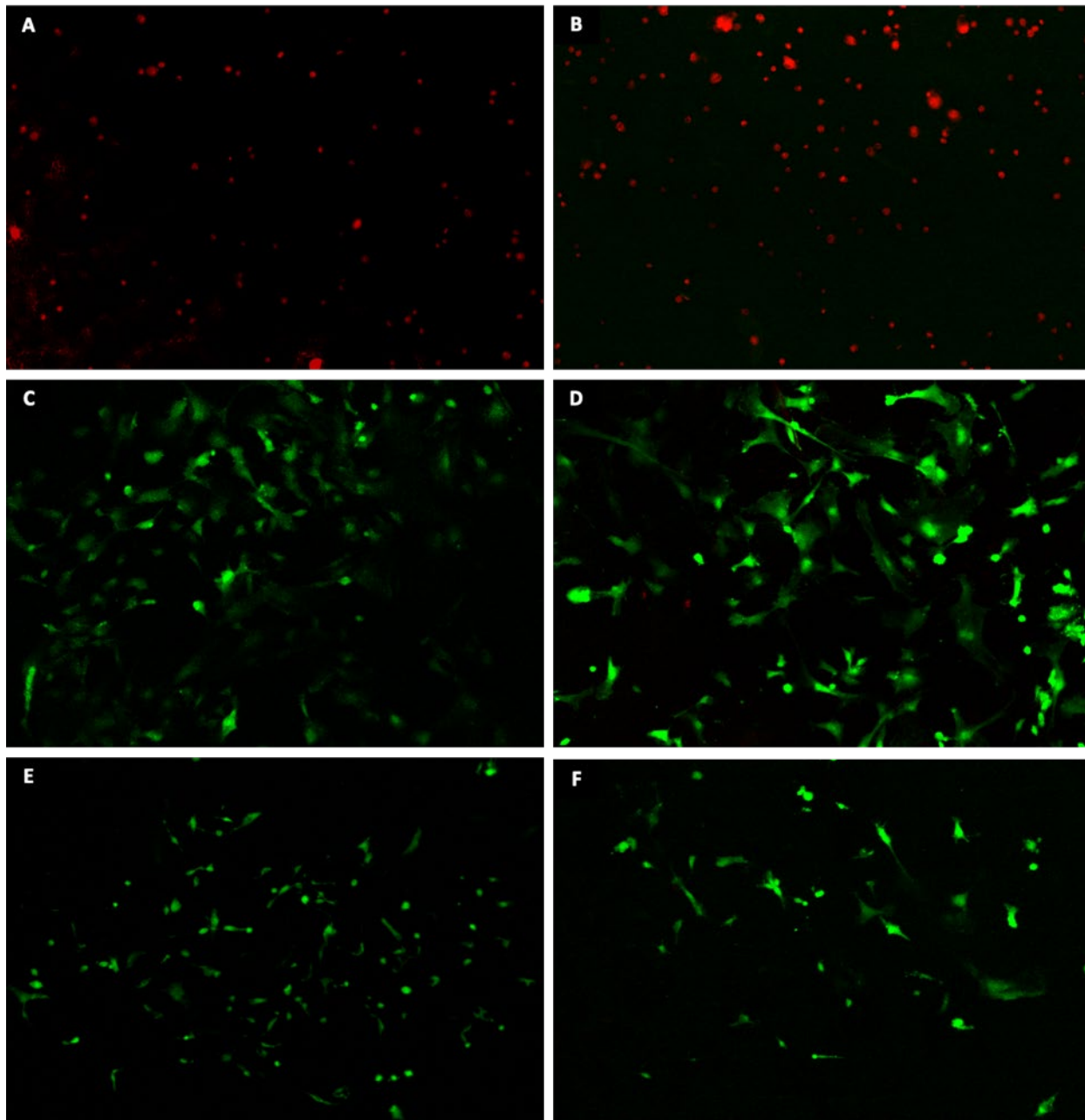
Figure 5.6 Fluorescent microscopy images of rat astrocytes stained with a live/dead assay on (A) peptoid monomer, (B) peptoid microspheres, (C) peptoid microspheres + 0.5 LbL (HEP)$_{0.5}$, (D) peptoid microspheres + 1.0 LbL (HEP/PLL)$_{1.0}$, (E) peptoid microspheres + 3.0 LbL (HEP/PLL)$_{3.0}$, and (F) peptoid microspheres + 3.5 LbL (HEP/PLL)$_{3.5}$.

5.4 Conclusion and Future Studies

Novel peptoid microsphere and LbL coatings were successfully fabricated for cell culturing applications. Peptoid microspheres are suitable anchors for HEP/PLL multilayer development to build biomaterials that combine the spherical topography of the peptoid and the biocomposition of the LbL polymers. Results revealed that the LbL films up to 3 bilayers are able to cover the peptoid microspheres without eliminating the spherical morphology of the microspheres. This is important because the end-goal of this material as an aECM substrate is to utilize the topography of the surface features to promote stem cell differentiation into specific adult cell types. For this, we proved that the novel peptoid and LbL substrates promote cell adhesion and are not cytotoxic to the astrocytes. Future plans include gaining a better understanding on the surface roughness, mechanical properties, and ability of the surfaces to promote stem cell proliferation and differentiation.

5.5 References

[1] A. K. Sato, M. Viswanathan, R. B. Kent and C. R. Wood, "Therapeutic peptides: technological advances driving peptides into development," *Current Opinions in Biotechnology,* vol. 17, no. 6, pp. 638-642, 2006.

[2] J. A. Patch, K. Kirshenbaum, S. L. Seurynck and A. Barron, "Versatile Oligo(N-Substituted) Glycines: The Many Roles of Peptoids in Drug Discovery," *ChemInform,* vol. 36, no. 36, pp. 1-31, 2005.

[3] A. Grob, C. Hashimoto, H. Sticht and J. Eichler, "Synthetic Peptides as Protein Mimics," *Frontiers in Bioengineering and Biotechnology ,* vol. 3, no. 211, 2015.

[4] J. Vagner, H. Qu and V. J. Hruby, "Peptidomimetics, a synthetic tool of drug discovery," *Curr Opin Chem Biol,* vol. 12, no. 3, pp. 292-296, 2008.

[5] K. Kirshenbaum, A. E. Barron, R. A. Goldsmith, P. B. E. K. Armand, K. T. Truong, K. A. Dill, F. E. Cohen and R. N. Zuckermann, "Sequence-specific polypeptids: A diverse family of heteropolymers with stable secondary structure," *PNAS,* vol. 95, no. 8, pp. 4303-4308, 1998.

[6] R. N. Zuckermann, J. M. Kerr, S. B. Kent and W. H. Moos, "Efficient method for the preparation of peptoids [oligo(N-substituted glycines)] by submonomer solid-phase synthesis," *Journal Of The American Chemical Society,* vol. 114, no. 26, pp. 10646-10647, 1992.

[7] C. Frantz, K. Stewart and V. Weaver, "The extracellular matrix at a glance," *Journal of Cell Science,* vol. 123, no. 24, pp. 4195-4200, 2010.

[8] R. Wade and J. Burdick, "Engineering ECM signals into biomaterials," *Materials Today,* vol. 15, no. 10, pp. 454-459, 2012.

[9] S. Pahal, R. Gakhar, A. Raichur and M. Varma, "Polyelectrolyte multilayers for bio-applications: recent advancements," *IET nanobiotechnology,* vol. 11, no. 8, pp. 903-908, 2017.

[10] K. Tang and N. Besseling, "Formation of polyelectrolyte multilayers: ionic strengths and growth regimes," *Soft Matter,* vol. 12, no. 4, pp. 1032-1040, 2016.

[11] S. Zhang, M. Xing and B. Li, "Biomimetic Layer-by-Layer Self-Assembly of Nanofilms, Nanocoatings, and 3D Scaffols for Tissue Engineering," *Int. J. Mol. Sci,* vol. 19, no. 6, p. 1641, 2018.

[12] N. Aggarwal, N. Altgarde, S. Svedhem, G. Michanetzis, Y. Missirlis and T. Groth, "Tuning Cell Adhesion and Growth on Biomimetic Polyelectrolyte Multilayers by Variation of pH During Layer-by-Layer Assembly," *Macomolecular Bioscience,* 2013.

[13] W. H. Burgess and T. Maciag, "The Heparin-Binding (Fibroblast) Growth Factor Family of Proteins," *Annual Review of Biochemistry,* vol. 58, pp. 575-606, 1989.

[14] M. S. LIberio, M. C. Sadowski, C. Soekmadji, R. A. Davis and C. C. Nelson, "Differential effects of tissue culture coating substrates on prostate cancer cell adherence, morphology and behavior," *PLoS One,* vol. 9, no. 11, 2014.

[15] M. L. Hebert, D. S. Shah, P. Blake, J. P. Turner and S. L. Servoss, "Tunable Peptoid Microspheres: Effects of Side Chain Chemistry and Sequence," *Organic & Biomolecular Chemistry,* vol. 11, no. 27, p. 4459, 2013.

[16] G. Perez Bakovic, J. Roberts, B. Colford, M. Joyce and S. Servoss, "Peptoid microsphere coatings: The effects of helicity, temperature, pH, and ionic strengths," *Biopolymers,* vol. 110, no. 6, 2019.

[17] A. Walker, J. Kim, J. Wyatt, A. Terlouw, K. Balachandran and J. Wolchok, "Repeated In Vitro Impact Conditioning of Astrocytes Decreases the Expression and Accumulation of Extracellular Matrix," *Annals of Biomedical Engineering,* vol. 47, pp. 967-979, 2019.

[18] M. Y. Ismail, M. Patanen, S. Kauppinen, H. Kosonen, M. Ristolainen, S. A. Hall and H. Liimatainen, "Surface analysis of tissue paper using laser scanning confocal microscopy and micro-computed topography," *Cellulose,* vol. 27, pp. 8989-9003, 2020.

[19] M. Rozenberg and G. Shoham, "FTIR spectra of solid poly-l-lysine in the stretching NH mode range," *Biophys Chem,* vol. 125, no. 1, pp. 166-171, 2007.

[20] D. Bratosin, L. Mitrofan, C. Palii, J. Estaquier and Montreuil, "Novel fluorescence assay using calcein-AM for the determination of human erythrocyte viability and aging," *Cytometry Part A,* vol. 66A, no. 1, pp. 78-84, 2005.

[21] S. Sanfilippo, M. Canis, L. Ouchchane, R. Botchorishvili, C. Artonne, L. Janny and F. Brugnon, "Viability assessment of fresh and frozen/thawed isolated human follicles: reliability of two methods (Trypan blue and Calcein AM/ethidium homodimer-1)," *Fertility Preservation,* vol. 28, pp. 1151-1156, 2011.

[22] E. M. Powell and H. M. Geller, "Dissection of astrocyte-mediated cues in neuronal guidance and process extension," *Glia,* vol. 26, no. 1, pp. 73-83, 1999.

6. Peptoid Interfaces for Stem Cell Culturing

6.1 Introduction

The extracellular matrix (ECM) is a network composed of proteins and macromolecules that physically supports the surrounding cells [1]. The ECM plays a major role in dictating stem cell fate, primarily due to biochemical, mechanical, and topographical cues [174, 175]. Numerous studies have demonstrated that cells are directly affected by specific chemical and mechanical properties of naturally occurring ECM components [4]. These cues induce cellular communication cascades that influence cell proliferation, differentiation, and apoptosis [5].

Engineering an artificial extracellular matrix that directly mimics the natural ECM is an extremely difficult but critical task for advancing the tissue engineering field. The aECM must possess excellent structural integrity and tunability, while also maintaining the bioactivity and biocompatibility of naturally occurring ECM components to help improve cellular microenvironments [6]. To date, many of the aECMs used for cell culturing have been limited to two-dimensional substrates. Since the natural ECM is three-dimensional, these 2-D substrates are not able to directly mimic the ECM network. Recently, it was determined that changes in the ECM are detected by cell receptors that can dictate cellular gene expression [7]. These changes can influence cell survival, shape, mitigation, proliferation, and differentiation [8]. The topography and spatial arrangement of features on artificial ECM surfaces have shown to guide stem cell attachment and differentiation into specific adult cell types [9]. In designing a nanocomposite scaffold that mimics the natural ECM it's important to combine specific features from various materials. The scaffold must have compatible biochemical cues that promote cellular adhesion, while also possessing topographical features that promote cellular proliferation and differentiation into adult cell types.

The main goal of this study was to create a three-dimensional, highly customizable substrate that mimics the natural features of the extracellular matrix to promote and guide stem cell proliferation and differentiation. The work here shows the development and characterization of peptoid microsphere and LbL coatings and their ability to enhance cell adhesion, proliferation, and differentiation.

## 6.2 Peptoid Substrates and Rat Neural Stem Cell Differentiation

The objective for this study was to determine the efficacy of the P3 peptoid microspheres as an ECM substrate by elucidating the mechanisms that topography plays on stem cell. We hypothesize that the topography of our peptoid microsphere surface will directly influence the differentiation pathway of neural stem cells into adult neurons or astrocyte cell types.

In collaboration with the Borrelli Lab at University of Arkansas Medical Sciences, the ability of our peptoid microsphere coatings to promote neural stem cell proliferation and differentiation was investigated by culturing rat neural stem cells (rNSCs) on our surfaces for 18 days. Peptoid microsphere coatings were prepared by dissolving the peptoids in 4:1 ethanol/water (v/v) solution at a concentration of 3 mg/mL. The peptoid solutions were applied to glass substrates using a pipette and allowed to dry at room temperature and 60% relative humidity for 1 hour. All materials were sterilized with 70% ethanol/water solution or autoclaved prior to making the peptoid microsphere coatings Since the peptoid is dissolved in ethanol/water, the peptoid coatings were sterilized using UV treatment for 10 minutes prior to culturing cells. Three different peptoid microsphere concentrations (1x, 2x, and 3x), or microsphere densities, were studied by altering the volume of microsphere solution applied to the glass to form the coatings (Figure 6.1).

The rNSCs were cultured to confluency prior to plating on the peptoid microsphere surfaces for differentiation. After 18 days of differentiation, the cells were fixed with paraformaldehyde and stained with β-tubulin for neurons and glial fibrillary acidic protein (GFAP) for glial cells. The slides were analyzed with a fluorescent microscope and the results displayed excellent cell viability and differentiation to primarily adult neurons (70-80%) versus glial cells (20-30%) (Figure 6.2). We believe that the topography of our peptoid microspheres plays a role in dictating stem cell differentiation fate.
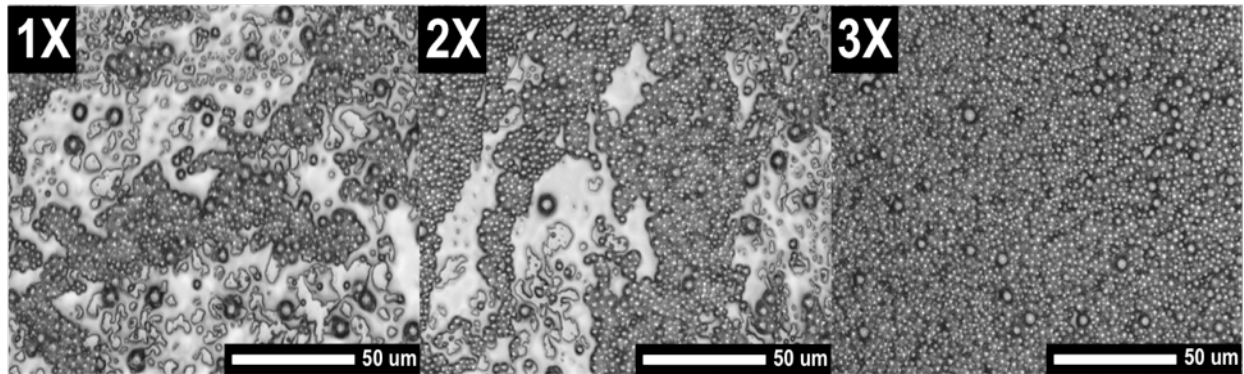

Figure 6.1 3D Laser Scanning Microscopy images of the peptoid microspheres coated at 1X, 2X, and 3X concentrations for experiments with rat neural stem cell differentiation.
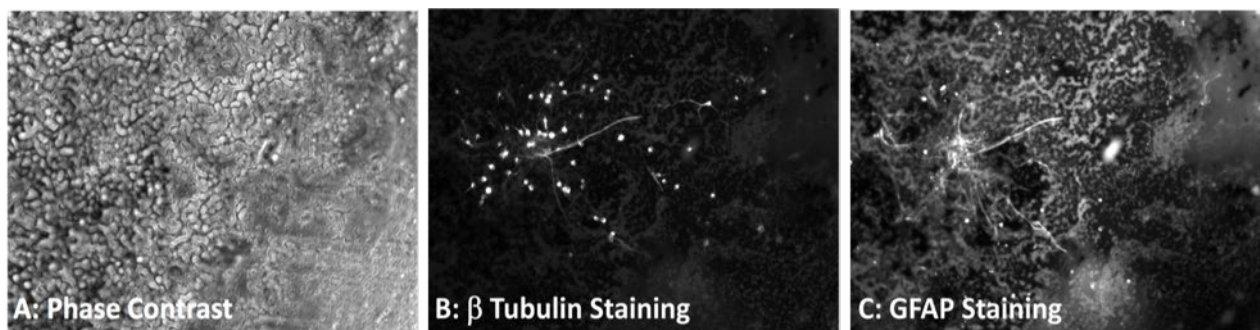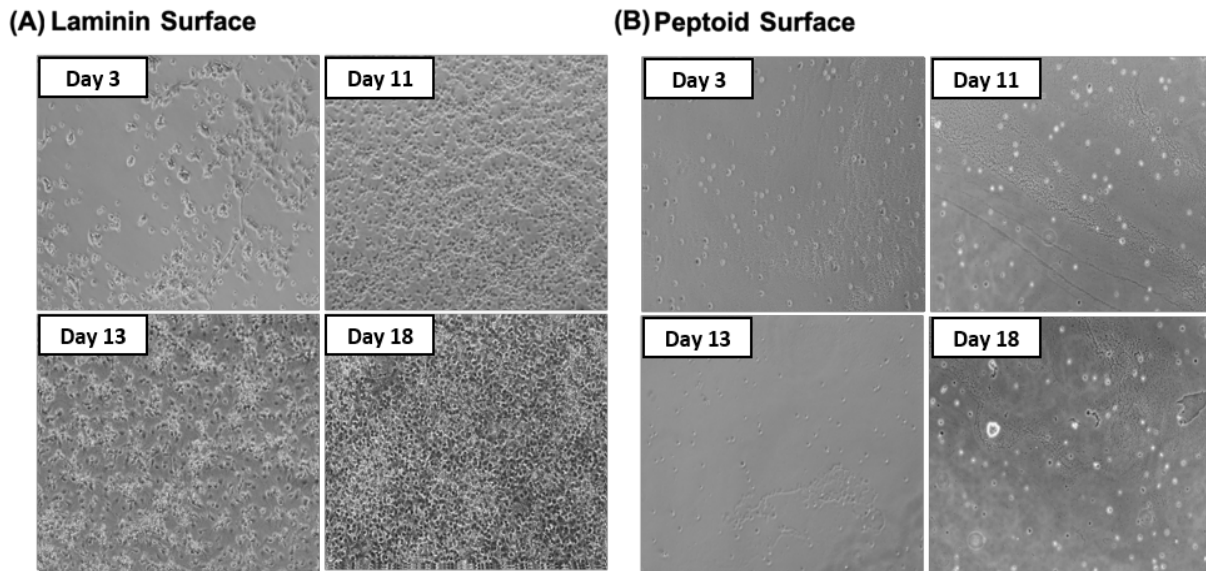

Figure 6.2 Day 18 of rat neural stem cell differentiation on peptoid microsphere coatings shown by (A) phase contrast microscopy, (B) beta-tubulin stain, and (C) GFAP stain fluorescent microscopy (Borrelli Lab).

To determine whether microsphere morphology played a role in rNSC differentiation, we comparatively cultured the cells on the peptoid monomer coating for 18 days. The peptoid monomer is the same P3 12mer sequence, but without forming microspheres. The monomer was coated on glass slides by dissolving the peptoid in 100% methanol at a concentration of 5 mg/mL. The peptoid monomer solution was pipetted onto the glass slides and allowed to dry for 1 hour at room temperature. The presence of the peptoid monomer on the slides was confirmed by using x-ray photoelectron spectroscopy (XPS) indicated by pi-pi bonds present on the surface of the coating (Figure 6.3). These pi-pi bond represent the aromatic groups of the methoxy-benzylamine and (S)-methylbenzylamine side chains present in the peptoid sequence. The rNSCs were grown to confluency and plated on the peptoid monomer surface and a laminin control surface for differentiation. At days 3, 11, 13, and 18 the surfaces were imaged using a confocal light microscope (Figure 6.4). The stem cells adhered to the peptoid monomer died by day 11 and no proliferation or differentiation was visually seen (Figure 6.4B). The cells on the laminin surface showed excellent cell viability and proliferated extensively over the 18 days (Figure 6.4A). From this study we concluded that the spherical morphology and surface topography of the peptoid microspheres plays a major role in neural stem cell proliferation and differentiation.
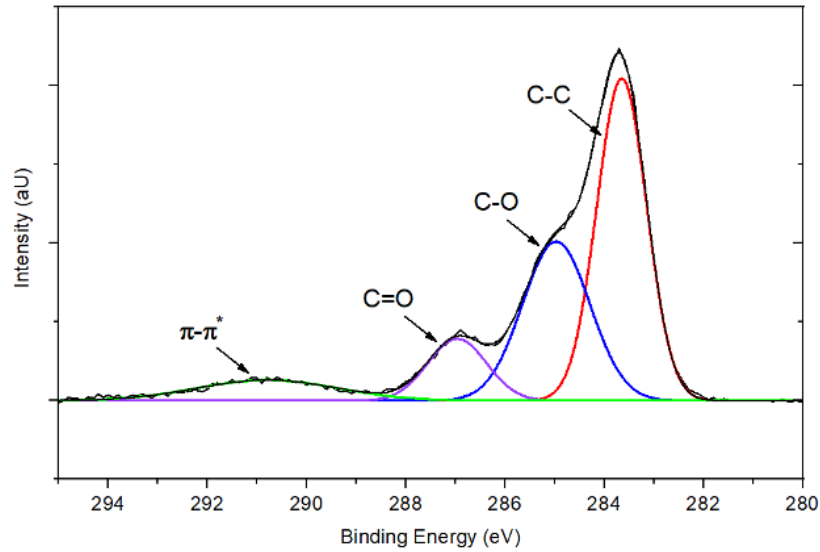
Figure 6.3 XPS analysis of peptoid monomer coatings on ultraclean glass slides.

Figure 6.4 Phase contrast microscopy of rat neural stem cell differentiation on (A) Laminin control and (B) peptoid monomer coated glass slide after 3, 11, 13, and 18 days (Borrelli Lab).

## 6.3   Peptoid Microsphere and PEM Coatings

The objective of this study was to combine the topography of the peptoid microsphere coatings with naturally occurring polymeric depositions in the form of PEMs. It was expected

95

that the PEMs would utilize the positive surface charge of the peptoid microspheres to create thin films across the top of the surface. Our work described here focused on the development of peptoid microsphere coatings that incorporate heparin and collagen or heparin and poly-L-lysine multilayered films. We determined that by adding 3-6 bilayers of heparin/collagen or heparin/poly(L-lysine) the films are thin enough to completely cover the microspheres, but the spherical morphology was still present. The layer-by-layer application method was tested and we determined that drop-coating (previous chapter), dip-coating, and spin-coating all created uniform PEM films on the peptoid microsphere surface. Schwann cells and bone-marrow derived human mesenchymal stem cells (hMSCs) were cultured on the newly developed substrates to test their efficacy in promoting cell adhesion and proliferation.

6.3.1   Dip-Coating Fabrication of PEM Films

Utilizing the positive surface charge of the peptoid microspheres and a previously established layer-by-layer method [10], we are able to fabricate heparin/poly(L-lysine) (HEP/PLL) and heparin/collagen (HEP/COL) thin films across the top of our microspheres. Peptoid microsphere coatings were made following the previously described method at a concentration of 3 mg/mL on ultraclean glass slides. All polymers (heparin, poly(L-lysine), and collagen) were held at a constant concentration of 1 mg/mL in PBS, except the type-1-collagen must be dissolved in an acetate buffer. The peptoid microsphere coated glass slide was dipped in the polymer solution for 5 minutes followed by a wash step in PBS for 3 minutes. This was repeated for each individual polymer layer until samples with a single layer of heparin (sample 0.5), a single bilayer (sample 1.0), and 6 bilayers (sample 6.0) were reached. To determine the efficiency of our coating method we visually analyzed the sample using SEM. The results showed that the peptoid microspheres formed uniform coatings alone (Figure 6.5A) and a single

layer of heparin (Figure 6.5B) added successfully to the peptoid microspheres. However, the 6

bilayers of heparin/poly(L-lysine) formed feather-like appendages that extended across the

surface (Figure 6.5C). The peptoid microspheres were present underneath 6 bilayers confirmed

by the cross-sectional SEM (Figure 6.5D), but little microsphere topography was preserved due

to the increased PEM thickness. The characterization process was repeated for the peptoid

microsphere and HEP/COL PEM coatings as well.
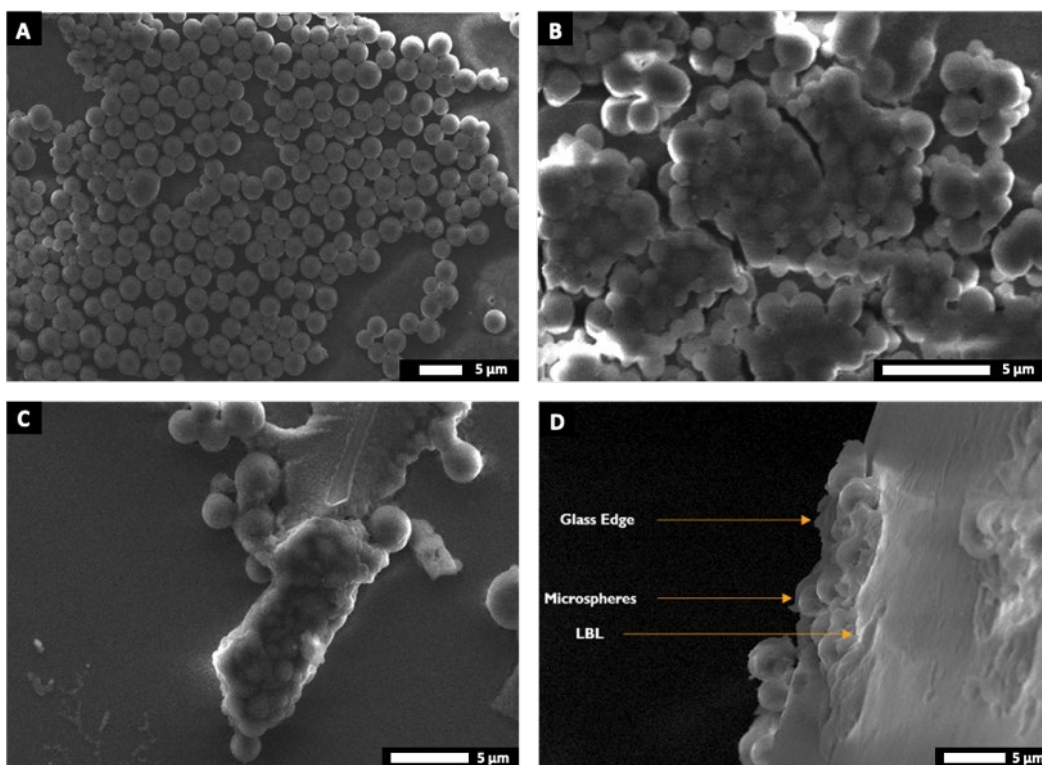
Figure 6.5 SEM images of (A) peptoid microspheres, (B) peptoid microspheres + 0.5 bilayers (Hep)$_{0.5}$, (C) peptoid microspheres + 6.0 bilayers (Hep/PLL)$_{6.0}$, and (D) cross section of peptoid microspheres + 6.0 bilayers (Hep/PLL)$_{6.0}$.

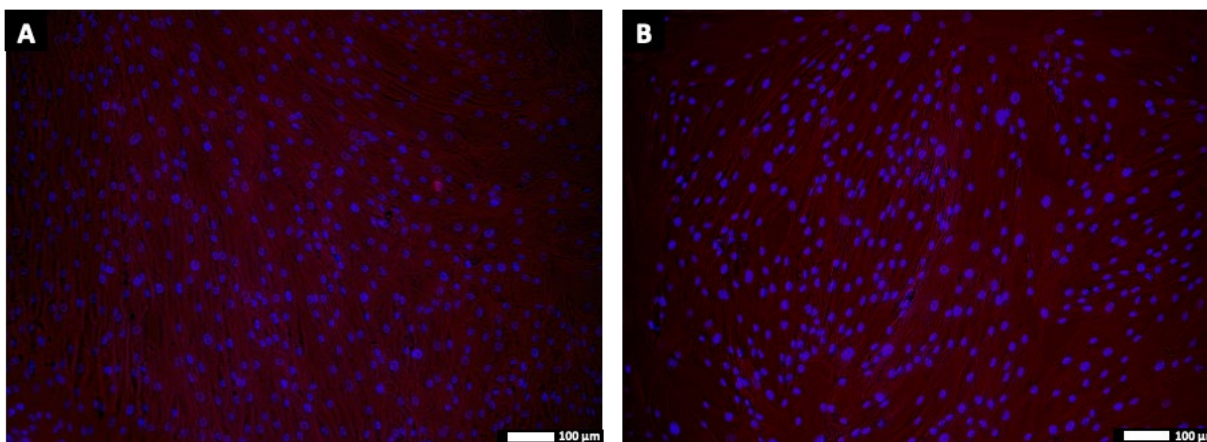### 6.3.2   Peptoid Microspheres + HEP/COL Coatings

PEM films of heparin/collagen were prepared on glass substrates (positive control) and

across the peptoid microsphere coatings by following the LbL method previously mentioned.

Both samples consisted of 6 bilayers of heparin and collagen. Schwann cells and hMSCs were

cultured on the LbL (HEP/COL)$_{6.0}$ and peptoid microspheres + LbL (HEP/COL)$_{6.0}$, surfaces for 3 days to determine the efficacy of the newly developed substrates for cell culturing. After day 3, the cells were fixed using paraformaldehyde and stained with Hoescht for the cell nuclei (blue) and Actin Red (red) for the cytoskeleton. Using ImageJ, the representative fluorescent microscope images of the Schwann cells and hMSCs were overlaid to display both cell nuclei and cytoskeleton directly. These images showed that the Schwann cells adhered to both surfaces and expanded (Figure 6.6). Both surfaces promoted excellent hMSC adhesion and expansion, while also enhanced cell proliferation (Figure 6.7). The hMSCs also displayed actin fiber filaments for both surfaces indicating healthy cellular behaviour. Actin filaments are a part of the MSCs cytoskeleton and has a major role in the mechanical properties of the cells by anchoring to the nucleus and holding it in place [11]. These studies provide necessary data to suggest further investigating the potential of peptoid microspheres and PEM films as aECM substrates.
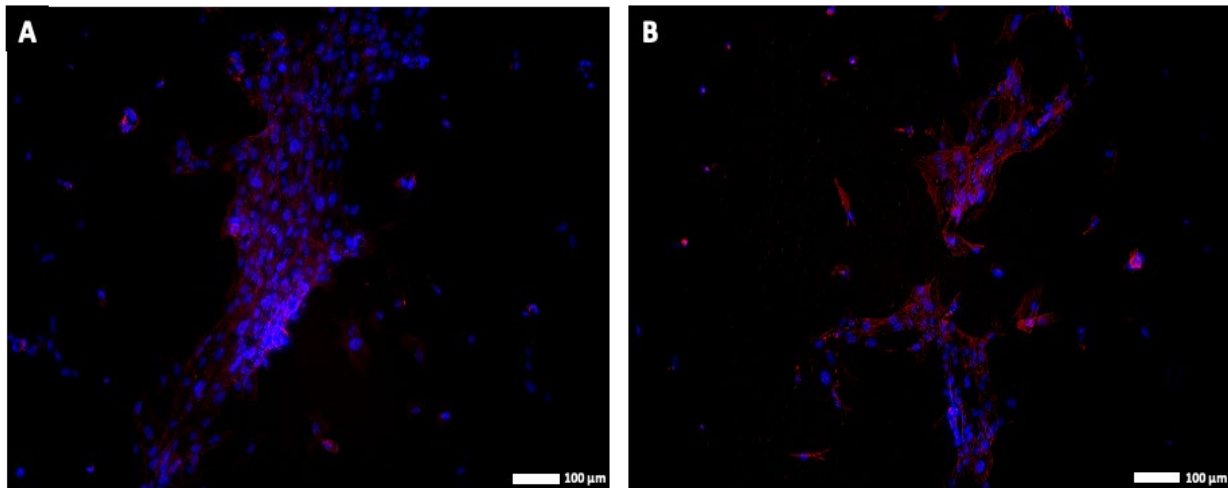
Figure 6.6 Study of morphology and extension of Schwann cells on (A) (HEP/COL)$_6$ and (B) peptoid microspheres + (HEP/COL)$_6$ surfaces. Representative fluorescence microscopic overlay images of Schwann Cells nuclei and actin labeled with Hoescht (blue) and Actin Red (red) after 3 days of culture.
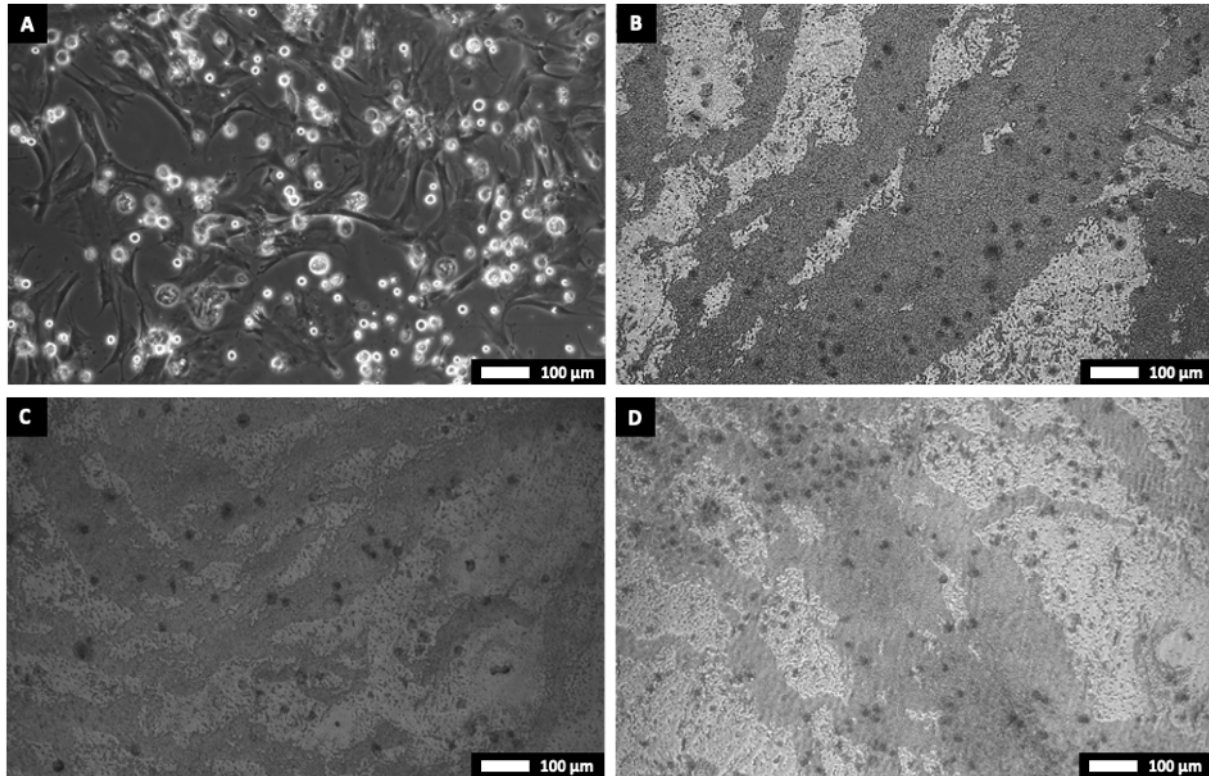
Figure 6.7 Study of morphology and extension of human mesenchymal stem cells (hMSCs) on (A) (HEP/COL)$_6$ and (B) peptoid microspheres + (HEP/COL)$_6$ surfaces. Representative fluorescence microscopic overlay images of MSC nuclei labeled with Hoescht (blue) and Actin Red (red), respectively, after 3 days of culture.

6.3.3 Peptoid Microspheres + HEP/PLL Coatings

PEM films of heparin/poly-L-lysine were prepared on glass substrates (positive control) and across the peptoid microsphere coatings by following the LbL method previously mentioned (Figure 6.5). Both samples consisted of 6 bilayers of heparin and PLL. hMSCs were cultured on the 6.0 LbL (HEP/PLL)$_{6.0}$ and peptoid microspheres + 6.0 LbL (HEP/PLL)$_{6.0}$, surfaces for 3 days to determine the efficacy of the newly developed substrates for cell culturing. After day 3, the cells were fixed using paraformaldehyde and stained with Hoescht for the cell nuclei (blue) and Actin Red (red) for the cytoskeleton. Optical microscopy showed the cells adhered to the glass control, peptoid microspheres, peptoid microspheres and 0.5 LbL (HEP)$_{0.5}$, and peptoid microspheres and 6.0 LbL (HEP/PLL)$_{6.0}$ coatings after 1 day (Figure 6.8). The cells on the peptoid microsphere samples were difficult to see using the inverted microscope due to the opaqueness of the coatings. The darker spots on the images represent the hMSCs (Figure 6.8B-D). Using ImageJ, the representative fluorescent microscope images of the hMSCs were overlaid to display both cell nuclei and cytoskeleton directly (Figure 6.9) The hMSCs grew extensively

on the glass control substrate indicated by the increased number and morphology of the cells on the surface (Figure 6.9A). The peptoid microsphere coatings had issues with background fluorescence, but the stained cells adhered to all of the coatings. The morphology of the cells on the peptoid and LbL coatings differed from the glass control in that the cells never spread out and stayed in a spheroid morphology (Figure 6.9C-D).

Figure 6.8 Light optical microscope images of human mesenchymal stem cells after 1 day on (A) Glass substrate (B) peptoid microspheres (C) peptoid microspheres and 0.5 LbL $(HEP)_{0.5}$, and (D) peptoid microspheres and 6.0 LbL $(HEP/PLL)_{6.0}$.
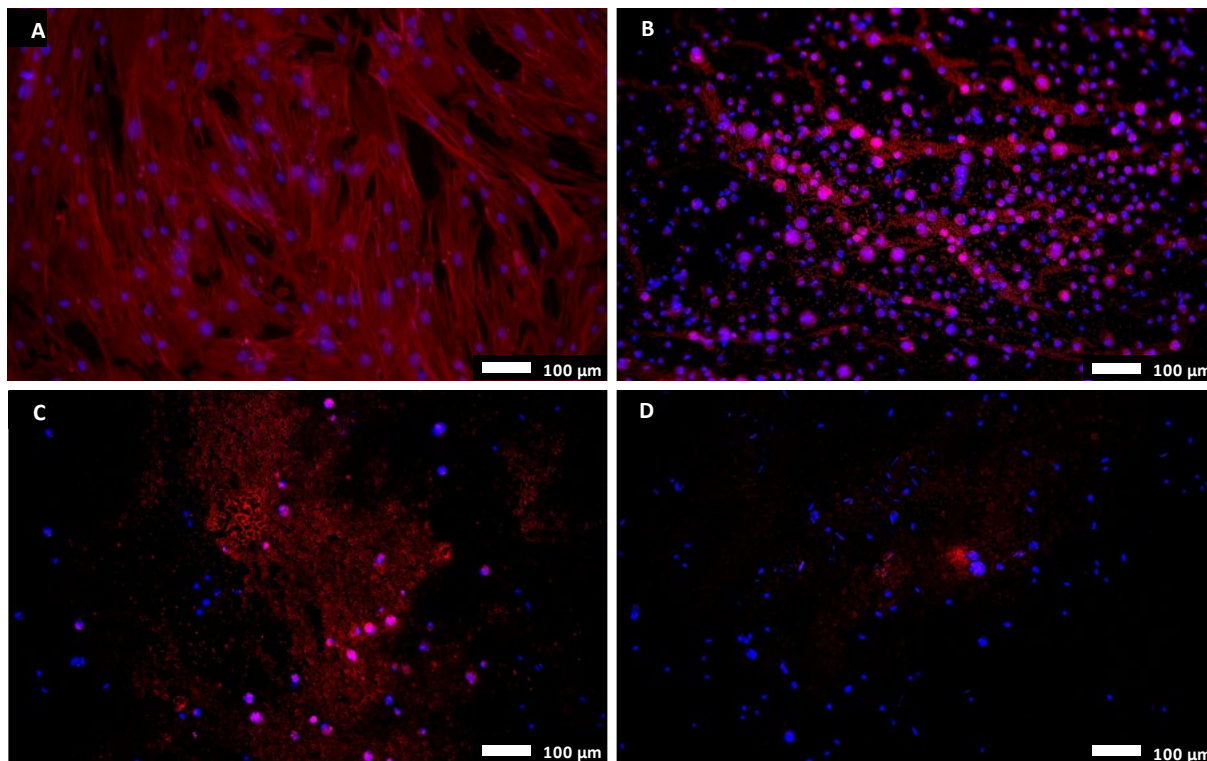
Figure 6.9 Study of morphology and extension of human mesenchymal stem cells (hMSCs) on (A) Glass substrate (B) peptoid microspheres (C) peptoid microspheres and 0.5 LbL (HEP)$_{0.5}$, and (D) peptoid microspheres and 6.0 LbL (HEP/PLL)$_{6.0}$. Representative fluorescence microscopic overlay images of MSC nuclei labeled with Hoescht (blue) and Actin Red (red), respectively, after 3 days of culture.
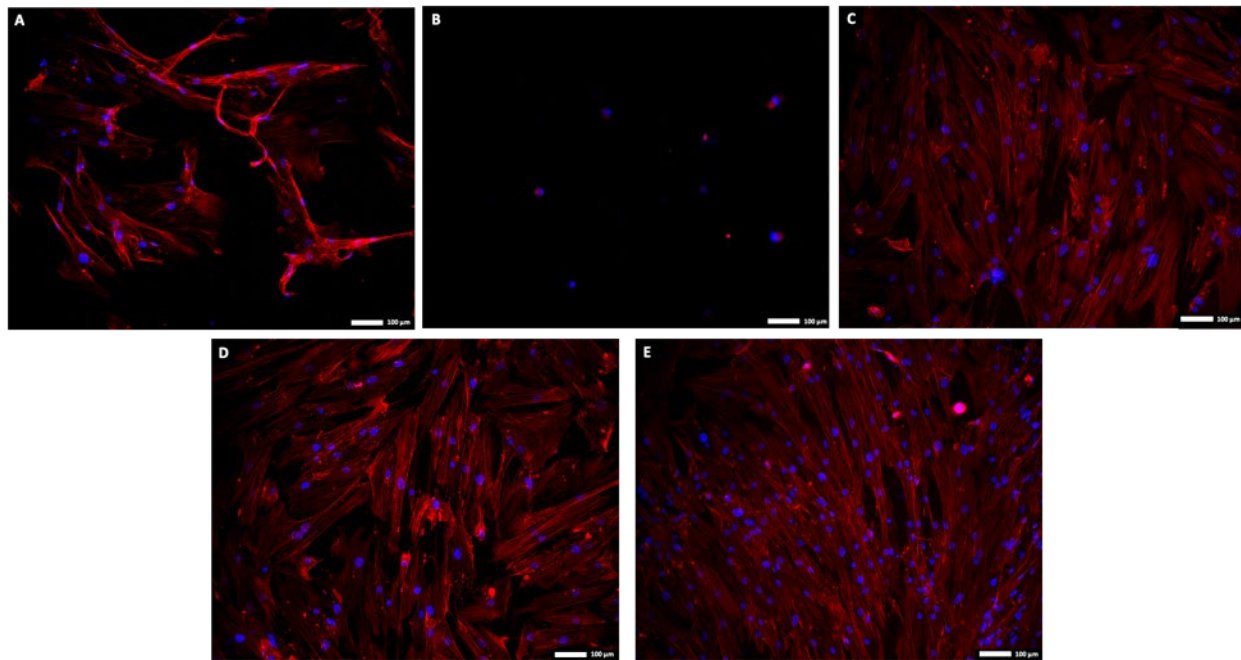
6.4   Peptoid Monomer and Microspheres in Solution

The goal of this study was to determine the effect that peptoid concentration had on hMSC growth. To do so, we investigated the cell growth by adding differing concentrations of peptoid monomer and microspheres directly to the cell media instead of forming peptoid coatings (Figure 6.10). In forming the peptoid monomer, the P3 peptide was dissolved in water and diluted to 1 mg/mL in PBS and 100 µL or 200 µL of the peptoid monomer solution was added to a well plate. The hMSCs in cell media were added to form a final volume of 1 mL per well. The final peptoid monomer concentrations were 0.1 mg/mL and 0.2 mg/mL in each of the two wells. Results showed that peptoid monomer concentration plays a role in hMSC viability as the higher

concentrated peptoid monomer solution had no cell adherence and growth. The lower

concentration, 0.1 mg/mL (Figure 6.10C), resulted in improved cell viability as compared to the

TCPS control (Figure 6.10A). The peptoid monomer at lower concentrations was proven to be

non-toxic to the MSCs.

The P3 microspheres were formed by dissolving the peptoid in 4:1 ethanol and water at a

concentration of 1 mg/mL. The peptoid microsphere solution was then diluted in dPBS to a

concentration of 0.1 mg/mL and the solution was centrifuged for 10 minutes. The top layer was

pipetted off to remove the ethanol. This was repeated 4 times and set in the hood to allow

residual ethanol to evaporate. The peptoid microsphere solution (100 µL or 200 µL) was added

to the well plate with hMSCs in media to a final volume of 1 mL per well, for a final peptoid

microsphere concentrations of ~0.01 mg/mL and ~0.02 mg/mL. Results showed that both

peptoid microsphere concentrations were below the threshold that prevents MSC from adhering

and extending out (Figure 6.10D-E). Both peptoid microsphere concentrations in solution had

better cell viability than the TCPS control sample. The hMSCs grown on the higher peptoid

microsphere concentration grew in more linear patterns, indicating that the microspheres in the

media might play a role in cell arrangement (Figure 6.10E).

Figure 6.10 Study of morphology and extension of human mesenchymal stem cells (hMSCs) on (A) tissue culturing polystyrene (well-plate), (B) 0.2 mg/mL peptoid monomer, and (C) 0.1 mg/mL peptoid monomer (D) 0.01 mg/mL peptoid microspheres, and (E) 0.02 mg/mL peptoid microspheres in solution. Representative fluorescence microscopic images of MSC nuclei (blue) and actin (red) labeled with Hoescht and Actin Red, respectively, after 4 days of culture.

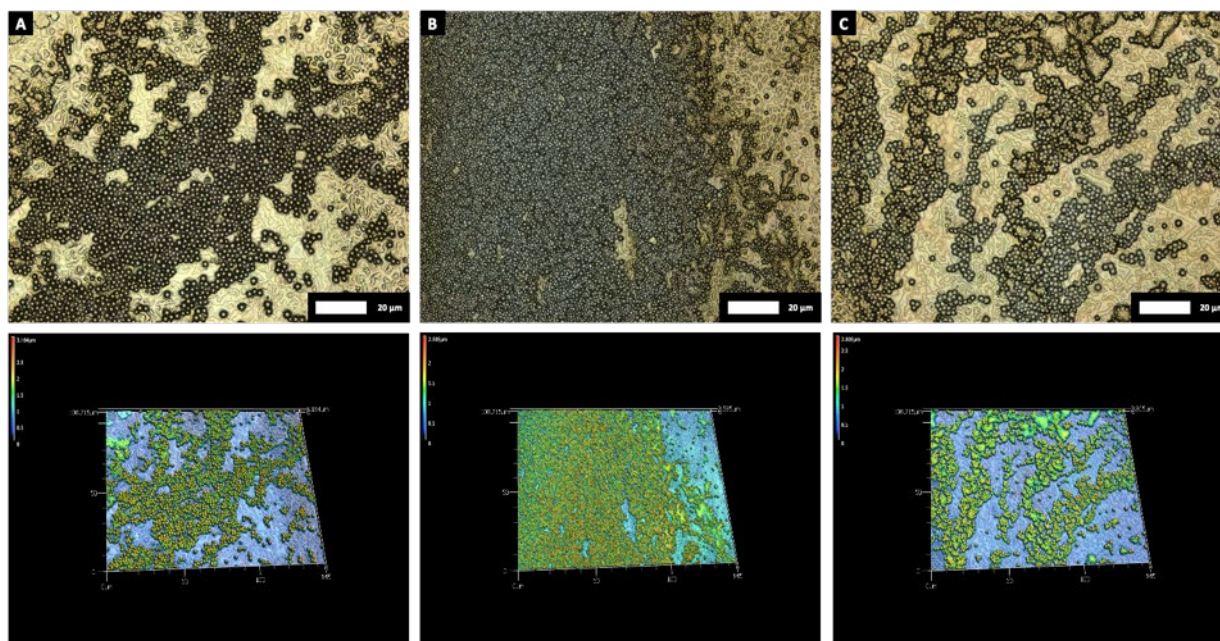## 6.5   Spin-Coating Peptoid Microspheres and LbL Films

Spin-coating is a widely used deposition method that can coat substrates uniformly with relative ease. It involves casting a material onto a spinning substrate, typically with a pipette [12]. The centrifugal force pushes the liquid outwards coating the entire substrate and allows for the fast evaporation of solvent. Since spin-coated is an efficient method of coating substrates, we decided to study its efficacy as a fabrication technique for our peptoid microspheres and LbL coatings. First, we wanted to see if spin-coating could drastically reduce the drying time and conditions (e.g. humidity, tween, airflow) that drop-coating peptoid microspheres required. For each sample, 30 µL of peptoid microsphere solution was pipetted onto a 25mm x 25mm

ultraclean glass slide and the solution was spun for 30 seconds at the desired speed. We investigated two spin-speeds of 500 RPM and 1,000 RPM. The coatings were characterized using 3D Laser Scanning Optical Microscopy (Figure 6.11). Both spin speeds formed peptoid microspheres on the surface, but the 1,000 RPM sample pushed the microspheres from the center due to the increased centrifugal force. This caused a ring-like effect where more microspheres were present at the edges of the glass slide (Figure 6.11A). The 500 RPM sample had more uniform coverage on the glass slide than the higher speed. Both samples had more efficient drying of the ethanol/water solvent mixture than the traditional drop-casting method. By spin-coating the peptoid microspheres onto the glass slides we were able to cut down the drying time from 30 minutes to 30 seconds.
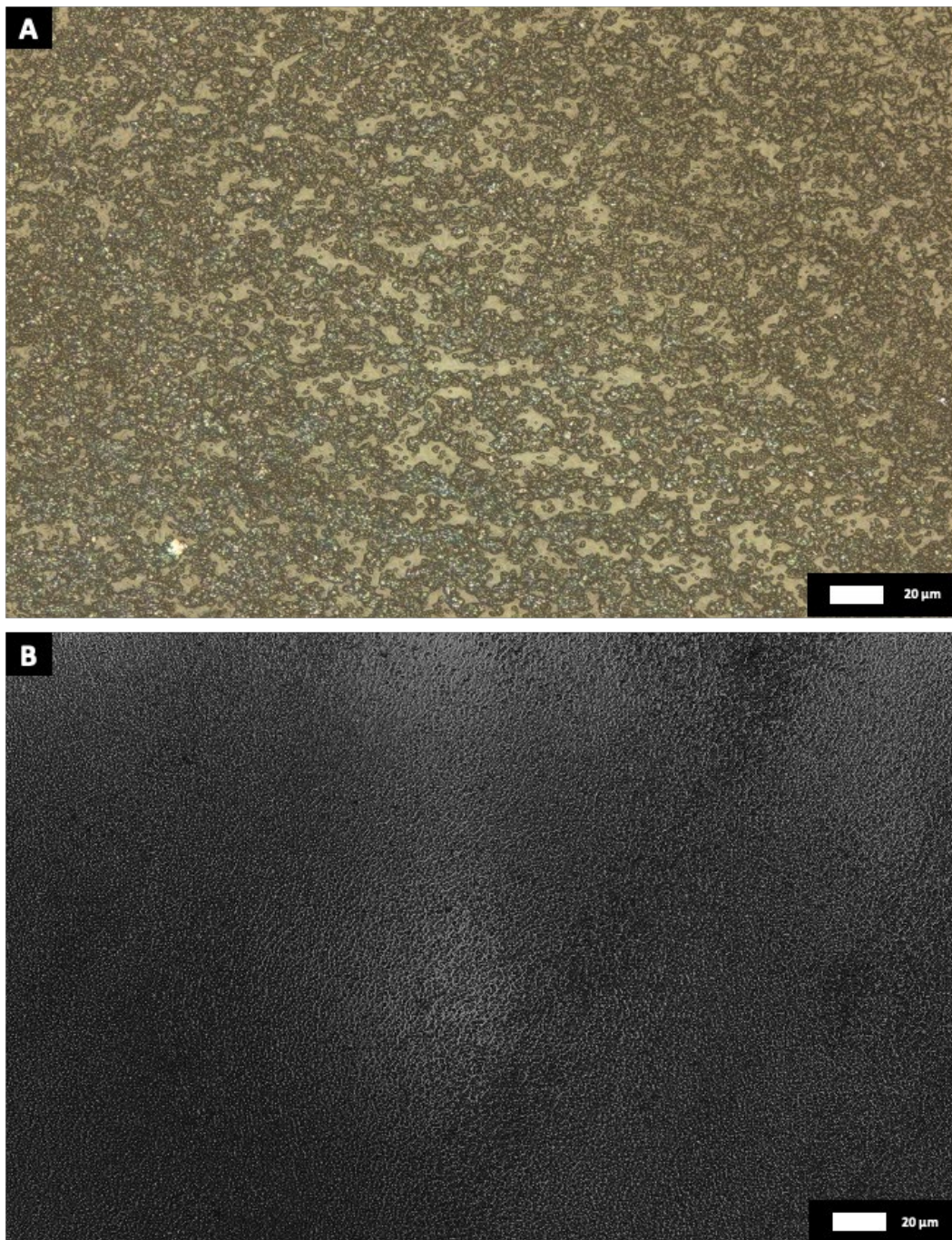
Figure 6.11 3D Laser Scanning Optical Microscope analysis of peptoid microspheres spin-coated onto an ultraclean glass slide at (A) 1,000 RPM (optical + laser) and (B) 500 RPM (laser only).

The ability to spin-coat LbL depositions on the microsphere substrates would potentially reduce synthesis time and create more uniform coatings. In doing so, a spin-coating technique that involved spinning each polymer at 5,000 RPM for 1 minute followed by a water wash at the same spin speed for 1 minute was used to form HEP/PLL bilayers. This process is repeated for each subsequent layer until the desired number of bilayers are formed. Once the bilayers were formed, the samples were fully dried with nitrogen gas and stored in a sterile environment for testing. Then, a single layer of heparin (HEP)$_{0.5}$, 1 bilayer (HEP/PLL)$_{1.0}$, and 3 bilayers (HEP/PLL)$_{3.0}$ were spin coated onto the peptoid microsphere substrates. 3D LSM images of the spin-coated LbL and peptoid microsphere coatings confirmed the presence of the films on the microspheres (Figure 6.12A-C). It is important that the spin-coating did not disrupt the peptoid microsphere morphology, since it will be utilized to potential dictate stem cell fate. All three coating thicknesses successfully preserved the microsphere morphology, while adding thin bilayers of the PEM films.

Figure 6.12 3D Laser Optical Microscope analysis of heparin/poly-L-lysine bilayers spin-coated on the peptoid microsphere coated glass slides. The samples were prepared by spin-coating (A) heparin only, (B) 1.0 bilayer (Hep/PLL)$_{1.0}$, (C) 3.0 bilayers (Hep/PLL)$_{3.0}$ on peptoid microsphere coated glass slides at 5,000 RPM for 1 minute each.

6.6 References

[1] B. Yue, "Biology of the Extracellular Matrix: An Overview," *J Glaucoma,* vol. 23, no. 8, pp. S20-23, 2015.

[2] W. P. Daley, S. B. Peters and M. Larsen, "Extracellular matrix dynamics in development and regenerative medicine," *Journal of Cell Science,* vol. 121, pp. 255-264, 2008.

[3] F. M. Watt and W. T. Huck, "Role of the extracellular matrix in regulating stem cell fate," *Nature Reviews Molecular Cell Biology,* vol. 14, pp. 467-473, 2013.

[4] I. A. Janson and A. J. Putnam, "Extracellular matrix elasticity and topography: material-based cues that affect cell function via conserved mechanisms," *Journal of Biomedical Material Res A,* vol. 103, no. 3, pp. 1246-1258, 2016.

[5] M. P. Lutolf, "Integration column: Artificial ECM: expanding the cell biology toolbox in 3D," *Integrative Biology,* vol. 1, no. 3, pp. 235-241, 2009.

[6] B.-S. Kim, I.-K. Park, T. Hoshiba, H.-L. Jiang, Y.-J. Choi, T. Akaike and C.-s. Cho, "Design of artificial extracellular matrices for tissue engineering," *Progress in Polymer Science,* vol. 36, no. 2, pp. 238-268, 2011.

[7] J. Heino and J. Kapyla, "Cellular receptors of extracellular matrix molecules," *Curr Pharm Des.,* vol. 15, no. 12, pp. 1309-1317, 2009.

[8] R. B. Gaynor, " A role for extracellular matrix binding receptors in regulating hematopoietic growth factor signaling," *PNAS,* vol. 100, no. 24, pp. 13737-13738, 2003.

[9] M. Akhmanova, E. Osidak, S. Domogatsky, S. Rodin and A. Domogatskaya, "Physical, Spatial, and Molecular Aspects of Extracellular Matrix of In Vivo Niches and Artificial Scaffolds Relevant to Stem Cells Research," *Stem Cells International,* vol. 2015, 2015.

[10] D. Dey, M. Islam, S. Hussain and D. Bhattacharjee, " Layer by Layer (LbL) Technique for fabrication of electrostatic Self assembled ultrathin films," *International Journal of Pure and Applied Physics,* vol. 4, no. 1, pp. 39-44, 2008.

[11] G. Yourek, M. A. Hussain and J. J. Mao, "Cytoskeletal Changes of Mesenchymal Stem Cells During Differentiation," *ASAIO J,* 2014.

[12] Q. Che, Z. Li, B. Pan, X. Duan, T. Jia and L. Liu, "Fabrication of layered membrane electrolytes with spin coating technique as anhydrous proton exchange membranes," *Journal of Colloid and Interface Science,* vol. 555, pp. 722-730, 2019.

7. Conclusion and Future Directions

The increased presence of biomimetic materials for biomedical applications has led to the development of more complex technologies. Specifically, there is a need for a material that is cost-effective, bioavailable, and tunable for various applications. This dissertation demonstrates the potential of peptoid microspheres as biomaterials for biosensing and cell manufacturing. In addition, the ability of the microspheres to serve as anchors for PEM development increases their potential in tissue engineering. The customizability and robustness of the peptoid microsphere substrate is invaluable as a biomimetic material. The use of peptoids in the form of uniform peptoid microsphere coatings offers a promising technology in biosensor and aECM substrate development. This dissertation studied (1) the physical and thermal properties of the peptoid microspheres along with their robustness in biological environments (Chapter 3), (2) the ability of peptoid microsphere coatings to enhance ELISA microarray technology (Chapter 4), (3) the tunability of the peptoid microsphere coatings by adding PEM films (chapter 5), and (4) the efficacy of peptoid microsphere and LbL coatings in cell culturing applications (Chapter 6). Our results found that varying peptoid chain length allows for the rational tuning of microsphere size. It has been demonstrated that the peptoid microsphere coatings are extremely robust for applications at physiological conditions. Results showed that the use of peptoid microsphere coatings as a novel surface for ELISA microarrays enhances the limits of detection and signal-to-noise ratios. It has also been proven that LbL technologies can be added to the surface of our peptoid microsphere coatings to create a more biocompatible and novel interface for cell culturing. These new materials have been proven to be non-toxic and effective in cell adhesion, proliferation, and viability.

Future studies for the physical properties of the peptoid microspheres should focus on

providing valuable insight into the mechanism of formation of the microsphere tertiary structure. By working with the Center for Integrative Nanotechnologies at Los Alamos National Lab the packing nature and self-assembly mechanism of the peptoid molecules can be further investigated. This study should conclude whether the peptoid microspheres are packed or hollow, the effect of peptoid chain length on packing density, and exactly how the peptoids are arranged in forming the microspheres. The charge distribution of the spheres could yield insight into the conformation and arrangement of peptoids in the microspheres. To gather this data, the use of grazing incidence small-angle x-ray scattering (GISAXS) from a synchrotron would provide the needed beam flux and q-resolution needed for the size of our peptoid molecules. From this data, it would be possible to create molecular dynamic simulations to model the formation of microspheres. These simulations could be carried over to provide an infrastructure to better model drug loading and delivery along with cell signaling interactions. For the LbL work, the uniformity of the depositions can be optimized, and the coatings characterized further using zeta-potential, XPS, and ellipsometry to provide feedback on the surface charge, chemical composition, and film thickness, respectively. It would be valuable to further determine the role that peptoid concentration and morphology plays on stem cells, and whether the peptoid microspheres influence the fate of stem cell differentiation.